Earth-Science Reviews 265 (2025) 105120

Contents lists available at ScienceDirect

Earth-Science Reviews

journal homepage: www.elsevier.com/locate/earscirev

# Magmatic complexes of the Tekturmas Fold-and-Thrust Belt, Central Kazakhstan: An overview and new implications for the early Paleozoic evolution of the Paleo-Asian Ocean☆

Inna Safonova [a,b], Alexandra Gurova [b,c], Alina Perfilova [a,c,*], Wenjiao Xiao [d,e,f], Pavel Kotler [b,c], Reimar Seltmann [g], Natalia Soloshenko [h], Alla Dolgopolova [g]

[a] Southwest Jiaotong University, Xi'an Road 999, Chengdu, China
[b] Sobolev Institute of Geology and Mineralogy, SB RAS, Koptyuga ave. 3, Novosibirsk, Russia
[c] Novosibirsk State University, Pirogova St. 2, Novosibirsk, Russia
[d] National Key Laboratory of Ecological Safety and Sustainable Development in Arid Lands, Xinjiang Institute of Ecology and Geography, Chinese Academy of Sciences, Urumqi 830011, China
[e] College of Earth and Planetary Sciences, University of Chinese Academy of Sciences, Beijing 100049, China
[f] Institute of Geology and Geophysics, Chinese Academy of Sciences, Beijing 100029, China
[g] Natural History Museum, Centre for Russian and Central EurAsian Mineral Studies, London, UK
[h] Zavaritskiy Institute of Geology and Geochemistry UrB RAS, Vonsovskogo ave. 15, Yekaterinburg, Russia

ARTICLE INFO

*Keywords:*
Central Asian Orogenic Belt
Paleo-Asian Ocean
U-Pb zircon ages
Isotopes
Intra-oceanic arcs
Seamounts

ABSTRACT

The Tekturmas Fold-and-Thrust Belt (TFTB) is an important structure of the Kazakhstan Orocline in the western Central Asian Orogenic Belt (CAOB), which formation is linked with the early-middle Paleozoic evolution of the Paleo-Asian Ocean (PAO). The TFTB includes accreted oceanic sediments and magmatic rocks, supra-subduction ophiolites and fore-arc and back-arc siliciclastic rocks of Cambrian to Silurian ages. There remains a deficiency in data from magmatic rocks of the TFTB and, as a result, the timing of magmatism, mantle sources and tectonic settings are still debatable and the general early Paleozoic evolution of the TFTB is not fully understood. In this paper we review previous geological and age data (U-Pb, microfauna) and present new geological, geochronological (U-Pb zircon ages) and geochemical data and first isotope data (Sm-Nd, Pb-Pb, Lu-Hf). We discuss these new results and the previously reported, but still limited data from both magmatic and clastic rocks. Granite and rhyolite yielded middle-late Ordovician U-Pb zircon ages, 462 and 449 Ma, respectively. There are three main groups of volcanic/subvolcanic and plutonic rocks: (1) high-Ti, (2) mid-Ti, and (3) low-Ti. The high-Ti basalts and andesites are enriched in high-field strength elements (HFSE) and light rare-earth elements (LREE); they were derived at 2–4 % melting of an enriched garnet-bearing peridotite ($\varepsilon Nd_t = +2.1\ldots +6.8$; $^{206}Pb/^{204}Pb = 19.2–22.8$) and erupted on an oceanic island or seamount. The mid-Ti gabbro is N-MORB formed from a 15 % melted depleted mantle source ($\varepsilon Nd_t = +8.1$; $^{206}Pb/^{204}Pb = 18.9$). The low-Ti group is depleted in HFSE, but not LREE, and formed at high degrees of melting (15–30 %) of depleted and ultra-depleted mantle sources ($\varepsilon Nd_t = +6.1\ldots +10.8$; $\varepsilon Hf_t = +17.6\ldots +19.3$) suggesting their emplacement in a supra-subduction setting. Based on all the available data, we present a model of double-sided subduction in this part of the PAO, which generated four intra-oceanic arcs at its opposite sides: early-middle Cambrian and Early Ordovician on one side and Early and Late Ordovician on another side. The early-middle Cambrian and Early Ordovician arcs were tectonically eroded and their fragments have been preserved in blocks of mélange and greywacke sandstones only. The pieces of all arcs were tectonically juxtaposed in the TFTB during the processes of subduction and accretion in the PAO. The early Paleozoic magmatism ceased in early Silurian time.

**Contents**

☆ This article is part of a Special issue entitled: 'WenjiaoAltaids' published in Earth-Science Reviews.

* Corresponding author at: Southwest Jiaotong University, Xi'an Road 999, Chengdu, China.
*E-mail address:* p.alina2808@mail.ru (A. Perfilova).

https://doi.org/10.1016/j.earscirev.2025.105120
Received 8 October 2024; Accepted 26 March 2025
Available online 30 March 2025

## 1. Introduction

Magmatic rocks emplaced in oceanic and supra-subduction settings and later incorporated into intra-continental orogenic belts, that result from oceanic suturing and continental collision, represent invaluable archives of information about magmatism of paleo-oceans and their active margins (or subduction zones). During oceanic subduction, the magmatic associations formed at mid-oceanic ridges (spreading) and oceanic islands, seamounts and plateaus (oceanic hot-spots) appear juxtaposed in accretionary prism and later, together with supra-subduction magmatic rocks of intra-oceanic and continental magmatic arcs, become parts of intra-continental Pacific-type orogenic belts formed in place of former oceans (e.g., Matsuda and Uyeda, 1971; Katz, 1973; Maruyama et al., 1997, 2011; Cawood et al., 2009; Stern, 2011; Safonova et al., 2011a; Safonova, 2017). During ocean closures and continental collisions, the accretionary and supra-subduction complexes undergo strong tectonic deformations and get intruded by collision-related and within-plate continental magmatic rocks. As a result, the orogenic belts, which we are studying now, may host magmatic rock associations formed in various tectonic environments: from ocean to continent. Identification of such magmatic rocks in fossil Pacific-type orogenic belts is rather challengeable due to their complicated structure, high degree of post-magmatic alteration, and often limited exposures. To differentiate those rocks, to trace the balance between crustal growth and recycling, and to develop a trustworthy tectonic model we must highlight the periods of oceanic, supra-subduction and collisional magmatism, i.e., to know the age, petrogenesis, mantle sources and geodynamic environments of formation of this or that rock.

The Central Asian Orogenic Belt (CAOB) is the world largest Phanerozoic Pacific-type or accretionary intra-continental orogen formed during the evolution and suturing of the Paleo-Asian Ocean (PAO) and by a subsequent series of dischronous collisions of the Siberian, North China, Tarim and East European continental blocks (clockwise from north to south) (e.g., Zonenshain et al., 1990; Sengör et al., 1993; Didenko et al., 1994; Dobretsov et al., 1995; Jahn et al., 2000; Buslov et al., 2001; Windley et al., 2007; Safonova et al., 2011a; Kröner et al., 2014, 2017; Xiao and Santosh, 2014; Safonova, 2017). The CAOB represents a puzzle of microcontinents, supra-subduction terranes and accretionary complexes hosting pieces of oceanic crust and passive margin strata (e.g., Badarch et al., 2002; Jahn, 2004; Degtyarev and Ryazantsev, 2007; Kröner et al., 2007; Volkova and Sklyarov, 2007; Sun et al., 2008; Kruk et al., 2010; Seltmann et al., 2010; Xiao et al., 2010; Wang et al., 2014; Safonova et al., 2017). The main controversy about the CAOB remains about the proportion of juvenile and recycled crust (Wang et al., 2023). To resolve that problem, we, again, must study CAOB magmatic rocks because the major sites of the formation of juvenile crust on Earth are intra-oceanic and, to a lesser degree, continental magmatic arcs (Clift et al., 2003; Stern and Scholl, 2010; Kröner et al., 2014). There have been found many intra-oceanic arc terranes in the CAOB (Safonova, 2017), however the magmatic formations of the western CAOB, in particular, those of early Paleozoic age remain insufficiently studied.

The Paleozoic history of the western CAOB is linked to the evolution several branches of the PAO: Ob–Zaysan (between Siberia and Kazakhstan), Uralia (between Baltica and Kazakhstan), Turkestan (between Kazakhstan and Tarim), and Junggar–Balkhash (between the limbs of the Kazakhstan Orocline) (e.g., Windley et al., 2007; Safonova et al., 2012, 2016; Shen et al., 2015; Liu et al., 2017; Li et al., 2018; Zhang et al., 2018, 2023). The early Paleozoic formations and complexes of the western CAOB are located in the hinge area of the Kazakhstan Orocline and north of it (Fig. 1) and are linked with the evolution of the Junggar–Balkhash branch of the PAO and/or Caledonian orogeny related to its suturing. The magmatism and orogeny formed numerous magmatic and clastic formations: Selety-Stepnyak volcanic arc in northern Kazakhstan, various accretionary wedges and suture zones and volcanic arcs of the Kazakhstan Orocline (Windley et al., 2007; Degtyarev, 2011, 2012; Shen et al., 2015), Songkul volcanic arc in Northern Kyrgyz Tien Shan (Konopelko et al., 2021), Tangbale-Barleik-Maylie ophiolites in West Junggar (Kwon et al., 1989; Zhang, 1997; Wen et al., 2016) (Fig. 1) and Kurai and Katun volcanic arcs in the Russian Altai (Buslov et al., 2001; Utsunomiya et al., 2009; Glorie et al., 2011; Chen et al., 2016). The main early Paleozoic terranes of the Kazakhstan Orocline are Zhaman-Sarusy, North Balkhash and Junggar-Balkhash suture zones with accretionary complexes and Baidaulet-Akbastau and Boshchekul-Chingiz volcanic arcs. The Tekturmas Fold-and-Trust Belt (TFTB) belongs to the Zhaman-Sarysu suture zone (Fig. 1).

Geographically, the TFTB is located in Central Kazakhstan, south of the city of Karaganda, and extended over a distance of more than 150 km from SWW to NEE (Fig. 2). It hosts Ordovician to early Silurian sedimentary and volcanogenic-sedimentary strata and several ophiolite complexes (e.g., Tortaul, Bazarbai) consisting of serpentinite mélange with blocks of ultramafic rocks, gabbro, plagiogranite, and basalt (Yakubchuk et al., 1989; Yakubchuk, 1991; Stepanets, 2016; Degtyarev et al., 2017, 2022, 2023). Recently there have been published several

papers on the TFTB reviewing available geological and stratigraphic data and presenting first high-precision geochronological and geochemical data from both magmatic and sedimentary rocks (Degtyarev et al., 2017, 2022; Khassen et al., 2020; Gurova et al., 2022; Perfilova et al., 2022a). However, it remains understudied in terms of igneous geochemistry and isotope systematics. Such data seems indeed necessary to develop more robust reconstructions of petrogenesis, mantle sources and geodynamic settings of eruption/emplacement of magmatic rocks and thus to contribute to the better understanding of the Paleozoic evolution of the PAO. In this paper we review the previous geological, biostratigraphic and geochemical data and present new geological, geochronological (U-Pb zircon ages) and detailed geochemical data and first isotope data (Sm-Nd and Pb-Pb bulk-rock and Hf-in-zircon) from TFTB magmatic rocks (for sampling sites see e-component supplementary figures) with deeper insights into their petrogenesis and mantle sources in an attempt to re-consider the magmatic processes involved in the early Paleozoic evolution of the PAO and to present a holistic story of the formation of the Tekturmas Fold-and-Thrust Belt.

## 2. A geological overview of the Tekturmas Fold-and-Thrust Belt

### 2.1. A historical retrospective

Some researchers believe the TFTB belongs to the northwestern part of the Junggar-Balkhash folded area/region or system (JBFA), which is extended from Central Kazakhstan to West Junggar in NW China (Bespalov, 1976; Degtyarev, 1999, 2011, 2012; Degtyarev et al., 2020, 2022; Seitmuratova et al., 2023). The JBFA is thought to be formed during the evolution of the Junggar-Balkhash branch of the PAO. It includes early-middle Paleozoic ophiolites, flysch deposits and accreted OPS units (basalt, chert, siliceous mudstone and siltstone) preciously referred to as basalt-siliceous sequences. Cambrian to Silurian ophiolitic belts have been found in the territories of Kazakhstan (Tekturmas, North Balkhash or Itmurundy in the NW and central JBFA, respectively) and NW China (Tangbale, Barleik-Maylie, Daerbute, Karamai in West Junggar). Windley B. with co-authors (2007) consider the TFTB a part of the Zhaman-Sarysu suture zone in the hinge of the Kazakhstan Orocline (Fig. 1) (Levashova et al., 2003, 2012; Abrajevitch et al., 2008; Li et al., 2018).

The Tekturmas Fold-and-Thrust Belt has been previously referred to as simply Tekturmas zone (Yakubchuk, 1991; Degtyarev et al., 2017) or Tekturmas ophiolite belt (Antonyuk et al., 2015; Khassen et al., 2020; Safonova et al., 2022) or ophiolite zone (Degtyarev et al., 2022) or Tekturmas accretionary prism or complex (Stepanets, 2016; Gurova et al., 2022). The geological survey in the Tekturmas Mountains started back in the 1930-ties (Bogdanov, 1939). That time they first reported about thick siliceous-volcanogenic deposits of the Tekturmas Mts. and considered then as an Urtynjal Series consisting of two formations, Karamurun (basalt-volcaniclastic) and Tekturmas (cherty and silici-clastic) and then they distinguished Bazarbai Formation including two sub-suites: lower (basaltic) and upper (siliceous-tuffogenic). In the 1970-ties, geologists and paleontologists obtained first data on the composition, age and stratigraphy of those deposits (Nazarov, 1975; Afonichev, 1976; Bespalov, 1976; Antonyuk, 1974; Zaitsev, 1977). Later, more detailed biostratigraphic data allowed improving previous geological maps and distinguishing more formations (older to younger): Karamurun, Kuzek, Tekturmas, Bazarbai and Yermek (Kurkovskaya, 1985; Novikova et al., 1991; Turmanidze et al., 1991; Gerasimova et al., 1992). Nowadays, most of researchers who have worked in the TFTB agree that it represents a polychronous suture-folded structure and consists of several tectonic sheets thrust northward at angles of 40° to 70° (Antonyuk, 1974; Yakubchuk, 1991).

Lithologically, the main constituents of the TFTB are the serpentinite mélange composing its axial part (Figs. 3, 4), Ordovician ophiolites,

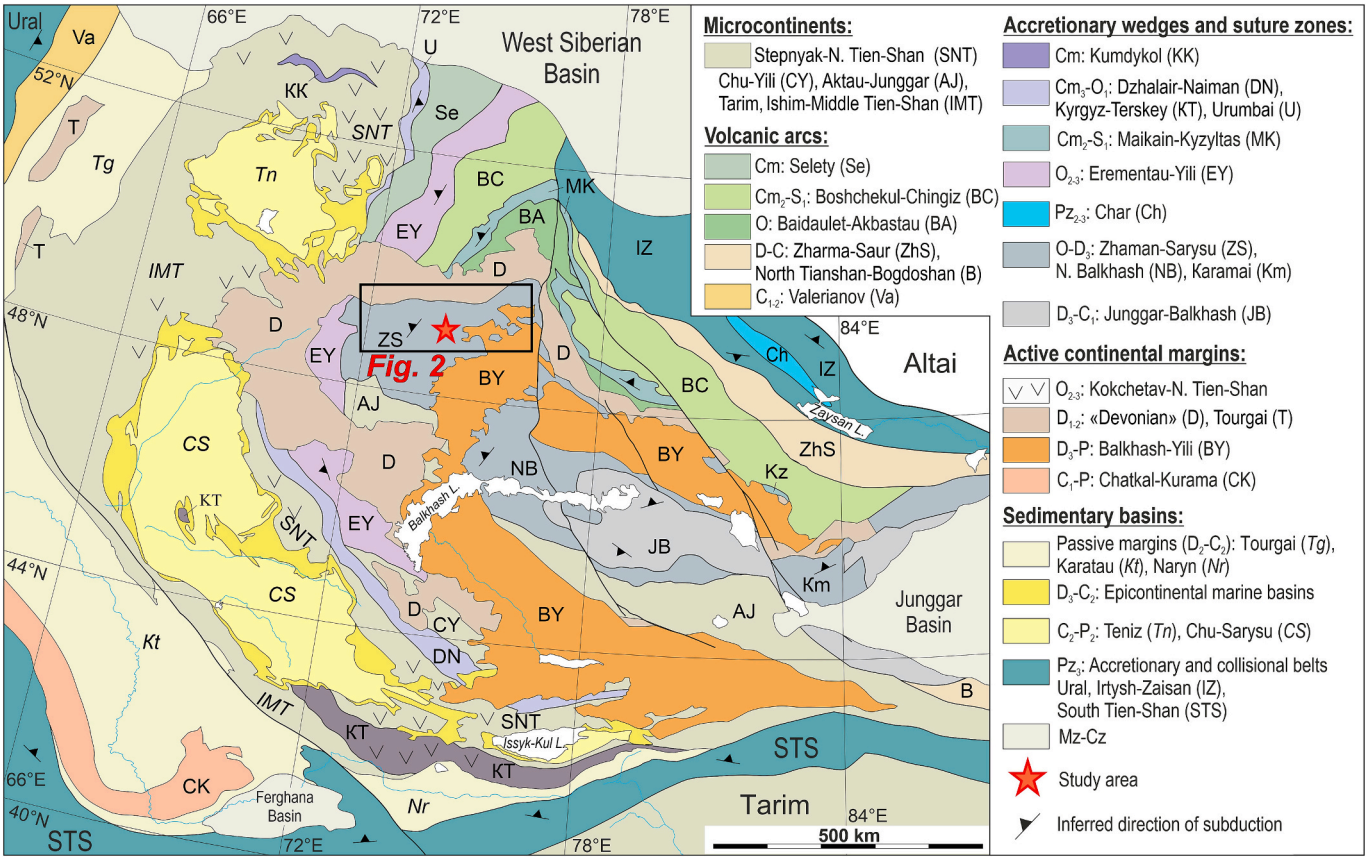


**Fig. 1.** Geotectonic map of the western Central Asian Orogenic Belt (after Windley et al., 2007, Xiao et al., 2015).

accretionary complex hosting coeval volcanogenic, cherty and siliciclastic strata, and Upper Ordovician-Lower Silurian clastic deposits and olistostromes (Gerasimova et al., 1992; Degtyarev et al., 2017, 2022; Khassen et al., 2020). The TFTB ophiolite association includes peridotite, gabbro and dolerite dikes and serpentinite mélange (Antonyuk, 1974; Stepanets, 2016; Khassen et al., 2020; Degtyarev et al., 2022; Gurova et al., 2022). The serpentinite mélange consists of blocks of gabbro and gabbro-amphibolite, dolerite, basalt and their metamorphosed analogues and siliceous sedimentary rocks submerged into apoharzburgite and apolherzolite matrix (Stepanets, 2016; Khassen et al., 2020; Degtyarev et al., 2022). The accretionary complex includes magmatic and sedimentary rocks formed over the oceanic plate: MORB and OIB-type basalts, pelagic chert, hemipelagic siliceous mudstone and siltstone, trench turbidites (Khassen et al., 2020; Degtyarev et al., 2022; Gurova et al., 2022; Perfilova et al., 2022a). Such rock assemblages are often called *ocean plate stratigraphy* or OPS (Isozaki et al., 1990; Safonova et al., 2016).

In different times and by different research groups the magmatic associations of the TFTB have been divided according to the timing of emplacement into early, late and residual (Degtyarev et al., 2017), then according to their geodynamic origin into Early Ordovician supra-subduction ophiolites, Middle Ordovician Karamurun oceanic intraplate basalts and Middle to Late Ordovician Bazarbai supra-subduction ophiolites (Figs. 3, 4) (Degtyarev et al., 2022). There have been more alternatives though, like: (1) the TFTB volcanic rocks were considered as parts of the Karamurun and Kuzek formations and the TFTB plutonic rocks as parts of ophiolite association (pyroxenite, gabbro, diorite, plagiogranite); (2) the plutonic rocks occur as blocks in serpentinite mélange (plagiogranite, tonalite, granodiorite) (Khassen et al., 2020; Safonova et al., 2022); (3) both the volcanic rocks and associated cherty and siliceous sediments are accreted units of oceanic plate stratigraphy (Khassen et al., 2020).

The first up-to-date geochemical data from magmatic rocks allowed identification of coherent and incoherent bodies of ophiolite associations of various origins, supra-subduction (fore-arc, back-arc and island-arc), mid-ocean ridge or seamounts (Fig. 4; Stepanets, 2016; Khassen et al., 2020; Degtyarev et al., 2022; Gurova et al., 2022). The first U-Pb zircon ages were obtained from supra-subduction plagiogranites (473 ± 2, 453 ± 4 Ma, Tortaul and Bazarbai complexes), Cpx-granulites (454–478 Ma), and syenites (463 ± 2 Ma) (Degtyarev et al., 2017, 2022) (Fig. 3; Table 1). The first U-Pb ages of detrital zircons from greywacke sandstones formed by erosion of intra-oceanic arcs showed the peaks of island-arc magmatism at ca. 510 and 450 Ma (Perfilova et al., 2022a) and suggested that the late Cambrian arc was tectonically eroded (Safonova and Perfilova, 2023).

### 2.2. TFTB structural-formational zones and their stratigraphy

Four structural-formational zones separated by regional faults have been traditionally recognized in the geological maps covering the TFTB (south to north): Uspenka, Tekturmas, Bazarbai and Nura (Fig. 3; Yakubchuk et al., 1988; Yakubchuk, 1991; Antonyuk et al., 1995). The main zones are Tekturmas and Bazarbai, which are dominated by oceanic and supra-subduction formations, respectively (Fig. 4; Antonyuk et al., 2015; Khassen et al., 2020; Degtyarev et al., 2022; Gurova et al., 2022). The main lithologies of both zones include serpentinite mélange, gabbroids, basaltic pillow-lavas, deep-marine chert, and various siliciclastic sedimentary rocks (siliceous mudstone and siltstones, and sandstones). The stratigraphic subdivision of the TFTB includes (from older to younger) eight Ordovician to Silurian formations: Karamurun, Tekturmas, Kuzek, Bazarbai, Airtau, Sarytau, Yermek and Isen' (Fig. 5).

The SW-NE trending Tekturmas Zone occupies a central position in the TFTB and is extended to a distance of more than 40 km (Figs. 3, 4, 6). The main lithologies are strongly deformed ophiolites, serpentinite mélange and gabbroids and their associated sedimentary rocks (Yakubchuk et al., 1988; Novikova et al., 1991; Stepanets, 2016). The mélange consists of fragments of harzburgite, dunite, layered gabbro, gabbro-amphibolite, dolerite, basalt, siliciclastic rocks, and, rarely, plagiogranites all submerged into serpentinite matrix. The main

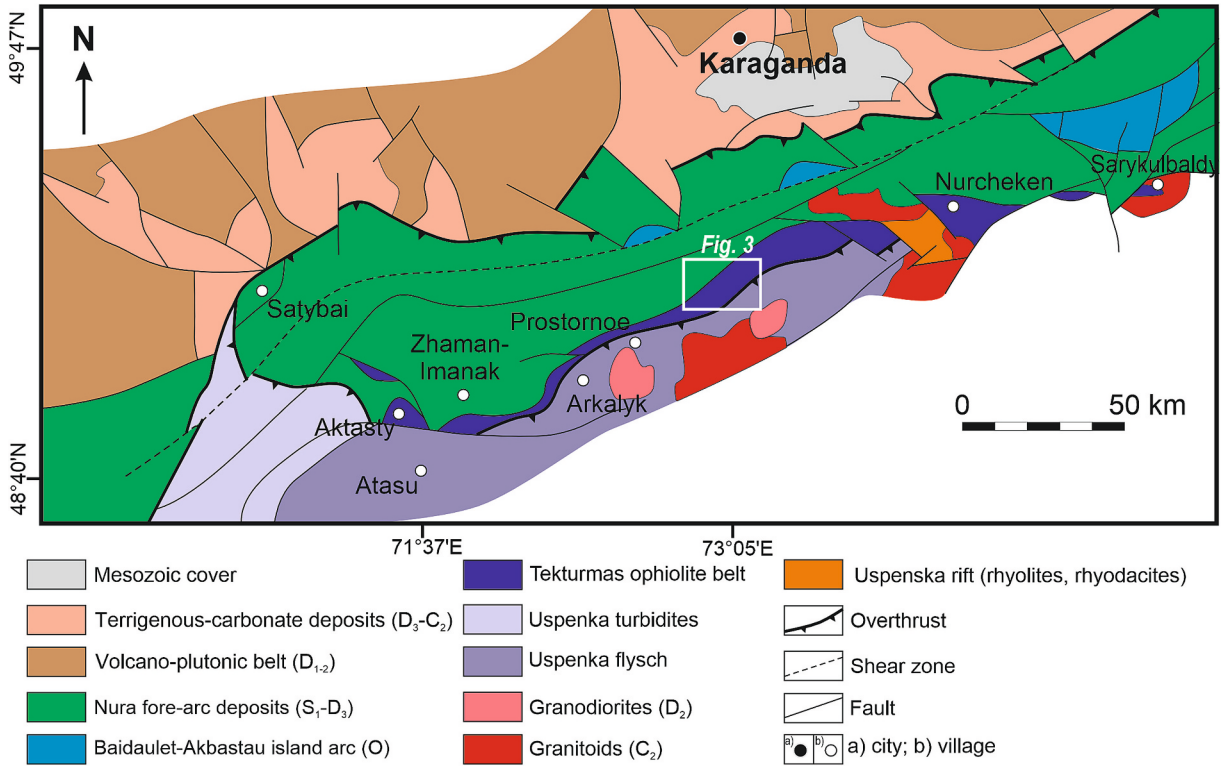


**Fig. 2.** Geodynamic scheme of the Tekturmas Fold-and-Thrust Belt and adjacent terranes (modified from Antonyuk et al., 1995; Stepanets, 2016).

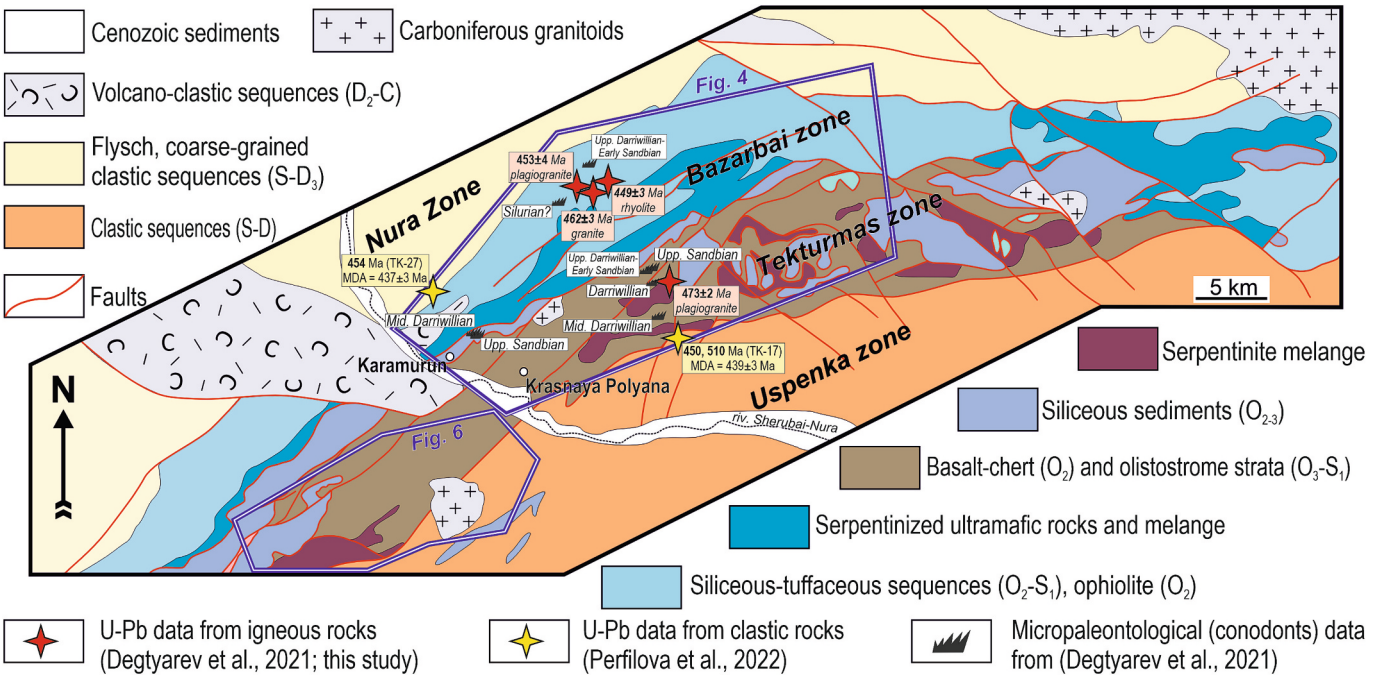


**Fig. 3.** Geological scheme of the Tekturmas Fold-and-Thrust Belt (adapted from Degtyarev et al., 2022).

formations are Karamurun, Tekturmas and Sarytau (Figs. 4–6). The Karamurun Fm. ($O_2$kr) consists of basalt and basaltic clastic lava, ribbon chert, siliceous mudstone and mafic to andesitic tuffs. The massive and amygdaloidal basalts are of OIB type (Khassen et al., 2020; Degtyarev et al., 2022). The Middle Ordovician age of the Karamurun Fm. was constrained by conodonts (Table 1; Gerasimova et al., 1992). The Tekturmas Fm. ($O_{2-3}$tk) is dominated by chert, siliceous mudstone, and siltstone; the rocks have variable colors, from light pink to red and dark-brown. The cherts and siliceous mudstones often possess a ribbon texture, that is typical of deep-water pelagic sediments now parts of accretionary complexes worldwide (Isozaki et al., 1990; Hori, 1992; Kusky et al., 2013; Safonova et al., 2016). The formation has middle-late Ordovician age as defined by conodonts of three zones from black and red cherts: lower Darriwilian, upper Darriwilian and lower Sandbian (Kurkovskaya, 1985; Novikova et al., 1991; Gridina, 2003). The Sarytau Fm. ($O_3$-$S_1$sr) is dominated by greenish siliceous siltstones, fine- to coarse-grained sandstones and other clastic rocks representing an olistostrome (Gerasimova et al., 1992; Novikova et al., 1991). The olistoliths are siliceous sedimentary rocks and basalts. The matrix consists of siliceous claystones, mudstones, siltstones, sandstones and tuffs carrying traces of re-deposition and solidification. The matrix contains late Ordovician conodonts and early Silurian graptolites (Gerasimova et al., 1992) (Table 1; Figs. 4, 5).

The Bazarbai Zone is located north of the Tekturmas Zone (Figs. 3, 4). Most of the rocks, both magmatic and sedimentary, occur as 500–600 m thick and 6–7 km long blocks or sheets aligned subparallel to the border with the Tekturmas Zone. The mafic volcanic and plutonic rocks are considered as ophiolites (Degtyarev et al., 2022). The main formations are Kuzek and Bazarbai overlapped by a Silurian flysch of the Nura Zone (Figs. 4, 5; Novikova et al., 1988). The Kuzek Fm. ($O_{2-3}$kz) is dominated by volcanic and subvolcanic rocks: amygdaloidal basalt (flows and pillow-lavas), dolerite, andesibasalt, tuffs interbedded with siliceous mudstones and siltstones. The Kuzek OPS, basalt, siliceous mudstones and siltstones, overlap the ophiolitic dike complex and plagiogranites. The basalts are associated with chert and siliceous mudstones containing middle Ordovician (upper Darriwilian) and upper Ordovician (lower Sandbian) conodonts (Degtyarev et al., 2017, 2022). The Bazarbai Fm. ($O_3$-$S_1$bz) is dominated by sedimentary and volcaniclastic rocks: chert, siliceous mudstone and siltstone, mafic to felsic tuffs. The Bazarbai tuffs carry interbeds of tuffaceous sandstones, greywacke sandstones and siliceous mudstones. The late Ordovician – early Silurian age of the Bazarbai Fm. was constrained by conodonts hosted by siliceous tuffs and cherts (Kurkovskaya, 1985; Novikova et al., 1991). The contacts between the Bazarbai Fm. and other formations are mostly tectonic (Fig. 4).

The Bazarbai and Tekturmas zones are bounded by the Nura and Uspenka zones from north and south, respectively (Figs. 3, 4). The Nura Zone is dominated by thick Silurian siliciclastic rocks (Orlov and Bespalov, 1981; Nikitin, 1991); the main formations are Yermek and Isen' (Fig. 5). The Yermek Fm. ($S_1$er) includes siltstones, sandstones, gravelstones (Fig. 5). The calcareous siltstones in the middle part of the formation carry early Silurian (Llandoverian) brachiopods and graptolites. The Isen' Fm. ($S_{2-3}$is) conformably overlaps the Yermek Fm. and consists of siltstones and sandstones with lenses of organogenic limestone hosting late Silurian brachiopods (Chetverikova et al., 1996). The greywacke sandstones of the Nura Zone yielded the maximum deposition age of 437 ± 3 Ma (Perfilova et al., 2022a). The Middle Paleozoic siliciclastic units of the Nura Zone stratigraphically overlay the older complexes of the Bazarbai Zone (Degtyarev, 1999; Khassen et al., 2020; Degtyarev et al., 2022).

The Uspenka Zone is located south of the Tekturmas Zone and is dominated by siliciclastic strata (flysch?) and olistostrome. It is characterized by a thrust-and-fold structure and, as a result, complex tectonic relationships with the early Paleozoic formations (Figs. 3, 4, 5). The olistostrome carries olistoliths or up to several kilometers long tectonic slivers of red cherts containing middle-late Ordovician conodonts (Gerasimova et al., 1992). These strata are thrust over the siliceous-tuffogenic rocks sitting on the top of the Middle-Late Ordovician magmatic complexes and sedimentary units of the Tekturmas Zone (Degtyarev et al., 2022). The main formations are Airtau and an early Silurian olistostrome (Fig. 5). The Airtau Fm. ($O_{2-3}$air) includes siliceous mudstones and siltstones, gravelstones and deep-marine cherts with thin interbeds of tuffs. No microfauna age constrains are available. The early Silurian olistostrome consists of greywacke sandstones with MDA 439 ± 3 Ma (Perfilova et al., 2022a) with interbeds and lenses of siliceous sediments, gravelstones and conglomerates. Cherty olistoliths contain

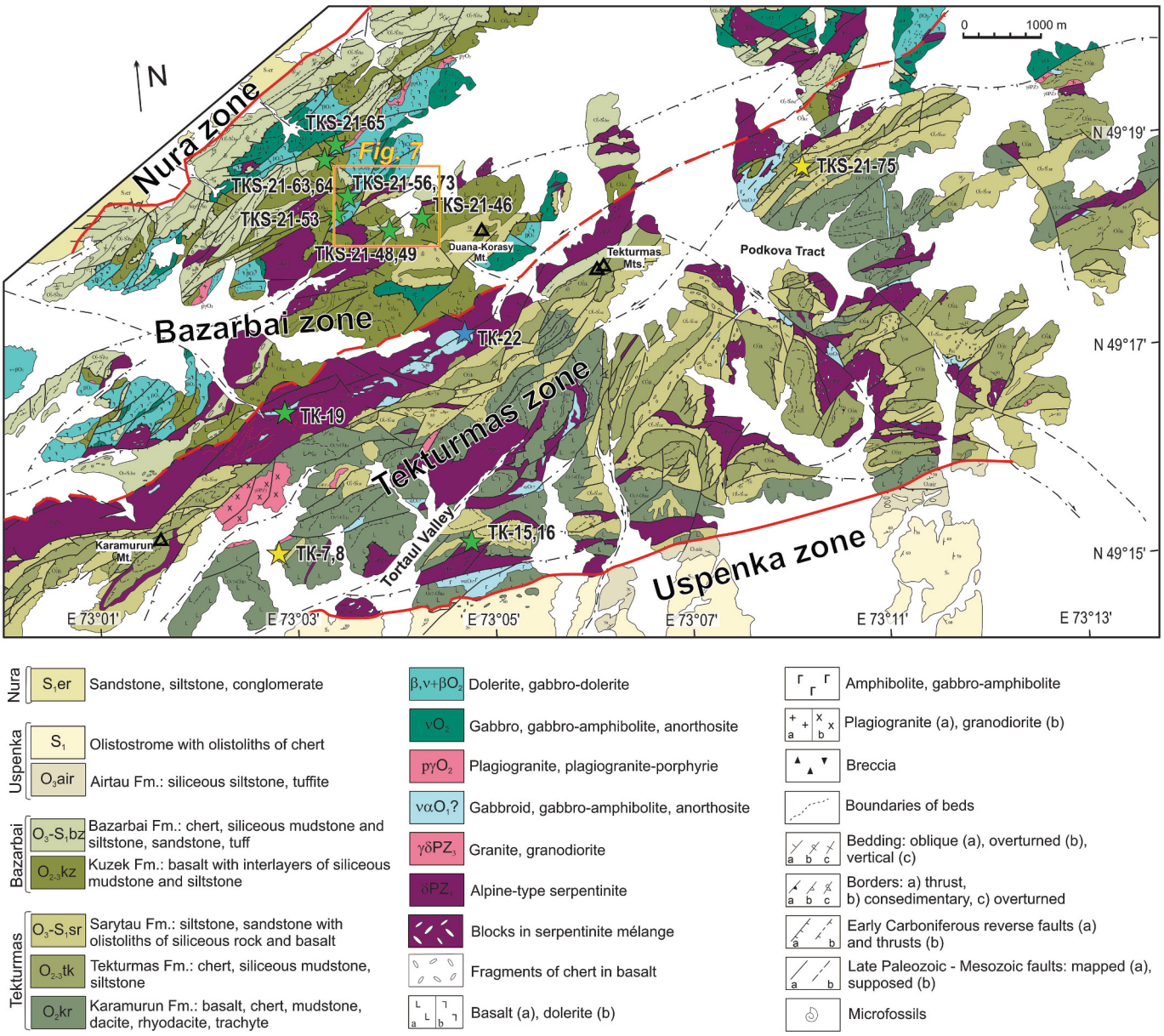


**Fig. 4.** Geological map of the central part of the Tekturmas Fold-and-Thrust Belt covering the Tekturmas Mts. and adjacent areas (modified from Yakubchuk, 1991). Stars and varieties: yellow – high-Ti andesites, blue – mid-Ti gabbro, green – low-Ti rocks. (For interpretation of the references to colour in this figure legend, the reader is referred to the web version of this article.)

early Silurian conodonts (Degtyarev et al., 2022).

### 2.3. Study area and sampling

The overall structure of the TFTB represents a pile of tectonic sheets thrust over each other (Fig. 6B) (e.g., Yakubchuk, 1991; Degtyarev et al., 2017, 2022, 2023; Gurova et al., 2022). Such a complicated structure is typical of most fossil accretionary complexes/orogens (Isozaki et al., 1990; Kojima et al., 2000; Wakita, 2012; Safonova et al., 2016, 2020). The magmatic rocks are affiliated either with the formations or with the ophiolites, were highly likely juxtaposed tectonically.

We studied outcrops and took samples of magmatic rocks in the Tekturmas and Sarytau Mts. of the Tekturmas Zone and north-west of the Duana-Korasy site of the Bazarbai Zone (Figs. 4, 6, 7). The scenario of the sampling covered the whole TFTB, however, we had to exclude the samples, which macroscopically and microscopically look altered by secondary processes (epidotization, chloritization) and tectonically deformed. At all sites, we sampled volcanic rocks of the Karamurun and Tekturmas formations and volcanic to plutonic mostly mafic (but not only) πrocks of the Tortaul and Bazarbai ophiolites after (Degtyarev et al., 2022) and mafic rocks of the Sarytau ophiolites (Table 2; Figs. 4, 6). The collection and the dataset of mafic rocks of the Tortaul and Bazarbai ophiolites is larger than that of (Degtyarev et al., 2022). For the first time, we recognized the Sarytau ophiolite in the Sarytau Mts. (Sarytau Segment; Fig. 8A), however, it may appear a continuation of the Tortaul ophiolites (Table 2; Figs. 4, 6A). The Sarytau Segment includes outcrops of ophiolites (plagiogranite, granite, gabbro-dolerite), volcanic and sedimentary rocks of the Karamurun, Tekturmas, Sarytau and Airtau formations and Silurian olistostrome (Figs. 5, 6). For the paper we selected samples of Sarytau ophiolites (Fig. 8B, C), volcanic rocks of the Karamurun and Tekturmas formations (Fig. 8D, E), subvolcanic to plutonic rocks of the Bazarbai ophiolites (Fig. 8F) and volcanic rocks of the Kuzek Fm. (Fig. 8G-I) (Table 2; Figs. 4, 6, 7).

The Sarytau ophiolites are represented by plagiogranite as a small

**Table 1**
A summary of biostratigraphic and U-Pb zircon age data from sedimentary, magmatic and metamorphic rocks of the TFTB.

| Locality | Rock type | Age | Reference |
|---|---|---|---|
| *Karamurun Fm.* | | | |
| 5.5 km east of Mt. Karamurun | Chert lens in basalt | middle Darriwilian<br>Conodonts: *Periodon aculeatus* Hadding | Degtyarev et al., 2022 |
| 7 km east of Mt. Karamurun | Chert lens in basalt | middle Darriwilian<br>Conodonts: *Periodon aculeatus* Hadding | Degtyarev et al., 2022 |
| Tortaul Valley | Chert | late Darriwilian<br>Conodonts: *Periodon aculeatus* Hadding, *Protopanderodus* cf. *parvibasis* Lofgren, *Histiodella holodentata* Ethington et Clark | Novikova et al., 1991; Gerasimova et al., 1992 |
| *Tekturmas Fm.* | | | |
| Mt. Tekturmas | Yellow chert | late Darriwilian – early Sandbian<br>Conodonts: *Periodon aculeatus* Hadding, *Pygodus anserinus* Lamont et Lindström, *Protopanderodus* sp., *Drepanodus arcuatus* Pander; Pygodus anserinus conodont zone | Degtyarev et al., 2022 |
| Mt. Tekturmas | Yellow chert | late Sandbian<br>Conodonts: *Periodon grandis* Ethington | Degtyarev et al., 2022 |
| 3.7 km SW of Mt. Karamurun | Red chert | middle Darriwilian - early Sandbian<br>Conodonts: *Periodon grandis* Ethington, *Periodon aculeatus* Hadding | Degtyarev et al., 2022 |
| Unknown | Chert | late Darriwilian<br>Conodonts: *Pygodus serra* Hadding, *Pygodus anserinus* Lamont et Lindström | Gerasimova et al., 1992; Nikitin, 2002; Baraboshkin and Chitalin, 1989 |
| Unknown | Chert | late Darriwilian – early Sandbian<br>Conodonts: *Drepanodus suberectus* Branson et Mehl *s.f.*, *Paroistodus* cf. *originalis* Sergeeva, *Periodon aculeatus* Hadding, *Drepanodus arcuatus* Pander, *Pygodus anserinus* Lamont et Lindström | Novikova et al., 1991 |
| *Kuzek Fm.* | | | |
| Northern Mt. Duana-Korasy | Chert | late Darriwilian – early Sandbian<br>Conodonts: *Periodon aculeatus* Hadding, *Pygodus serra* Hadding, *Pygodus anserinus* Lamont et Lindström | Novikova et al., 1991 |
| 3.2 km NW of Mt. Duana-Korasy | Siliceous siltstone | late Darriwilian-early Sandbian<br>Conodonts: *Pygodus anserinus* Lamont et Lindström, *Periodon aculeatus* Hadding, *Cornuodus longibasis* Lindström, *Protopanderodus* sp., *Drepanodus* sp.; Pygodus anserinus conodont zone | Novikova et al., 1991; Degtyarev et al., 2017 |
| *Bazarbai Fm.* | | | |
| 1.3 km SW of Mt. Duana-Korasy | Red chert | upper Sandbian<br>Conodonts: *Periodon grandis* Ethington | Degtyarev et al., 2022 |
| Unknown | Red chert | upper Sandbian<br>Conodonts: *Periodon grandis* Ethington, *Panderodus mutatus* Branson et Mehl, *Scabbardella* cf. *altipes* Heningsmoen | Magmatic complexes…, 1988 |
| 7 km NE of Mt. Karamurun | Plagiogranite | 473 ± 2 Ma | Degtyarev et al., 2022 |
| 2.5 km NW of Mt. Duana-Korasy | Plagiogranite | 453 ± 4 Ma | Degtyarev et al., 2022 |
| 2.4 km NW of Mt. Duana-Korasy | Rhyolite | 449 ± 3 Ma | This study |
| 2.4 km NW of Mt. Duana-Korasy | Granite | 462 ± 3 Ma | This study |
| *Sarytau Fm.* | | | |
| 3.2 km NW of Mt. Duana-Korasy | Siliceous siltstone | Silurian (?)<br>Conodonts: *Drepanoistodus* sp., *Decoriconus* sp. | Degtyarev et al., 2022 |
| 2.6 km NW of Mt. Duana-Korasy | Siliceous siltstone | Silurian (?)<br>Conodonts: *Drepanoistodus* sp., *Decoriconus* sp. | Degtyarev et al., 2022 |
| Mt. Duana-Korasy | Chert | upper Ordovician (Sandbian-Katian stage) – lower Silurian<br>Conodonts: *Periodon grandis* Ethington, *Drepanodus suberectus* Branson et Mehl, *Scabbardella altipes* Henningsmoen<br>Graptolites: *Coronograptus gregarious* Lapworth, *Monograptus convolutes* Hisinger | Gerasimova et al., 1992 |
| *Metamorphic complex* | | | |
| 6.2 km NE of Mt. Karamurun | Cpx granulite | 454–478, 830, 1880, 2530 Ma (main peaks) | Degtyarev et al., 2022 |
| | Ga-bearing gneiss | 461–507, 914–112 Ma (main peaks) | Degtyarev et al., 2022 |
| *Yermek Fm.* | | | |
| 7 km NW of Krasnaya Polyana | Sandstone | 450, 510 Ma (main peaks); MDA* = 439 ± 3 Ma | Perfilova et al., 2022a |
| *Uspenka olistostrome* | | | |
| 7 km east of Krasnaya Polyana | Sandstone | 453 Ma (main peak); MDA = 437 ± 3 Ma | Perfilova et al., 2022a |

* MDA - maximum depositional age as inferred from the U-Pb ages of detrital zircons from greywacke sandstones. Cpx, clinopyroxene; Ga, garnet.

body (Fig. 8B) and dolerite dike (Fig. 8C). The Karamurun basalts occur as flows and pillow-lavas in hot or cold contacts with chert and siliceous mudstone (Fig. 8D, E). There are also clastic lavas with lenses of deep-marine sediments. The thickness of the lava flows reaches 20–50 m. The association of basalts with ribbon chert and siliceous mudstone suggests that all these lithologies are parts of OPS (Isozaki et al., 1990; Safonova et al., 2016). A section made across the central part of the ridge show the complicated structure of the south-western part of the Tekturmas Zone (Fig. 6A). In more details, we studied variable lithologies outcropping in the northwestern part of the Sarytau Segment, where Karamurun OPS pillow-lavas in contact with pelagic chert and siliceous mudstone (Fig. 8D) are tectonically juxtaposed with the gabbros (Fig. 6B).

In the central part of the Tekturmas Zone, we studied several outcrops of gabbro, basalt and andesite along the Tortaul Valley in its axial part (Fig. 4; Table 2). The 0.5 to 2 m packages of red, pink and chocolate ribbon cherts of the Tekturmas Fm. are folded, boudinaged and carry signature of gravitation slumping down. The cherts are intercalated with

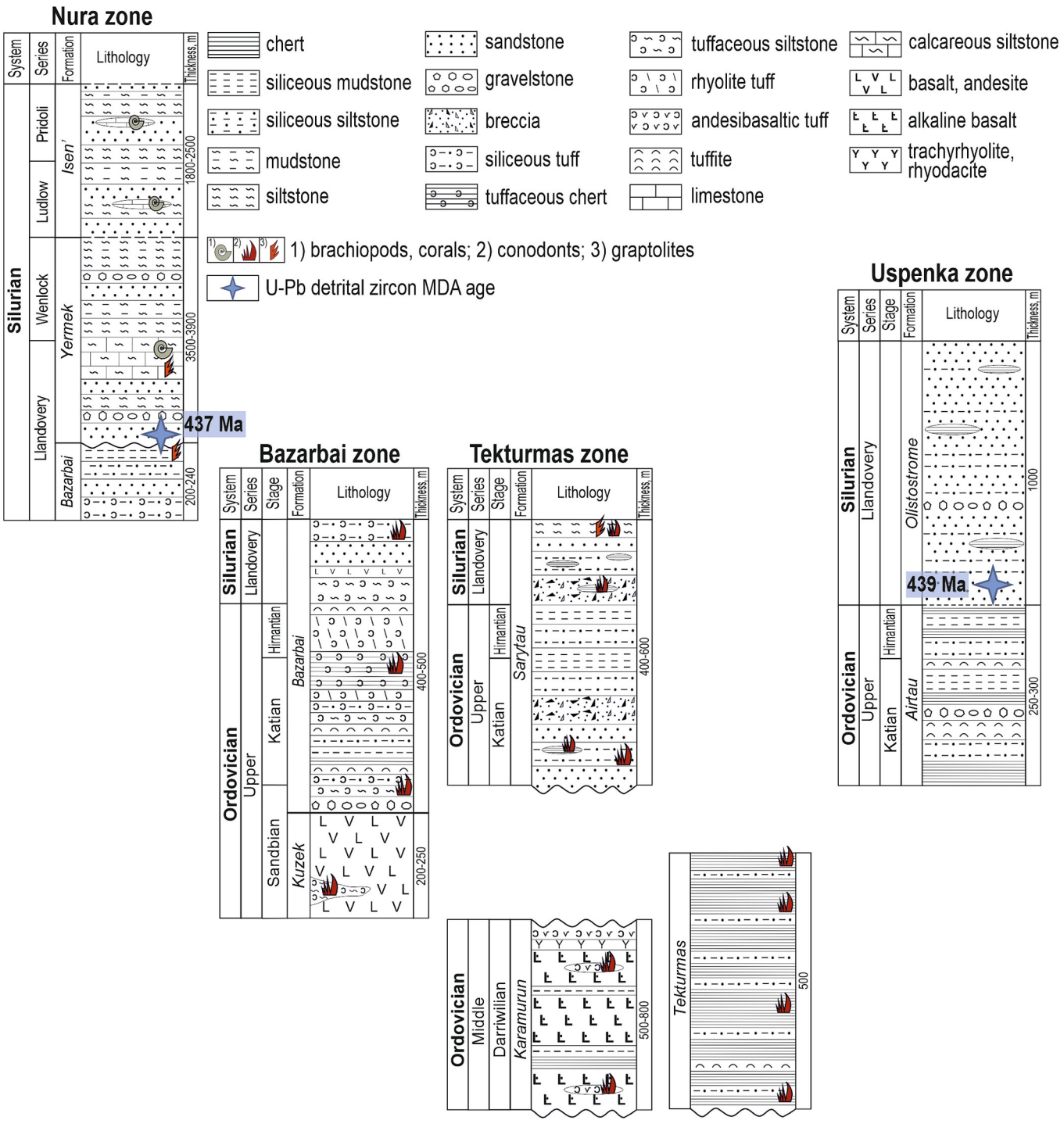


**Fig. 5.** Stratigraphic columns of the Tekturmas Fold-and-Thrust Belt showing levels of microfauna and detrital zircon age data (Zholtaev et al., 2021; Degtyarev et al., 2022; Perfilova, 2023).

siliceous mudstone, tuff and breccia and may occur in contact with magmatic rocks (basalt) and as olistoliths in the Sarytau olistostrome cropping out south of the Tekturmas Zone. No clear relationships between the sedimentary rocks of the Tekturmas Fm. and other formations have been found in the study area.

In the Bazarbai Zone we sampled various magmatic rocks of the Bazarbai ophiolite: gabbro, dolerite, basalt, andesibasalt, andesite, dacite, rhyolite and granite (Fig. 4; Table 2). The outcrops of gabbro (Fig. 8F) are surrounded by deep-marine sediment but the contact is hidden. Although previously all those rocks have been considered as members of the ophiolite association (Degtyarev et al., 2022), we refer the pillowed basalts (Fig. 8G) in contact with chert and siliceous mudstone as parts of OPS and accordingly attribute them to the Kuzek Fm. (Fig. 5). In general, the magmatic rocks of the Bazarbai Zone are dominated by mafic to andesitic volcanic rocks and mafic plutonic rocks, but there are also small outcrops of felsic rocks (Table 2). Up the section, above the volcanics, there are interbedded sedimentary and volcanogenic-sedimentary rocks of the Bazarbai Fm.: basalt, red ribbon chert, chocolate siliceous mudstone, greenish-gray siliceous siltstone, tuff and tuffaceous and volcanomictic sandstones (Figs. 4, 5, 8H, I). The Bazarbai Fm. overlies the serpentinite mélange and is overlain by the Silurian flysch with angular and/or tectonic unconformities (Antonyuk,

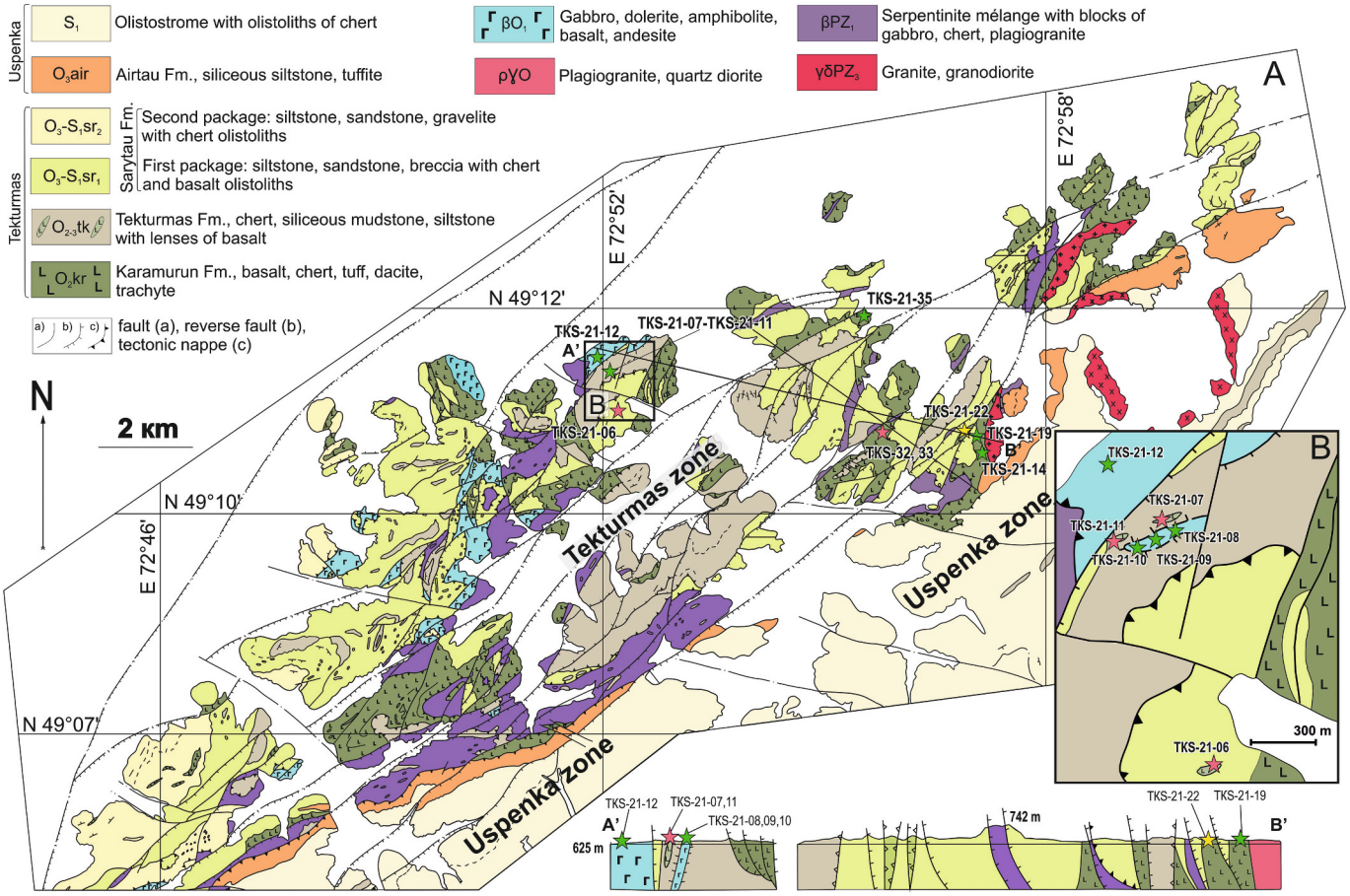


**Fig. 6.** A, geological map of the Sarytau Mts. showing the extension of the Uspenka and Tekturmas zones to the southwest (modified from Novikova et al., 1988); B, geological scheme of a site with magmatic rocks of different origins juxtaposed. Q – Quaternary. Stars and varieties: pink - high-Ti basalts, yellow - high-Ti andesites, green - low-Ti rocks.

1974; Yakubchuk, 1991). In Duana-Korasy Site, we sampled andesibasalts of the Kuzek Fm., dolerite of the Bazarbai ophiolite and gabbro occurring as a block in serpentinite mélange (Fig. 7).

Thus, the TFTB, in general, consists of formations of three dominant lithological types: basaltic (Karamurun, Tekturmas and Kuzek), siliceous (Tekturmas and Bazarbai) and clastic (Sarytau, Airtau, Yermek and Isen') and several ophiolitic complexes (Sarytau, Tortaul, Bazarbai). In this paper, we consider three main associations of magmatic rocks. Mafic volcanic rocks of Ocean Plate Stratigraphy are associated with deep-marine sedimentary rocks (chert, siliceous mudstone and siltstone), and, to a lesser degree, turbidites of the Karamurun, Tekturmas and Bazarbai formations. The central parts of thick lava flows or large "pillows" are often composed of microgabbro and dolerite. Ophiolitic complexes consist of pyroxenites, gabbros, dolerites, and plagiogranites exposed in the Sarytau Segment, Tortaul Mts. and Bazarbai Zone (Figs. 4, 6). Gabbros often form separate bodies (Fig. 8A, F). Serpentinite mélange hosts blocks of gabbro, plagiogranite and granodiorite (Figs. 4, 6, 7). The collection of samples selected for this study includes OPS magmatic rocks (mostly mafic volcanics) and ophiolites (mostly gabbroids, but also several samples of volcanic rocks and granitoids) (Table 2).

## 3. Petrography

The magmatic rocks of the TFTB are variable, volcanic and plutonic, mafic to felsic. The most abundant varieties are basalt and andesibasalt, often as pillow-lavas and at contact with deep-marine sediments (Fig. 8D, E, G-I), gabbro and dolerite (Fig. 8A, C, F). The volcanic rocks typically have massive and/or amygdaloidal textures and aphyric and porphyric microstructures (Fig. 9A-E). The porphyric varieties (Fig. 9A-C) carry phenocrysts of plagioclase (up to 2.5 mm long; 5–25 vol%), clinopyroxene (up to 2.5 mm size) and olivine typically replaced by chlorite. The 0.1–0.3 mm opaque minerals, commonly Fe-oxides (Ti-magnetite?), in places changed to hydroxides, form euhedral and subhedral grains. The microstructure of the mesostasis is interstitial or poikiloophitic and consists of volcanic glass and microliths of plagioclase, pyroxene and opaque minerals. The aphyric varieties consist of small plagioclase laths and volcanic glass (Fig. 9D). Some aphyric volcanic rocks carry amygdules that may occupy up to 25 % of rock volume and are 1 to 5 mm in diameter; they are typically filled by calcite, quartz, and chlorite. In a part of basaltic samples, clinopyroxene grains show parallel cleavage and pleochroism from light pink to colorless that is indicative of Ti-rich augite typical of alkaline basalts (Ichiyama et al., 2014; Safonova et al., 2016).

The more felsic varieties of TFTB volcanic rocks are andesite, dacite and rhyolite (Fig. 9D, E). The andesites have porphyric, seldom aphyric microstructures and massive texture. The phenocrysts (5–10 % of the bulk rock) are plagioclase. The mesostasis has pilotaxitic or hyalopilitic microstructure and consists of small plagioclase laths and chloritized volcanic glass. Dacite has massive texture and porphyric structure with phenocrysts of plagioclase; the mesostasis consist of plagioclase laths, quartz, altered volcanic glass and accessory opaque minerals. Rhyolite is a relatively rare type of volcanic rocks. The rhyolite sampled in the Bazarbai Zone for the U-Pb zircon dating (TKS-21-63) has porphyric microstructure and massive texture (Fig. 9E). The phenocrysts are plagioclase, often forming agglomerations, and quartz; the mesostasis is

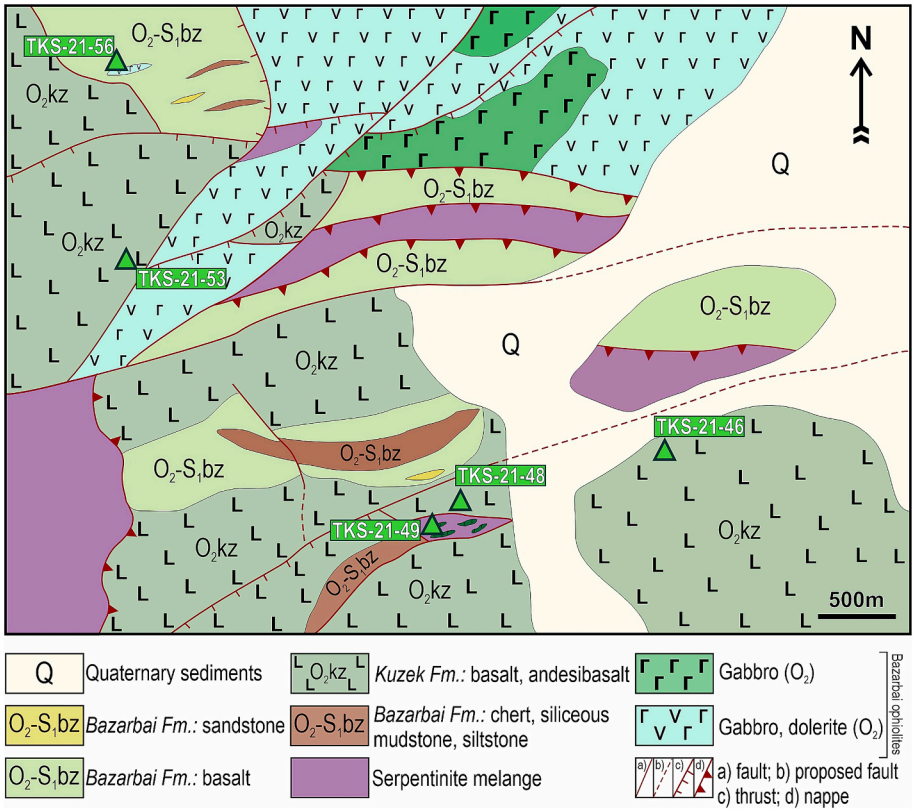


**Fig. 7.** A detailed geological map of a sampling plot in the Duana-Korasy site showing relationships between magmatic and sedimentary rocks of the Kuzek and Bazarbai fms. and Bazarbai ophiolites. Green triangles are for the sampling points (see also Table 2). (For interpretation of the references to colour in this figure legend, the reader is referred to the web version of this article.)

**Table 2**
Description of magmatic rocks of the Tekturmas Fold-and-Thrust Belt.

| | Sample no. | Rock type | Zone/segment | Complex | Site | Lat.; N | Long.; E |
|---|---|---|---|---|---|---|---|
| 1 | **TKS-21-06** | Basalt | Sarytau | Karamurun Fm. | N. Sarytau | 49°11′35.5″ | 72°52′10.2″ |
| 2 | **TKS-21-07** | Basalt | Sarytau | Karamurun Fm. | N. Sarytau | 49°12′11.3″ | 72°52′03.0″ |
| 3 | **TKS-21-08** | Gabbro | Sarytau | Sarytau ophiolite | N. Sarytau | 49°12′09.7″ | 72°52′02.5″ |
| 4 | **TKS-21-10** | Gabbro | Sarytau | Sarytau ophiolite | N. Sarytau | 49°12′08.1″ | 72°51′58.1″ |
| 5 | **TKS-21-12** | Gabbro | Sarytau | Sarytau ophiolite | N. Sarytau | 49°12′20.4″ | 72°51′50.5″ |
| 6 | **TKS-21-19** | Andesibasalt | Sarytau | Karamurun Fm. | SE Sarytau | 49°11′24.5″ | 72°57′00.6″ |
| 7 | **TKS-21-22** | Phonolite | Sarytau | Karamurun Fm. | SE Sarytau | 49°11′24.1″ | 72°56′52.5″ |
| 8 | **TKS-21-32** | Basalt | Sarytau | Karamurun Fm. | SE Sarytau | 49°11′31.8″ | 72°55′04.0″ |
| 9 | **TKS-21-33** | Basalt | Sarytau | Karamurun Fm. | SE Sarytau | 49°11′27.3″ | 72°55′37.2″ |
| 10 | **TKS-21-35** | Andesibasalt | Sarytau | Karamurun Fm. | N. Sarytau | 49°11′31.7″ | 72°55′52.9″ |
| 11 | **TK-7** | Trachyandesite | Tekturmas | Karamurun Fm. | Tortaul Valley | 49°15′03.5″ | 73°03′05.9″ |
| 12 | **TK-8** | Andesite | Tekturmas | Karamurun Fm. | Tortaul Valley | 49°15′03.5″ | 73°03′05.9″ |
| 13 | **TK-15** | Basalt | Tekturmas | Karamurun Fm. | Tortaul Valley | 49°15′11.3″ | 73°05′49.4″ |
| 14 | **TK-16** | Gabbro | Tekturmas | Tortaul ophiolite | Tortaul Valley | 49°15′11.3″ | 73°05′49.4″ |
| 15 | **TK-19** | Gabbro | Tekturmas | Tortaul ophiolite | Tortaul Valley | 49°16′24.0″ | 73°03′16.9″ |
| 16 | **TKS-21-41** | Gabbro | Tekturmas | Tortaul ophiolite | Krasnaya Polyana | 49°13′16.7″ | 73° 4′28.1″ |
| 17 | **TKS-21-42** | Andesibasalt | Tekturmas | Tortaul ophiolite | Krasnaya Polyana | 49°13′15.8″ | 73°04′27.3″ |
| 18 | **TKS-21-75** | Trachyandesite | Tekturmas | Tekturmas Fm. | Podkova Tract | 49°18′46.3″ | 73°10′33.9″ |
| 19 | **TK-22** | Gabbro | Bazarbai | Bazarbai ophiolite | Duana-Korasy Mt. | 49°17′25.2″ | 73°05′48.0″ |
| 20 | **TKS-21-01** | Dolerite | Bazarbai | Bazarbai ophiolite | Krasnaya Polyana | 49°15′36.3″ | 72°57′08.7″ |
| 21 | **TKS-21-04** | Basalt | Bazarbai | Kuzek Fm. | Krasnaya Polyana | 49°15′35.4″ | 72°57′02.5″ |
| 22 | **TKS-21-46** | Andesibasalt | Bazarbai | Kuzek Fm. | Duana-Korasy Mt. | 49°18′26.7″ | 73°05′16.4″ |
| 23 | **TKS-21-48** | Andesibasalt | Bazarbai | Kuzek Fm. | Duana-Korasy Mt. | 49°18′18.5″ | 73°04′46.8″ |
| 24 | **TKS-21-49** | Gabbro | Bazarbai | Bazarbai ophiolite | Duana-Korasy Mt. | 49°18′19.3″ | 73°04′45.5″ |
| 25 | **TKS-21-53** | Andesibasalt | Bazarbai | Kuzek Fm. | Duana-Korasy Mt. | 49°18′33.1″ | 73°04′16.5″ |
| 26 | **TKS-21-56** | Dolerite | Bazarbai | Bazarbai ophiolite | Duana-Korasy Mt. | 49°18′44.5″ | 73°04′11.1″ |
| 27 | **TKS-21-63** | Rhyolite | Bazarbai | Kuzek Fm. (?) | Duana-Korasy Mt. | 49°19′01.9″ | 73°04′01.3″ |
| 28 | **TKS-21-64** | Dacite | Bazarbai | Kuzek Fm. (?) | Duana-Korasy Mt. | 49°19′01.9″ | 73°04′01.3″ |
| 29 | **TKS-21-65** | Granite | Bazarbai | Bazarbai ophiolite | Duana-Korasy Mt. | 49°19′04.3″ | 73°04′11.6″ |
| 30 | **TKS-21-73** | Andesibasalt | Bazarbai | Kuzek Fm. | Duana-Korasy Mt. | 49°18′43.8″ | 73°04′05.5″ |

The names of sites are given after (Yakubchuk, 1991; Antonyuk et al., 1995), the names of complexes are given after (Degtyarev et al., 2022); see Figs. 4 and 6 for the geographic outline.

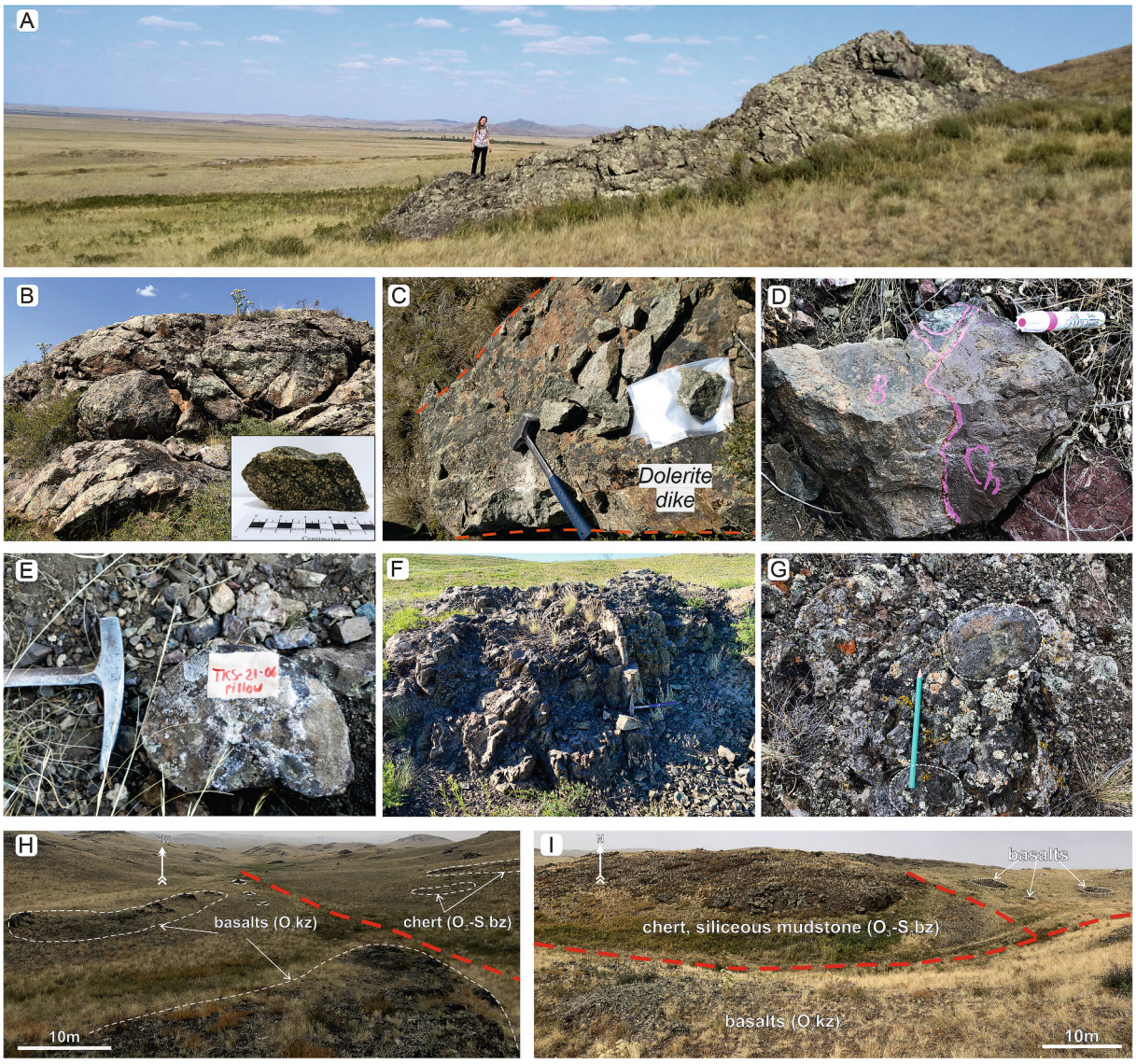


**Fig. 8.** Field photos of outcrops in the TFTB (A-E, Sarytau Segment; F-I, Bazarbai Zone): A, gabbro; B, plagiogranite; C, dolerite dike; D, aphyric pillow-basalt in direct «cold» contact with chert; E, pillow-basalt; F, gabbro; G, altered pillow-basalt; H, contact between basalt of the Kuzek Fm. and siliceous sediments of the Bazarbai Fm.; I, small outcrops of basalt and a contact between basalt and siliceous mudstone.

microfelsitic. There are also felsic tuffs with clasts of plagioclase, quartz, volcanic glass and andesitic to felsic volcanic rocks (Fig. 9F) and one sample of leucitic phonolite with massive texture and porphyric structure consisting of phenocrysts of plagioclase, K-feldspar and possibly leucite and vitreous mesostasis (volcanic glass, small laths of plagioclase and K-feldspar, opaque minerals). The mafic to felsic volcanic rocks belong to the Karamurum, Tekturmas and Kuzek formations (see section 2, Table 2; Figs. 4–7).

The plutonic varieties of magmatic rocks are gabbro or microgabbro (Fig. 8A, C, F), dolerite and granitoids (Fig. 8B). The observed gabbros have massive texture and are dominated by clinopyroxene and plagioclase with subordinate orthopyroxene and olivine (Fig. 9G, H). The dolerites have microdoleritic and microophitic structures, massive texture and consist of clino- and orthopyroxene and plagioclase. The granitoids, plagiogranite and granite, are less abundant and occur as separate small bodies or blocks in serpentinite mélange. The Hbl-granite sampled for the U-Pb dating has hypidiomorphic structure, massive texture and consists of plagioclase (35 vol%), K-feldspar (35 %), hornblende (about 10 %) and quartz (20 %) (Fig. 9I). In this paper we consider the plutonic varieties as parts of the Sarytau, Tortaul and Bazarbai ophiolites as after (Degtyarev et al., 2022) (Figs. 4, 6).

The most of the rocks, in particular mafic to andesitic varieties (Fig. 9A-D), visually and under microscope show alteration of the phenocrysts of olivine, pyroxene and plagioclase and the mesostasis by processes of post-magmatic alteration, probably, ocean-floor hydrothermal metamorphism and accretion-related greenschist metamorphism. The most typical secondary minerals are chlorite, epidote, zoisite, prehnite, actinolite, calcite, leucoxene, opaque minerals, chalcedony plus saussurite aggregates.

## 4. Results

For details on the analytical methods, that were used for the determination of the U-Pb ages of zircons, concentrations of major oxides and trace element, bulk-rock isotopic measurements (Pb-Pb, Sm-Nd) and Hf-in-zircon isotopes see supplementary electronic materials.

### 4.1. U-Pb zircon ages

We separated zircons from two samples, rhyolite (TKS-21-63) and

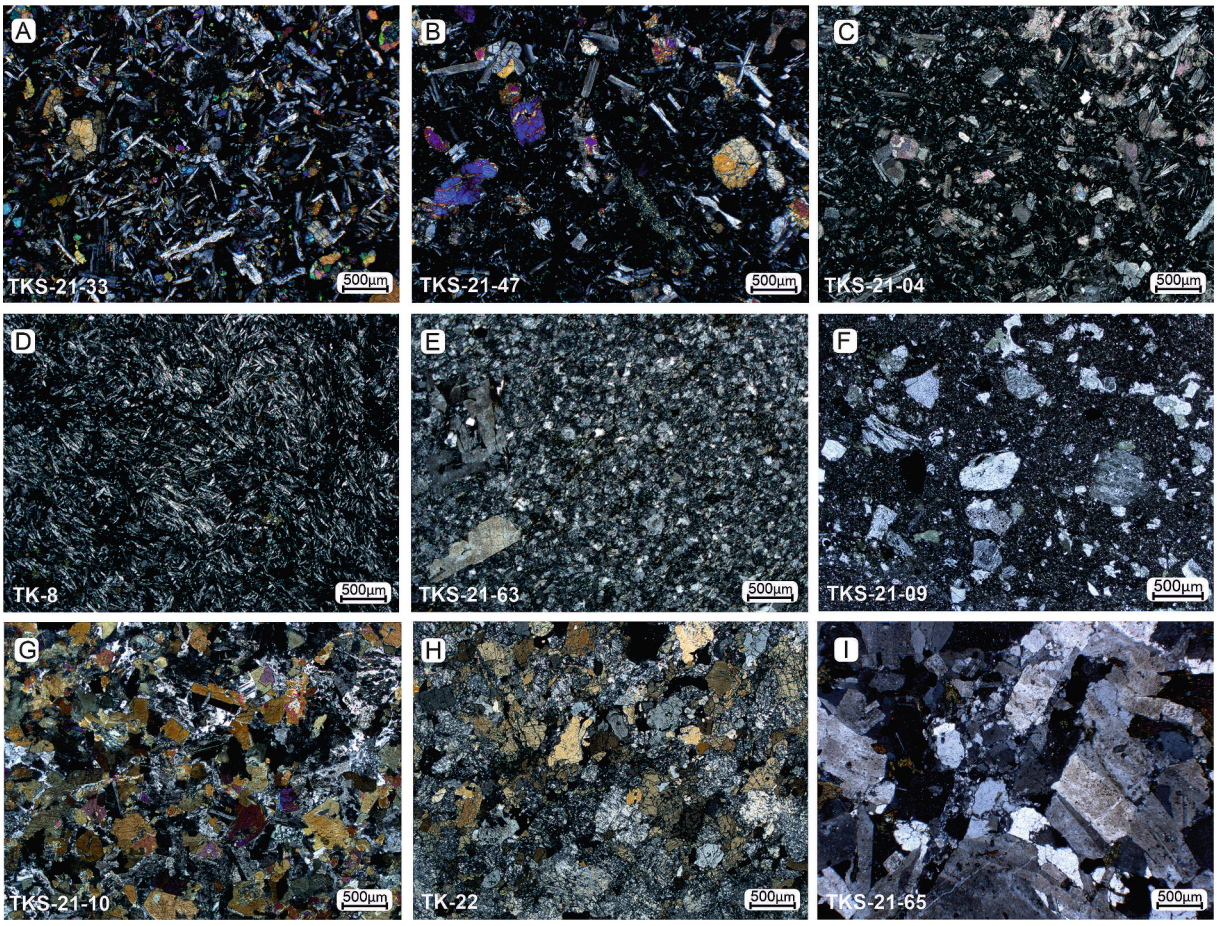


**Fig. 9.** Microphotos of thin-sections of magmatic rocks of the TFTB. A, Px-porphyric basalt; B, Ol-porhyric basalt; C, amygdaloidal andesibasalt; D, trachyandesite; E, rhyolite; F, andesitic tuff; G, gabbro; H, altered gabbro; I, granite. See Table 2 for the description of samples.

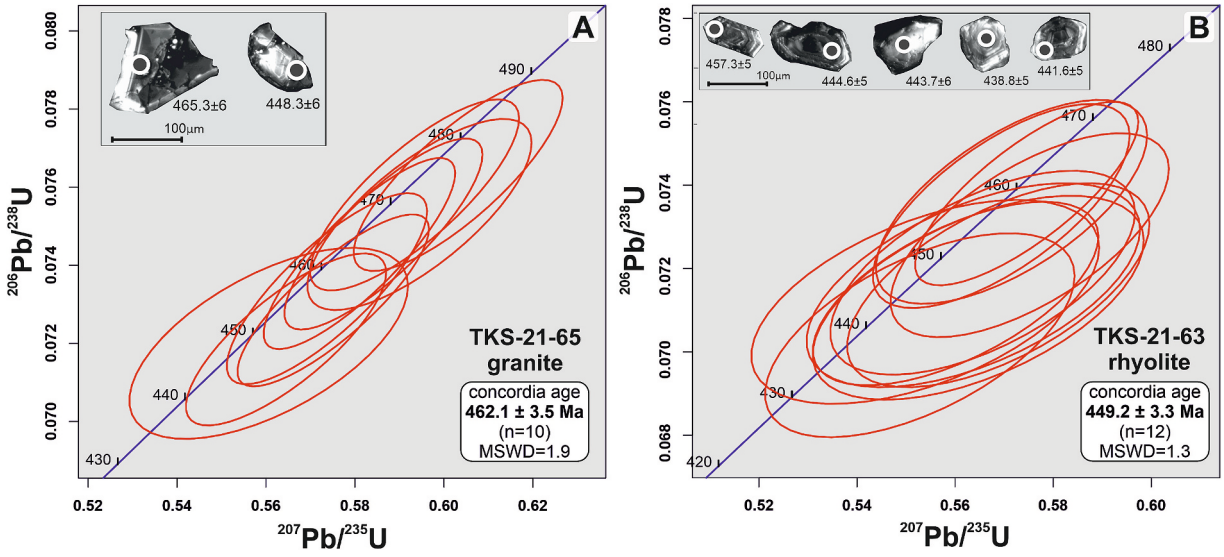


**Fig. 10.** CL photos of zircons and concordia plots of U-Pb isotope ratios of zircons from granite (A) and rhyolite (B) of the Bazarbai Zone of the TFTB.

granite (TKS-21-65), of the central Bazarbai Zone (Fig. 4). The LA-ICP MS zircon U-Pb dating results are listed in the supplementary materials (Supplementary table S1). Fig. 10 shows the CL images of representative zircon grains and the U-Pb isotope concordia diagrams. All zircons are subhedral to euhedral with aspect ratios of 1:2 or 1:3, colorless or slightly yellow and transparent, and show oscillatory or banded zoning. Forteen zircons from granite TKS-21-65 were analyzed, of which 13 appeared 96 to 100 % concordant. They yielded $^{206}Pb/^{238}U$ ages spanning 481.7 ± 6.0 to 442.9 ± 5.6 Ma and a weighted mean age of 458.5 ± 6 Ma (Fig. 10A). Ten zircons from TKS-21-65 yielded best age estimates ranging from 474.1 ± 5.9 to 448.3 ± 5.9 Ma and a weighted mean age of 462.1 ± 3.5 Ma (MSWD = 1.9). Twenty one zircons from

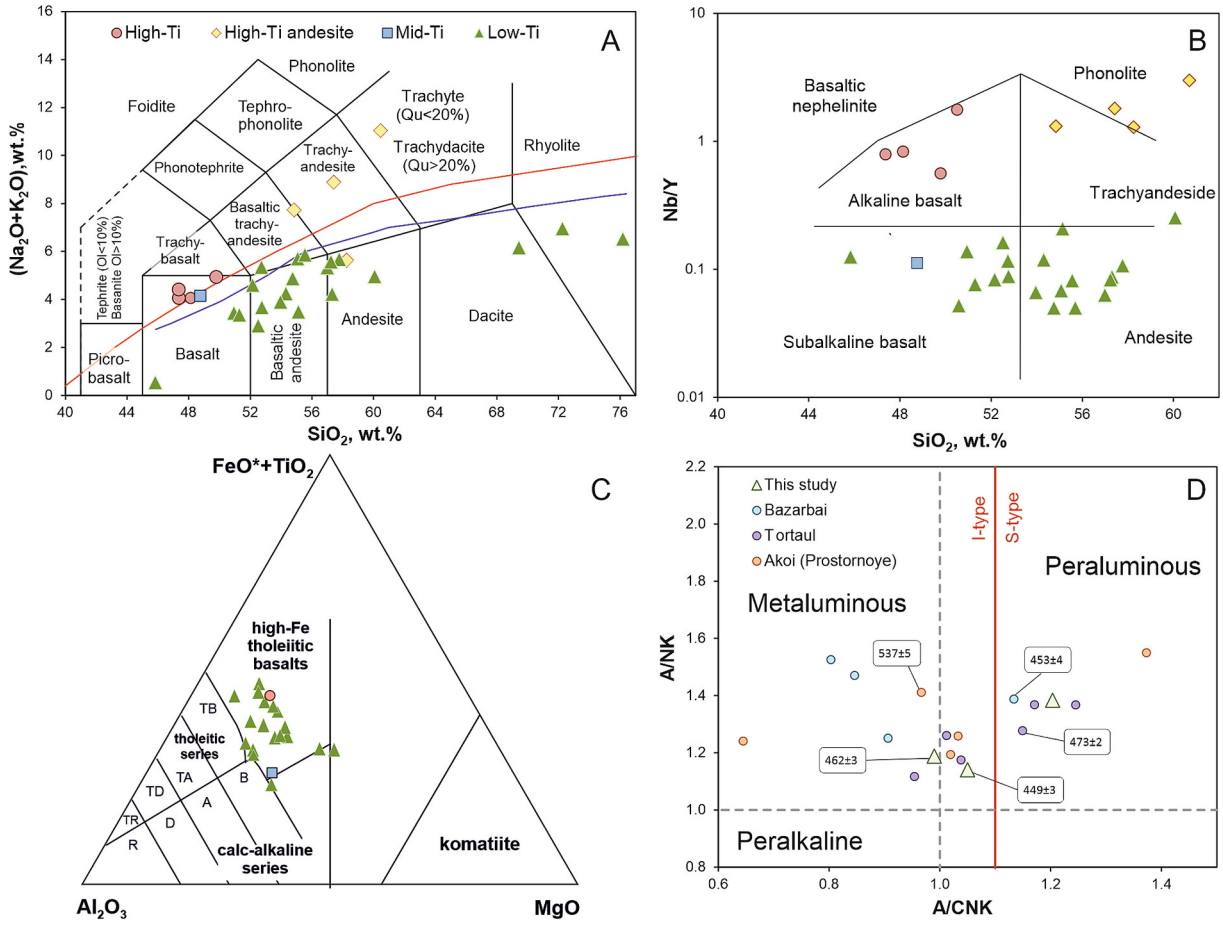


**Fig. 11.** Classification diagrams for igneous rocks of the TFTB, central Kazakhstan. A, $SiO_2$ total alkali (Le Maitre et al., 2002). B, $SiO_2$ – Nb/Y diagram (Winchester and Floyd, 1977). C, $Al_2O_3$ – FeO* + $TiO_2$ – MgO diagram (Jensen, 1976); tholeiitic series: TB – basalt, TA – andesite, TD – dacite, TR – rhyolite; calc-alkaline series: B – basalt, A – andesite, D – dacite, R – rhyolite. D, the A/CNK [molar $Al_2O_3/(CaO + Na_2O + K_2O)$] versus A/NK [molar $Al_2O_3/(Na_2O + K_2O)$] diagram for granitoids, the boundary line is from (Maniar and Piccoli, 1989). Data from Bazarbai and Tortaul granites after (Degtyarev et al., 2022) and Akoi (Prostornoye) granites after (Degtyarev et al., 2023).

rhyolite TKS-21-63 were dated and 18 of those yielded concordances of 97 to 100 %, $^{206}Pb/^{238}U$ ages ranging from 470.8 ± 5.9 to438.8 ± 5.7 Ma, and a weighted mean age of 451 ± 4 Ma (Fig. 10B). Of those twelve grains yielded best age estimates ranging from 459.2 ± 5.6 to 438.8 ± 5.7 and a weighted mean age of 449.2 ± 3.3 Ma (MSWD = 1.3), which we consider as an average age of crystallization. In summary, the U-Pb dating of zircons shows that the dated granite is a bit older (Middle Ordovician, Darriwillian) than the rhyolite (Late Ordovician, Katian).

### 4.2. Major and trace elements

Several recent papers have presented limited major and trace element data from Tekturmas magmatic rocks, mostly from plutonic granitoids (Degtyarev et al., 2022, 2023) and from volcanic rocks, but gave no detailed information about localities, sampling coordinates and/or formations (e.g., Stepanets, 2016; Khassen et al., 2020; Gurova et al., 2022). In this paper, we present full major and trace element data from mafic to felsic magmatic rocks sampled at several localities of the TFTB, including the first data from those of the Sarytau Segment of the Tekturmas Zone, of which each sample has precise coordinates and well-defined geological affinity (Table 2; Fig. 6; Supplementary figure S1 and table S2). The collection of volcanic, subvolcanic and plutonic rocks from all localities includes mostly subalkaline varieties plus several samples of alkaline basalt, trachyandesite and trachydacite. Most of them plot in the fields of basalt and basaltic andesite in the TAS diagram (Fig. 11A). As the volcanic rocks often occur in direct contact with deep-sea sediments (Fig. 8D, H, I), they probably experienced alteration of oceanic water and related migration of LILE and other mobile elements (e.g., Humphris and Thompson, 1978; Thompson, 1991). In the $SiO_2$ - Nb/Y diagram based on relatively immobile elements, the samples plot also in the fields of subalkaline basalt and andesite, alkaline basalt, trachyandesite and phonolite (Fig. 11B). According to different diagrams, the group of subalkaline varieties is either dominated by tholeiites (Fig. 11C). The granitoids are mainly metaluminous (granite and rhyolite); the peraluminous varieties are less abundant (dacite) (Fig. 11D). The analyses showing L.O.I. higher than 5 % were excluded from the dataset (Supplementary table S2).

The mafic to andesitic volcanic and subvolcanic rocks, basalt, andesibasalt, dolerite and gabbro (Fig. 9) ($SiO_2$ = 44.2–57.3 wt%) are characterized by the value of Mg# (atomic ratio of $Mg/(Mg + Fe^{2+})$) ranging from 24 to 71 at MgO = 2.5–13.4 wt% and $Fe_2O_3$ = 8.6–15.7 wt % (Supplementary table S2). The rocks show variable contents of $TiO_2$ (0.5–2.6 wt%), CaO (2.2–15.1 wt%) and $Al_2O_3$ (11.8–18.3 wt%). We preliminary divided the samples into three groups: high-Ti ($TiO_2$ > 2.1 wt%; 4 samples), medium-Ti ($TiO_2$ = 1.1 wt%; 1 sample) and low-Ti ($TiO_2$ = 0.3–0.9 wt%; 15 samples). The high- and medium-Ti samples possess, in average, lower contents of MgO (5.8 wt%) compared to the low-Ti varieties (6.3 wt%). In the MgO vs. major oxides binary diagrams, there are trends suggesting fractionation of olivine and pyroxenes (Fig. 12A, C, D); in other plots we can see no clear trends (Fig. 12B, E, F). The high-Ti varieties are characterized by higher concentrations of incompatible elements, such as rare-earth elements (REE) and Nb

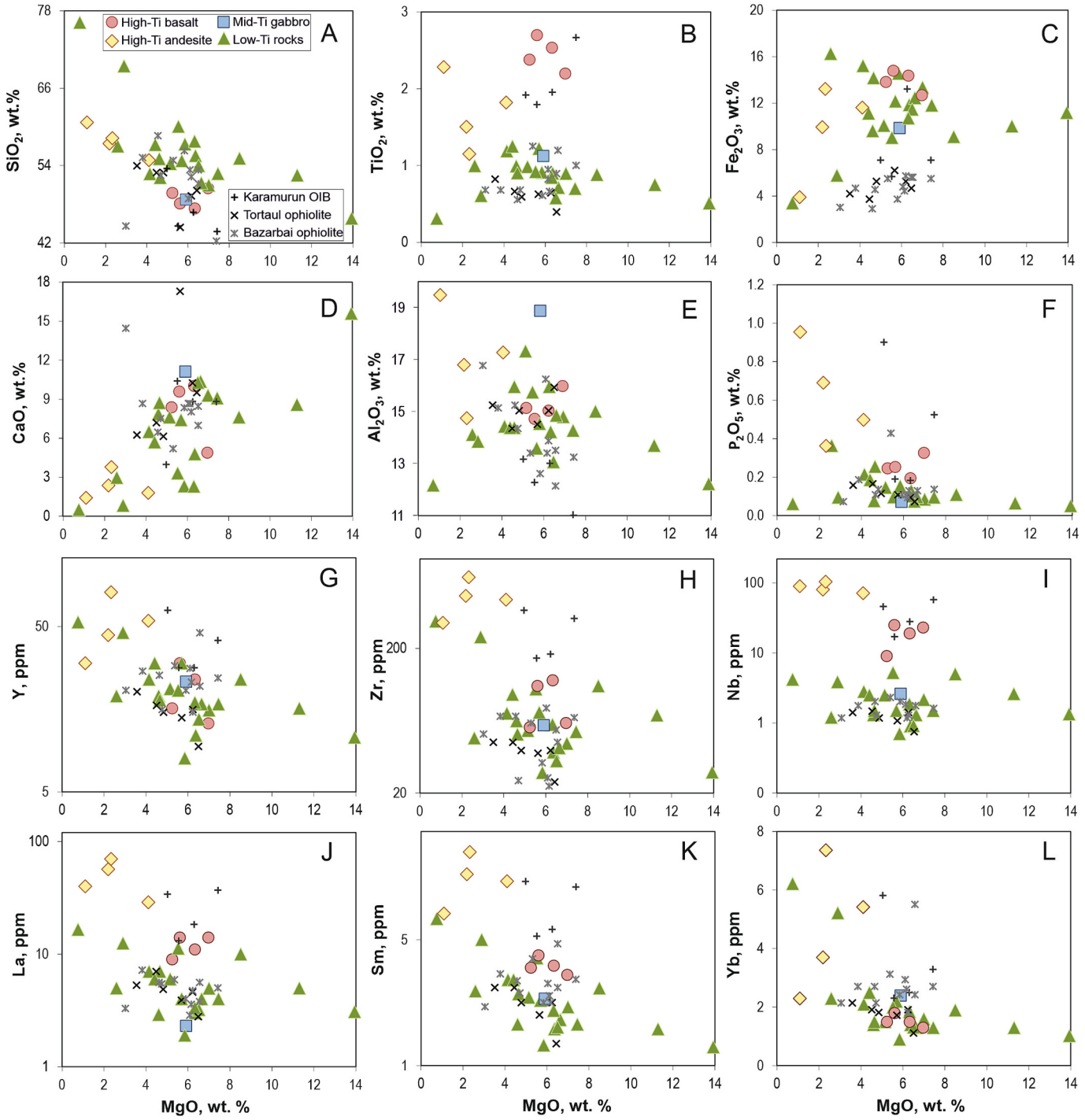


**Fig. 12.** MgO vs. major oxides and trace elements of magmatic rocks of the TFTB, central Kazakhstan. Data from Tortaul and Bazarbai ophiolites and Karamurun OIB after (Degtyarev et al., 2022).

(Fig. 12G-L) and show the lowest values of Zr/Nb (2.7–6.3) compared to the low-Ti samples.

The chondrite-normalized REE spectra of the high-Ti samples (Fig. 13A) are typically enriched in LREE ($La/Yb_n = 4.1–7.3$) and display differentiated heavy REE or HREE ($Gd/Yb_n = 2.2–2.7$). The REE spectrum of the medium-Ti gabbro (Fig. 13C) is slightly depleted in LREE ($La/Yb_n = 0.7$) and show undifferentiated HREE ($Gd/Yb_n = 1.1$). The low-Ti is characterized by flat to LREE-enriched and differentiated HREE ($La/Yb_n = 1.2–3.8$; $Gd/Yb_n = 1.0–1.7$) (Fig. 13D). Most samples show zero to weak Eu anomalies (Fig. 13A-D). The primitive mantle normalized multi-component spectra for the most of the high-Ti basalts are characterized by positive Nb anomalies ($Nb/Th_{pm} = 1.3–2.5$, $Nb/La_{pm} = 1.0–1.7$; Fig. 13E; Supplementary table S2), which are typical of many accreted OIB-type basalts (e.g., Polat et al., 1999; Ichiyama et al., 2008; Safonova and Santosh, 2014; Safonova et al., 2015, 2016). The medium-Ti gabbro displays no notable Nb enrichment relative to La, but strong enrichment in respect to Th ($Nb/La_{pm} = 1.1$, $Nb/Th_{pm} = 2.1$; Fig. 13G), that is more typical of MORB. The multi-element spectra for the low-Ti samples (Fig. 13H) possess clear Nb depletion relative to Th and La ($Nb/La_{pm} = 0.2–0.5$; $Nb/Th_{pm} = 0.2–0.6$).

The high-Ti andesites and dacite ($SiO_2 = 52.8–59.6$; $TiO_2 = 1.1–2.2$ wt%; 4 samples) are characterized by low Mg# (26 to 41) at MgO =

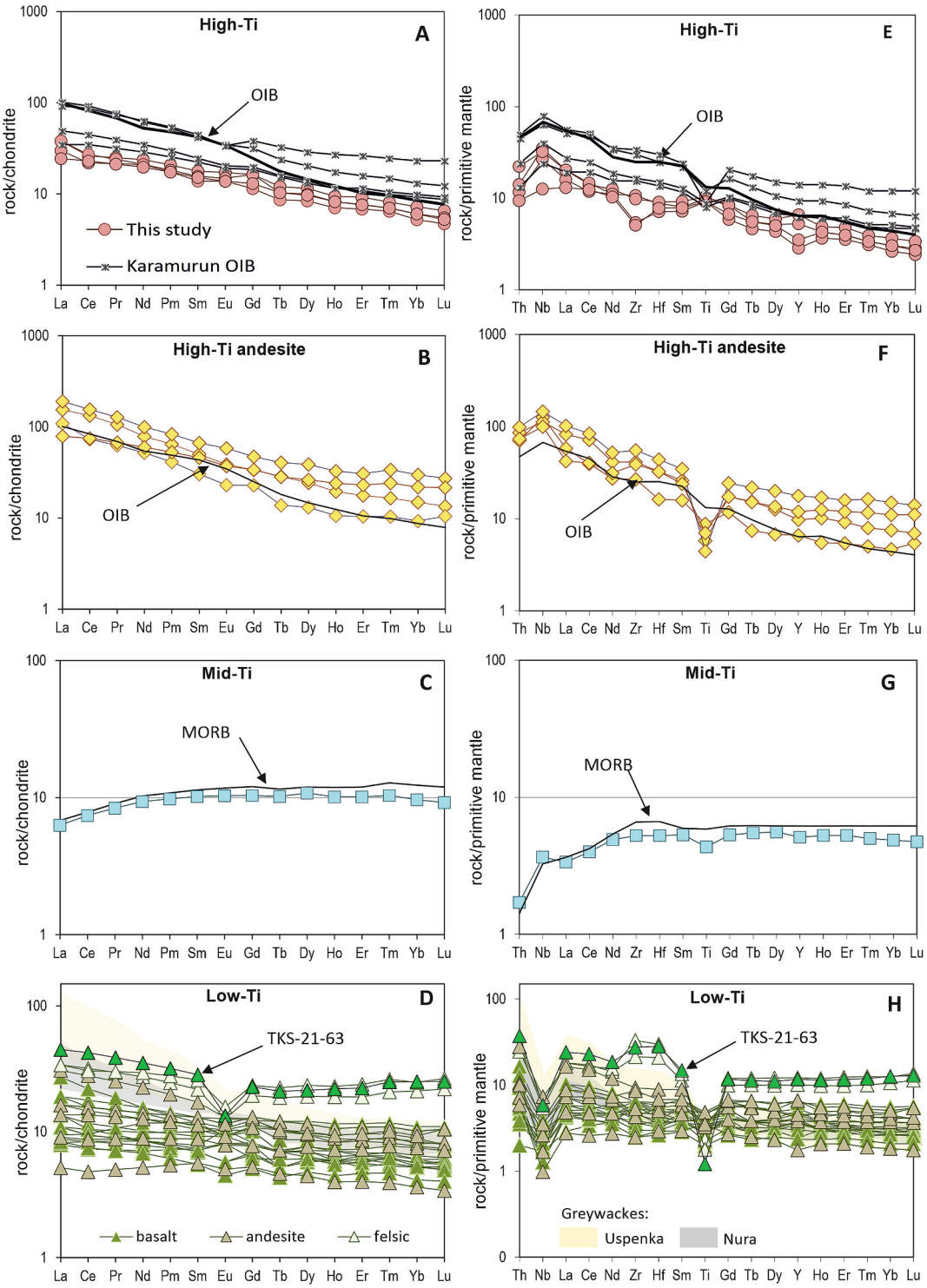


**Fig. 13.** Chondrite-normalized rare-earth element patterns (A–D) and primitive mantle-normalized multi-component trace element patterns (spider diagrams; E–H) for igneous rocks of the TFTB, central Kazakhstan. Normalization values are from Sun and McDonough (1989). Data from Karamurun OIB after (Degtyarev et al., 2022). Data from greywackes of the Nura and Uspenka zones of the TFTB after (Perfilova et al., 2022a).

1.1–4.0 wt% and $Fe_2O_3$ = 3.8–12, low CaO (1.4 to 3.7 wt%) and medium to high $Al_2O_3$ spanning 14.3 to 19.1 wt% (Supplementary table S2). In the classification diagrams they plot in the fields of trachyandesite and trachydacite (Fig. 11A, B). As the "trachyandesite" lacks quartz (see section 3) and is characterized by a very high concentration of $K_2O$, we will refer it to as phonolite (Table 2). In the diagrams of MgO vs. major oxides (Fig. 12A-F), they form trends in respect to MgO and $P_2O_5$ suggesting fractionation of olivine and/or orthopyroxene and apatite during the crystallization and differentiation of a parental magma. In the diagrams of MgO vs. trace elements (Fig. 12G-L), the high-Ti andesites and dacite show increased concentrations of REE such as La, Sm, Nb, and Zr. Their REE spectra are similar in shape to OIB and have close concentrations to those (Fig. 13B); they are enriched in the LREE and differentiated in HREE ($La/Yb_n$ = 3.6–11.8; $Gd/Yb_n$ = 1.5–2.5). The spidergrams (Fig. 13F) are characterized by positive Nb anomalies ($Nb/Th_{pm}$ = 1.3–1.8, $Nb/La_{pm}$ = 1.4–2.4), but also display a negative

anomaly at Ti (Ti/Ti* = 0.2–0.6). Similar to the high-Ti basalts and in contrast to the low-Ti andesitic lavas they have low Zr/Nb ratios (3.3–6.1).

More felsic rocks are low-Ti dacite, rhyolite and granite ($SiO_2$ = 67.5–75.0; $TiO_2$ = 0.3–0.6; 3 samples). They are characterized by Mg# ranging from 24 to 51, MgO = 0.7–2.8, $Fe_2O_3$ = 3.3–5.6, CaO = 0.1–0.8, and $Al_2O_3$ = 12.0–13.5 wt%. The 462 Ma granite is metaluminous and the 449 Ma rhyolite and dacite are peraluminous (Fig. 11D). The granitoids are most REE-enriched relative to the other low-Ti rocks and show no HREE differentiation ($La/Yb_n$ = 1.4–1.8; $Gd/Yb_n$ = 0.91–0.95), and show distinct Eu anomalies in the REE spectra (Eu/Eu* = 0.5–0.6; Fig. 13D). Their multi-component patterns are characterized by negative Nb ($Nb/La_{pm}$ = 0.2–0.3; $Nb/Th_{pm}$ = 0.2–0.3; Fig. 13H) and Ti anomalies (Ti/Ti* = 0.1–0.2).

### 4.3. Isotopes: bulk-rock Sm-Nd, Pb-Pb and Lu-Hf-in-zircon

Bulk-rock Sm-Nd isotopic compositions of magmatic rocks are typically used to estimate the modal age and juvenile or recycled character of their mantle sources. In this work we present the first Nd and Pb bulk-rock and Hf-in-zircon isotope data from the magmatic rocks of the TFTB. To calculate the initial isotope ratios (Supplementary table S3), we used the microfauna and U-Pb zircon ages (Figs. 3, 5, 10; Table 1; Supplementary table S1). The low-Ti samples from Tortaul, Sarytau and Duana-Korasy and other sites (Table 2) have higher $^{143}Nd/^{144}Nd$ (0.512806–0.513015), whereas the high-Ti samples from the Sarytay and Tortaul have lower $^{143}Nd/^{144}Nd$ (0.512485–0.512666). The age versus $\varepsilon Nd_t$ plot (Fig. 14A) shows that all samples are characterized by positive values $\varepsilon Nd_t$. The highest of $\varepsilon Nd_t$ values indicating highly depleted mantle sources have been recorded for the supra-subduction rhyolite (+10.82) and the MORB-type gabbro (+8.05). The other low-Ti volcanics possessing supra-subduction geochemical features show the values of $\varepsilon Nd_t$ spanning +6.02 and +7.85. The high-Ti samples (OIB-type basalt, phonolite and andesite) show the widest range of $\varepsilon Nd_t$ from +2.01 to +6.77, that is typical of OIB-type lavas worldwide (e.g., Zindler and Hart, 1986; Safonova et al., 2011b, 2011c, 2015, 2020). The εNdt-evolution diagram (Fig. 14A) demonstrates that the volcanic rocks are derived from different sources: the growth lines are sub-horizontal for most rocks, except for the high-Ti andesites and rhyolite, as typical of mantle rocks.

Bulk-rock Pb-Pb isotope systematics is a powerful tool in identifying recycled material of the continental crust to the mantle and is often used to discuss the different types of initial mantle sources (DM, HIMU or EM), tectonic settings (island arc, oceanic island, mid-oceanic ridge) and

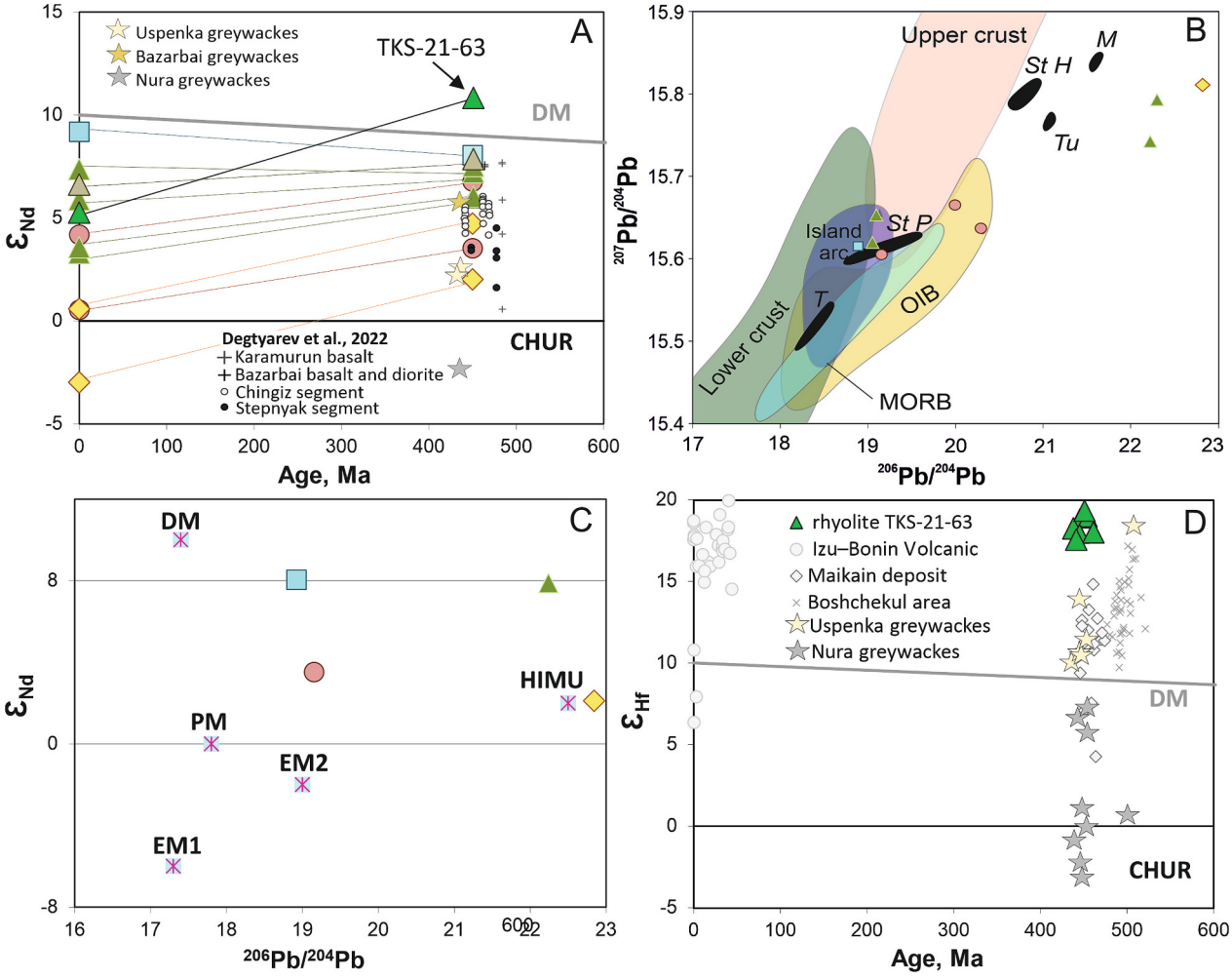


**Fig. 14.** Isotope diagrams for igneous rocks of the TFTB. A, age vs. $\varepsilon Nd_t$ plot. B, measured $^{206}Pb/^{204}Pb$ vs. $^{207}Pb/^{204}Pb$ data of igneous rocks (the fields are after Zartman and Doe, 1981; Sun and McDonough, 1989); black fields are for oceanic islands: M, Mangaia; Tu, Tubuai; StH, St. Helena; StP, St. Paul's Rocks; T, Tristan da Cunha. C, $^{206}Pb/^{204}Pb$ vs. $\varepsilon Nd_t$ plot; DM, depleted mantle; PM, primitive mantle; EM, enriched mantle; HIMU, high μ sources (Zindler and Hart, 1986). D, age vs. $\varepsilon Hf_t$ in zircon plot for rhyolite TKS-21-63; light gray circles are glasses of basalt to dacite compositions from tephra of the early Izu-Bonin arc (after Straub et al., 2010). Isotope data from greywacke sandstones of the TFTB after (Perfilova et al., 2022a; Safonova and Perfilova, 2023; Perfilova, 2023), from Maikain deposit after (Pan et al., 2015), and Boshchekul area after (Shen et al., 2015). Symbols in A-C are as in Fig. 11.

possible isotope fractionation in terms of secondary alteration, e.g., decoupling of Nd and Pb isotopes (Cohen and O'Nions, 1982; Sun and McDonough, 1989). The initial Pb isotopic composition of the samples ranges in $^{206}Pb/^{204}Pb$ from 19.2 to 20.3 for the high-Ti basalts, 18.9 for the mid-Ti gabbro and 19.1–22.3 for the low-Ti volcanics (Supplementary table S3). The highest value of $^{206}Pb/^{204}Pb$ (22.8) has been recorded for the high-Ti phonolite. In the $^{206}Pb/^{204}Pb$ vs $^{207}Pb/^{204}Pb$ diagram all samples plot along the orogenic trend at its high-radiogenic end (Fig. 14B). The trend of the Pb isotopes suggests a variable contrasting contribution of mantle and crustal Pb to the samples. The highest value of $^{207}Pb/^{204}Pb$ can be linked to the presence of a crustal component as a result of either the contamination of the rocks during their emplacement or enrichment of initial mafic melts in subducted crust materials. In the combined $^{206}Pb/^{204}Pb$ vs $\varepsilon Nd_t$ diagram, the high-, mid- and low-Ti basalts plot in between the reference points for the primitive mantle (PM), depleted mantle (DM) and HIMU enriched mantle, and the high-Ti phonolite plots near the HIMU point (Fig. 14C). The Nd isotope systematics shows that a part of the low-Ti magmatic rocks and the mid-Ti gabbro were derived from isotopically similar mantle sources, that is quite possible as both MORB and supra-subduction rocks, in particular those formed at young intra-oceanic arcs, are derived from depleted sources (Fig. 14A). However, the Pb isotope systematics indicate that the depleted source which produced the arc magmas is different from that of the MORB-gabbro by a higher value of $^{206}Pb/^{204}Pb$, that is typical of continental crust (Fig. 14B, C).

Hf-in-zircon isotopes can be used to track the differentiation of crustal and mantle associated elements in order to trace crustal evolutionary paths (Kemp et al., 2007; Collins et al., 2011). The ratios of Lu and Hf isotopes were measured in zircons from rhyolite TKS-21-63 possessing supra-subduction geochemical characteristics. The zircons show initial $^{176}Hf/^{177}Hf$ ratios varying from 0.283012 to 0.283055 and yielded extremely positive $\varepsilon Hf_t$ values of +17.6 to +19.3 (Fig. 14D). Such high ratios have been recorded in Izu-Bonin volcanic arc lavas derived from extremely depleted harzburgite mantle (Straub et al., 2010).

## 5. Petrogenesis

Given that a part of the samples under study carries phenocrysts (section 3; Fig. 9), we can suggest fractional crystallization of parental melts. The high-Ti volcanic rocks (Fig. 12B) are characterized by the lowest Zr/Nb of 2.7 to 6.3 (Supplementary table S2) and highest Nb, La and Sm (Fig. 12I-K). The fractionation of olivine and orthopyroxene is possible because there are phenocrysts of those minerals in the basalts of this group and moderate correlations between $SiO_2$ vs MgO and $Fe_2O_3$ (Figs. 9A, B, 12 A, C).

The most representative group of TFTB of mafic to felsic low-Ti rock varieties (Fig. 12B) is characterized by lower concentrations of other incompatible elements (Fig. 12G-L), in particular, Nb and Sm, and, as a result, the highest Zr/Nb ratios (20–82) (Supplementary table S2). The low-Ti volcanic rocks, but not the high-Ti varieties, exhibit a wide range of the contents of MgO (Fig. 12). The presence of olivine (though altered; Fig. 9B) and the negative trends in the MgO vs $SiO_2$ (Fig. 12A) suggest fractionation of Mg-bearing minerals, e.g. olivine and orthopyroxene. The negative trend in the MgO vs $TiO_2$ plot (Fig. 12B), the negative anomalies of Ti and Nb in the multi-element spectra of the low-Ti samples (Fig. 13H), and the presence of magnetite in thin sections (Fig. 9B-E) and variable $Al_2O_3/TiO_2$ ratios (11.1–23.9; Supplementary table S2) suggest fractionation of Ti-Fe oxides during crystallization of a primary magmatic melt. There are two parallel trends in the MgO vs CaO plot (Fig. 12D) suggesting fractionation of two Ca-bearing minerals, e.g., clinopyroxene and plagioclase. More evidence for the fractionation of plagioclase comes from the phenocrysts of plagioclase and the negative Eu anomalies in the REE spectra present in the most of the low-Ti samples (Figs. 9C, E, 13D).

The granitoids are both I-type (the dated granite and rhyolite; Fig. 11D), whereas the dacite is S-type suggesting different conditions of magma generation: derivation from igneous or intracrustal sources versus anatexis of metasedimentary or supracrustal protoliths (Chappell and White, 1992). A special case is the low-Ti rhyolite (TKS-21-63; Fig. 9E) (Supplementary tables S2, S3), which is characterized by not only highly positive $\varepsilon Nd_t$ (+10.8), but also strongly positive $\varepsilon Hf_t$ (+17.6 − +19.3) (Fig. 14A, D). During magmatic crystallization, a high molar ratio of Al/(Ca + Na + K) > 1.0 (index ASI > 1.0) would decrease the Zr/Hf ratios at a later stage, i.e. at a low-temperature crystallization of zircon (Linnen and Keppler, 2002; Yin et al., 2013). Rhyolite TKS-21-63 shows ASI = 1.05, we suggest that those extremely high values of $\varepsilon Hf_t$ resulted from the low-temperature crystallization of a high-Al magma.

## 6. Mantle sources and degrees of melting

In general, only the high-Ti basalts (but not high-Ti andesites) are characterized by differentiated HREE (Fig. 13A; $Gd/Yb_n > 2$) indicating derivation of primary melts from garnet-bearing mantle sources (Hirschmann and Stolper, 1996). The other varieties, both mid- and low-Ti, were derived from spinel-bearing mantle sources (Fig. 13C, D; $Gd/Yb_n$ = 0.9–1.7; Supplementary table S2). Note that the REE patterns from the low-Ti varieties of this work and from the Tortaul and Bazarbai ophiolites published in (Degtyarev et al., 2022) are absolutely identical (Supplementary figure S3). According to the bulk-rock Sm-Nd and Pb-Pb isotope systematics, the rocks were derived from generally juvenile mantle sources (Fig. 14A) or primitive to HIMU mantle sources (Fig. 14C).

The low-Ti varies of the Kuzek and Tekturmas fms., Tortaul and Bazarbai ophiolites (Table 2; supplementary table S2) yielded increased concentrations of Th relative Yb in the low-Ti rocks that move the points above the mantle trend into the area of magma-crust interaction under a volcanic arc (Fig. 15A). A probable mantle source of rhyolite TKS-21-63, as seen from both the Sm-Nd and Lu-Hf systematics (Fig. 14A, D), is a strongly depleted fore-arc mantle source, that is typical of the Izu-Bonin-Mariana intra-oceanic arc system (Straub et al., 2010).

The mid-Ti gabbro is compositionally very close to the "classic" N-MORB (Fig. 13C, G). It is characterized by the highest, among the TFTB basalts, value of $\varepsilon Nd$ (+8.05) and the lowest value of $^{206}Pb/^{204}Pb$ (18.92) that are indicative of a DM-type source (Fig. 14A-C). The mid-Ti gabbro plots within the mantle array and close to the point of N-MORB (Fig. 15A).

The high-Ti basalts yielded LREE enriched, HREE differentiated REE patterns and Nb peaked multi-element patterns (Fig. 13A, E) and medium to high $\varepsilon Nd$ (+3.5 − +6.7) and $^{206}Pb/^{204}Pb$ ratios plotted in the field of OIB (Fig. 14 A-C) suggesting their derivation from an enriched garnet-bearing mantle source, possibly, EM2. The Nb/Yb vs Th/Yb systematics plots the high-Ti basalts near the OIB point within the mantle array (Fig. 15A).

A special group is the high-Ti andesites and phonolite (Fig. 11A, B, 12B), that are also characterized by increased concentrations of Zr, Nb, La and Sm (Supplementary table S2; Fig. 12H-K) and yielded REE and multi-element patterns similar to those of typical OIBs (Fig. 13B, F). Their Sm-Nd and Pb-Pb isotope systematics indicate a HIMU-like mantle source that typically produces OIB-type within-plate oceanic lavas (Fig. 14A-C). HIMU mantle sources probably result from subducted and recycled oceanic crust (possibly contaminated by seawater) that has not been homogenized with the rest of the mantle (e.g., Chauvel et al., 1992; Hanyu et al., 2011). In the Nb/Yb vs Th/Yb diagram (Fig. 15A), these high-Ti volcanics plot close to the mantle array, the OIB point (Sun and McDonough, 1989) and Tristan-da-Cunya within-plate oceanic island basalts and andesites (Weit et al., 2017).

In general, OIB-type lavas can be produced from both juvenile (variably depleted) and enriched mantle sources (Fig. 14B, C), but intra-oceanic arc magmatic rocks are typically produced from depleted/juvenile sources (Fig. 14A, D). In the western CAOB, most of the early Paleozoic magmatic formations emplaced in supra-subduction settings

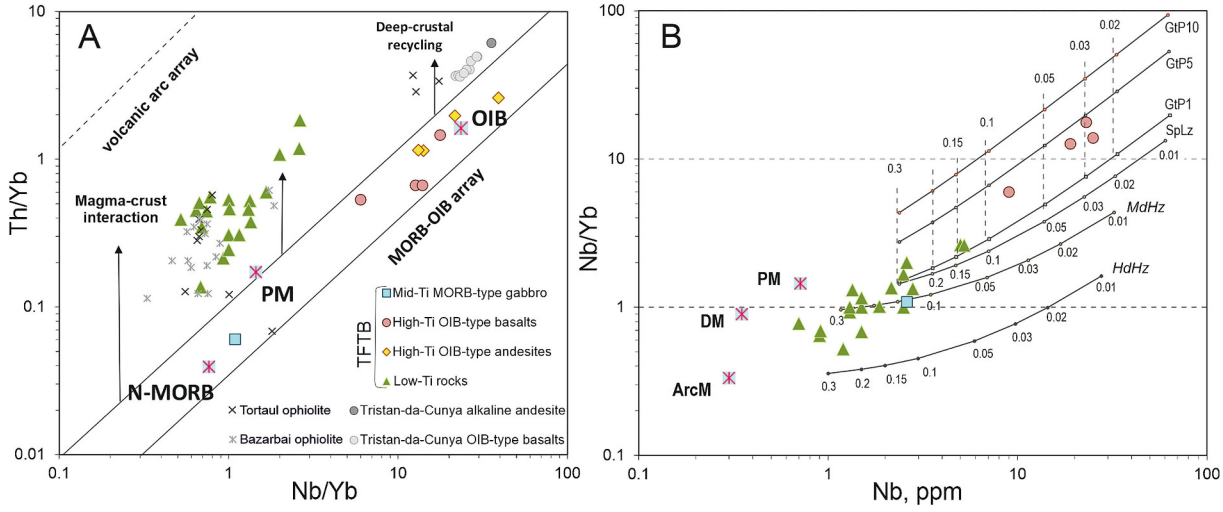


**Fig. 15.** A, Nb/Yb vs. Th/Yb plot after (Pearce, 2008) showing high-Ti andesite and OIB-type basalts of Tristan-da-Cunya (Weit et al., 2017) and ophiolites of Tortaul and Bazarbai zones of the TFTB (Degtyarev et al., 2022). PM, OIB and MORB are after (Sun and McDonough, 1989). B, Nb vs Nb/Yb modeling based on partition coefficients from (Johnson, 1998; Bédard, 1994). The calculated melting curves are for spinel lherzolite (SpLz) and garnet peridotite containing 1, 5 and 10 % of garnet (GtP) from primitive mantle (PM), moderate depleted harzburgite (MdHz) and highly depleted sub-arc harzburgite (HdHz). PM – primitive mantle, DM – depleted mantle, ArcM – arc mantle. Numbers denote degrees of melting. Symbols as in Fig. 11.

are characterized by positive values of εNd and εHf, i.e. were derived from juvenile mantle sources (Table 4).

To understand better the composition/type of parental melts, that produced the volcanic rocks of the TFTB, we performed geochemical modeling of basalts to andesibasalts of all three groups in the Nb – Nb/Yb system (Fig. 15B) following the method of Pfänder with co-authors (Pfänder et al., 2002) in order to estimate the composition of melts generated at variable melting degrees of different mantle. These elements are low-mobile during a possible subduction-related migration from the slab to the mantle wedge and therefore their concentrations reflect those in the mantle source (Pearce and Peate, 1995). For calculating the degree of melting of a probable source (primitive, depleted) we used the non-modal batch-melting equation (Albarède, 1995). As probable mantle sources we chose primitive mantle (PM) spinel lherzolite, primitive garnet lherzolite (containing 1, 5 and 10 % of garnet), depleted mantle peridotite (DM) and highly depleted sub-arc harzburgite (HdHz) (Safonova et al., 2012). The initial concentrations of Nb and Yb were taken as, respectively, as 0.71 and 0.49 ppm for PM, 0.35 and 0.45 ppm for DM (Sun and McDonough, 1989), 0.20 and 0.45 ppm for a highly depleted harzburgite of the Izu-Bonin-Mariana fore-arc (Parkinson and Pearce, 1998). The primitive values correspond to those in the N-MORB calculated for 10 % batch melting of depleted mantle peridotite by (Hofmann, 1988). We chose the Izu-Bonin sub-arc mantle harzburgite as a highly depleted mantle source with the value of Nb/Yb (because Yb is more compatible than Nb) to be lower than that in the TFTB mafic volcanics, of which the lowest is 0.52 (Supplementary table S2; sample TKS-21-73). For the mineral compositions of the mantle sources and information about distribution coefficients see Supplementary table S4. The results show that the high-Ti basalts formed at the 2 to 4 % melting of garnet peridotites with 1 to 5 % of garnet. The mid-Ti gabbro was derived by the 15 % melting of a "classic" DM that is typical of most MORBs. The parental melts of the most of the low-Ti basalts and andesibasalts were derived at significantly higher degrees of melting (15 to 30 %) of variable mantle sources: from 1 % garnet peridotite to DM and highly depleted harzburgite (Fig. 15B).

## 7. Tectonic settings of magmatism

The geological relationships, geochemical and isotopic characteristics of the magmatic rocks of the TFTB are all indicative of their eruption/emplacement in different tectonic settings. Such a tectonic juxtaposition of magmatic, presumably volcanic, rocks of different origins is typical of many fossil Pacific-type orogenic belts (e.g., Utsunomiya et al., 2009; Safonova et al., 2011b, 2012, 2020; Dagva-Ochir et al., 2020). In our case, we will discuss the settings that are most typical of Pacific-type orogens: oceanic and supra-subduction.

Oceanic. The high-Ti volcanic rocks are typically associated with volcaniclastic rocks, i.e. slope facies suggesting their formation at oceanic rises. The overall geochemical features suggest that the high-Ti basalts are, in parallel, enriched in LREE and Nb, that is typical of OIB-type or plume-type basalts, i.e. similar to those of the Hawaii system of within-plate seamounts and islands (Hofmann, 1997). The overall levels of the concentrations of REE and other trace elements in the OIB-type volcanics of the TFTB (Fig. 13A, E) are bit lower than that of an average OIB (Sun and McDonough, 1989). This by no way rises doubts on the within-plate origin of the high-Ti volcanics rocks of the TFTB, but the variable degrees of enrichment in incompatible elements suggest their derivation by low to medium degrees melting of enriched sources (Fig. 15B) under a relatively thin oceanic lithosphere moving over a hot spot/mantle plume (e.g., Regelous et al., 2003; Niu and O'Hara, 2008; Safonova, 2008; Safonova and Santosh, 2014). Their variable isotope systematics suggest their derivation from enriched mantle sources that is also typical of OIBs (Fig. 14; Zindler and Hart, 1986; Sun and McDonough, 1989; Regelous et al., 2003). The high-Ti andesites and phonolite possess have higher concentrations of REE (Fig. 13B) and their spidergrams also show the peaks at Nb (Fig. 13F). As they are similar to OIB in terms of trace elements, they could be also emplaced in intraplate oceanic environments, like the andesite of the Tristan da Cunha islands (An et al., 2016; Weit et al., 2017). In discrimination diagrams, the high-Ti mafic to felsic volcanic rocks plot in the field of oceanic island tholeiites (Fig. 16A) or within-plate tholeiites and alkaline basalts (Fig. 16B).

The only mid-Ti sample (gabbro) is geochemically similar to MORB (Fig. 13C, G). Indeed, MORB-type mafic rocks are rare in the fossil Pacific-type orogenic belts, because after their birth at mid-oceanic ridges and constituting a major portion of oceanic crust, they typically get subducted back to the mantle leaving us only small pieces in accretionary prisms, usually as parts/bottoms of accreted oceanic islands, to find and explore (e.g., Safonova et al., 2011c, 2016, 2024b). Its Sm-Nd isotope characteristics suggest a depleted mantle source as typical of most MORB-type basalts (e.g., White et al., 1987; Hofmann, 1997; Bezard et al., 2016). In the discrimination diagrams, the mid-Ti

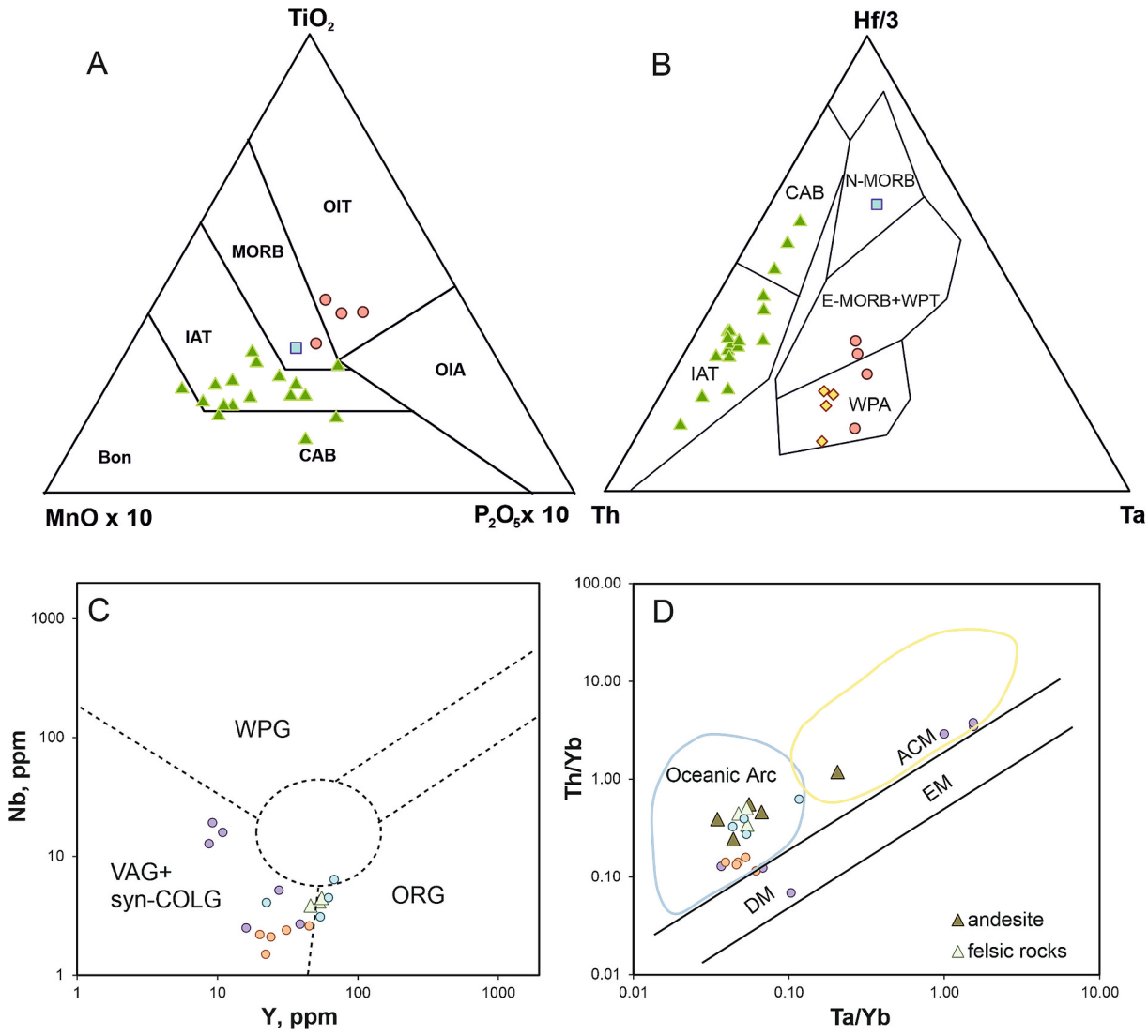


**Fig. 16.** Tectonic discrimination diagrams for igneous rocks of the TFTB, central Kazakhstan. For mafic to andesitic volcanic rocks (A, B): A, MnO*10 – $TiO_2$ – $P_2O_5$*10 (Mullen, 1983); B, Th – Hf/3 – Ta (Wood et al., 1979). WPA – within-plate alkaline basalts; WPT – within-plate tholeiites; IAT – island-arc tholeiites; CAB – calc-alkaline basalts; OIT – oceanic islands tholeiites; OIA – oceanic islands alkaline basalts; Bon – boninites; MORB – mid-ocean ridge basalts. For felsic rocks (C, D): C, Y vs. Nb (Pearce et al., 1984); Syn-COLG – *syn*-collisional granite, VAG – volcanic arc granite, WPG – within-plate granite, ORG – ocean ridge granite; D, Ta/Yb vs. Th/Yb (Pearce, 1983); ACM – active continental margin, DM – depleted mantle, EM – enriched mantle. The data from Bazarbai, Tortaul and Akoi, small light-blue, purple and orange circles, respectively, are from (Degtyarev et al., 2022; Degtyarev et al., 2023). Other symbols as in Figs. 11, 12. (For interpretation of the references to colour in this figure legend, the reader is referred to the web version of this article.)

gabbro plots in the field of N-MORB (Fig. 16A, B).

Supra-subduction. All numerous low-Ti samples show no direct contacts with deep-marine sediments as most contacts are concealed (Fig. 8B, C, F). Compositionally, they range from basalt to rhyolite (Fig. 11A). The felsic varieties are mostly metaluminous and I-type, although the peralumnous and S-type varieties have been diagnosed as well (Fig. 11D). The low-Ti varieties are characterized by clear crystallization trends (Fig. 12A, B) and Nb troughs in the spidergrams (Fig. 13H), i.e., possess geochemical features typical of supra-subduction magmatic series. In the discrimination diagrams, the low-Ti basalts and andesibasalts plot in the fields of island-arc tholeiites and calc-alkaline basalts (Fig. 16A, B). These features, coupled with the highly positive values of $\varepsilon Nd_t$ and $\varepsilon Hf_t$ (Fig. 14A, C, D) and the unimodal distributions of the U-Pb detrital zircon ages (Fig. 17; Perfilova et al., 2022a), indicate their eruption in an intra-oceanic arc setting. The discrimination diagrams for the felsic varieties (granite, rhyolite, dacite) indicate their emplacement in orogenic settings and oceanic arc setting (Fig. 16C, D).

## 8. Other localities of early Paleozoic oceanic and arc magmatism of the PAO

The formation of the TFTB is closely related to the early Paleozoic evolution of the PAO and with the multi-stage amalgamation of the Kazakhstan composite continent (Windley et al., 2007; Buslov, 2011). The proto-Kazakhstan continent, i.e. its "protolithic" magmatic arcs separated the PAO into four interconnected oceans: Ob–Zaisan (between Siberia and Kazakhstan), Uralia (between Baltica and Kazakhstan), Turkestan (between Kazakhstan and Tarim), and Junggar–Balkash (between the limbs of the Kazakhstan Orocline) (Windley et al., 2007). Middle-late Cambrian to late Ordovician island arcs have been preserved, though in variable degree, within the Early Paleozoic structure of the Kazakhstan continent, in West Junggar and Northern Tienshan (Fig. 1). Although previously it was suggested that some arcs were built upon oceanic crust, i.e. represent intra-oceanic arcs (Baidaulet–Akbastau arc), while many others have heterogeneous basement consisting of both oceanic and continental segments

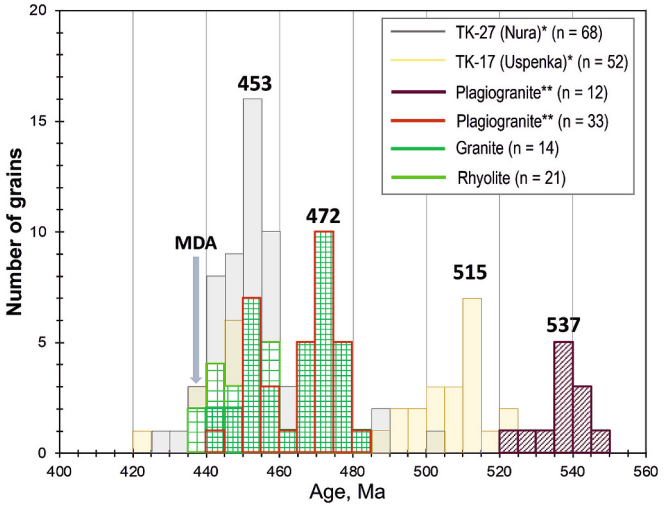


**Fig. 17.** A histogram of magmatic and detrital zircon ages from the TFTB: *, ** – borrowed from (Perfilova et al., 2022a) and (Degtyarev et al., 2022, 2023), respectively, and new data (granite, rhyolite; Fig. 10).

(Boshchekul–Chingiz and Selety-Urumbai), or fully on continental-type basement (Stepnyak–North Tian Shan arc) (Degtyarev, 1999; Filippova et al., 2001; Windley et al., 2007). Recently there have been obtained new geochronological and isotope data from magmatic and clastic rocks, which confidently show that most of the arcs, which fragments have been preserved in the Kazakhstan collage/orocline, but not in the northern Tienshan, represent intra-oceanic arcs, i.e., built upon oceanic crust (Shen et al., 2015; Safonova et al., 2017, 2020, 2022; Safonova and Perfilova, 2023; Zhang et al., 2023). Those data argue in favor of the model suggesting a continuous arc magmatism from the Vendian to the Early Paleozoic in the western PAO in contrast to the model of suggests several independent and short-lived arc systems (Filippova et al., 2001). The island-arc terranes of the Kazakhstan Orocline formed by the evolution of the Junggar–Balkhash Ocean, a south-western branch of the PAO. In early Paleozoic time, accretionary prisms formed in front of the intra-oceanic arcs; they incorporated deep-marine volcanic and sedimentary formations, i.e. ocean plate stratigraphy units. Thus formed accretionary complexes also included ophiolites. Amalgamation of the early Paleozoic island arcs and Precambrian microcontinents formed the Kazakhstan continent and ceased in Late Silurian or early Devonian time (Korobkin and Buslov, 2011).

High-Ti oceanic basalts of OIB-type often as pillow-lavas have been found in many accretionary complexes of the CAOB (Safonova and Santosh, 2014; Safonova, 2017). However, as mentioned in section 7 few, if any, basalts of MORB-type have been found in those. The early Paleozoic oceanic magmatism (OIB and MORB types) of the PAO has been reconstructed in the Katun' accretionary complex (AC) (Safonova et al., 2011b), Zasur'ya AC (Safonova et al., 2011c) of the Russian Altai, Itmurundy AC of Central Kazakhstan (Safonova et al., 2020), Fan–Karategin AC in Tajikistan (Volkova and Budanov, 1999), Tangbale and Barleik–Mayile in West Junggar (Wang et al., 2003). All those ACs include not only thrust-duplexed OPS units with OIB-type basalts and, to a lesser degree, MORB-types basalts, pelagic and hemipelagic sediments, but also serpentinite mélanges also referred to as ophiolitic mélanges with peridotite, gabbro and dolerite. Basaltic lavas are often associated with radiolarian chert and limestone in accretionary complexes and ophiolites of West Junggar (Wang et al., 2003 and references therein). A part of Tangbale and Mayile diabases and basalts are characterized by high $TiO_2$ contents (up to 3 wt%), enriched LREE ($La/Yb_n > 2$) and high Nb (Wang et al., 2003). The Tangbale and Mayile oceanic units are spatially related to island-arc units of similar ages and accretionary units of younger ages (Zhang et al., 2023).

The Early Paleozoic supra-subduction magmatism in the western CAOB is represented by respective terranes in Northern and Central Kazakhstan, Northern Tienshan and West Junggar. Note that those in Central Kazakhstan and West Junggar are dominated by magmatic associations formed in intra-oceanic arcs (Fig. 1, Table 4) and those in Northern Tienshan includes both continental and intra-oceanic arc formations. The intra-oceanic arc terranes in Kazakhstan are the early-middle Cambrian Selety-Urumbai arc (NE Kazakhstan; Degtyarev and Ryazantsev, 2007), Cambrian – early Ordovician Bozshakol-Chingiz arc, the same as Boshchekul, (NE and east; Shen et al., 2015) and Baidaulet-Akbastau arc (west; Degtyarev, 2011; Pan et al., 2015), Ordovician Itmurundy and Tekturmas arcs (center; Safonova et al., 2020, 2022; this paper). In West Junggar, the Cambrian-Ordovician Tangbale-Mayile-Barleik-Xiemisitai-Hongguleleng ophiolitic belt includes, similarly to Itmurundy and Tekturmas, magmatic rocks of MORB and OIB affinities and supra-subduction rocks (Zhang et al., 2023). The Kyrgyz Northern Tienshan hosts the Songkultau intra-oceanic juvenile arc of Cambrian age (Konopelko et al., 2021) and Mazarashiu-Shamsi recycled continental arc (unpublished data).

## 9. Geodynamic model: four intra-oceanic arcs and tectonic erosion

We summarized all available U-Pb ages of zircons from both magmatic and clastic rocks of the TFTB and made a single histogram (Fig. 17). The histogram clearly shows four major peaks at ca. 537, 515, 472 and 453 Ma, that are separated by clear troughs. Such a combination of four almost unimodal distributions suggests the presence of several intra-oceanic arcs at one or more Pacific-type convergent margins of the PAO in early Paleozoic time (Fig. 18).

Several recent publications on Central Kazakhstan have shown that the Tekturmas and Itmurundy zones host Ordovician island-arc complexes and, to a lesser degree, early-middle Cambrian magmatic rocks possessing supra-subduction geochemical features (Safonova et al., 2020; Degtyarev et al., 2022, 2023; Perfilova et al., 2022b; Gurova et al., 2022). The tectonic model presented in (Degtyarev et al., 2022) considered the Tekturmas, Bazarbai and Tortaul ophiolites separately from the other Ordovician formations of the TFTB (Degtyarev et al., 2017, 2022) and linked the latter with the Baidaulet-Akbastau and Boshchekul-Chingiz intra-oceanic arcs (see Safonova et al., 2017 for review and references cited therein). In this paper, we present a partly alternative three-stage model for the evolution of an active margins of the PAO and establishment of the TFTB from early Cambrian to early Silurian times (Fig. 17) based on a summary of all data from TFTB magmatic rocks, previous and new, and, in consideration with the published data from coeval arc complexes of Kazakhstan and West Junggar (Table 4).

A key point of the model is the presence of a "true" MORB-type basalt in the axial zone of the TFTB (see point TK-22 in Fig. 3; Table 2), close to the serpentinite-dominated Tekturmas Zone (section 2), which pelagic cherts span the middle Darriwilian to the early Sandbian in age (Table 1). In our model we will consider the Tekturmas zone as an axial part of the reconstruction (Fig. 18). The areas north and south of the axial serpentinite zone are characterized by different dominating lithologies and their associations (Figs. 3, 4): magmatic-dominated and siliciclastic-dominated, respectively. In addition, they host greywacke sandstones of different compositions, basaltic to felsic to the north (Bazarbai and Nura zones) and andesitic to felsic to the south (Safonova and Perfilova, 2023; Perfilova, 2023), which also yielded different distributions of U-Pb detrital zircon ages (Table 3; Fig. 17; Supplementary figure S2). These facts allow us to propose a model of double-sided subduction under two Pacific-type convergent margins, both intra-oceanic: Nura-Bazarbai to the north of the proposed MORB-axis and Uspenka-Tekturmas to the south of it (Figs. 3, 4).

The oldest early-middle Cambrian intra-oceanic arc (ca. 537 Ma; Fig. 18A) was constrained, as mentioned above, by the age of zircons from granitoids in mélange south of the axis (Fig. 17; Degtyarev et al.,

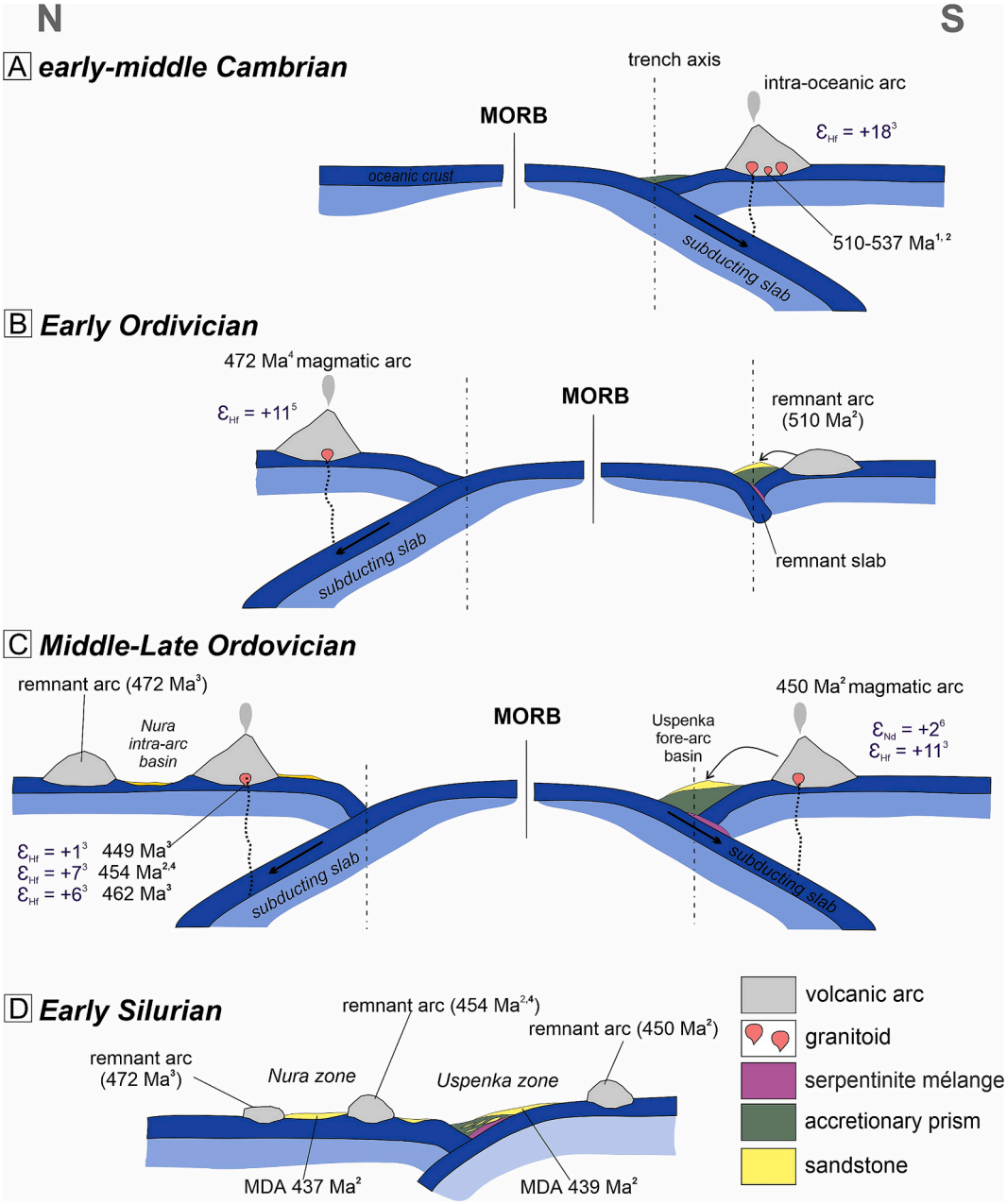


**Fig. 18.** A new tectonic model for the early Paleozoic magmatism of the Paleo-Asian Ocean based on the data from the Tekturmas Fold-and-Thrust Belt. Age data: 1 – Degtyarev et al., 2023; 2 – Perfilova et al., 2022a; 3 – this study; 4 – Degtyarev et al., 2022; 5 – Pan et al., 2015; 6 – Safonova and Perfilova, 2023.

2023). No coeval coherent magmatic complexes have been found in the TFTB, although fragments of an early Cambrian arc have been found in the Itmurundy Zone of Central Kazakhstan located south of the TFTB (Fig. 1; the ca. 500 ages of zircons from mélange-hosted supra-subduction granitoids; Safonova et al., 2020; Degtyarev et al., 2022). In the western CAOB, juvenile arc complexes occur in the Tangbale and Barleik-Mayile areas of West Junggar in NW China (Kwon et al., 1989; Jian et al., 2005; Ren et al., 2014; Zhao and He, 2014; Weng et al., 2016; Wen et al., 2016; Zhang et al., 2023) and in the Songkul area of Northern Tienshan in Kyrgyzstan (Konopelko et al., 2021) (Table 4). More evidence for that early-middle Cambrian arc south of the TTFB axis (Fig. 18A) comes from the U-Pb ages of detrital zircons of a greywacke sandstone of the Uspenka Zone (510 Ma, Figs. 3, 4, 17; Perfilova et al., 2022a). As there are few zircons younger 519 Ma, but older 455 Ma (Fig. 17), we suggest that the early-middle Cambrian arc was tectonically eroded and the trench axes shifted landward (Fig. 18B). Processes of tectonic or subduction erosion and related shifts of trench axes have been reported before in the modern Circum-Pacific (e.g., Stern and Scholl, 2010; Suzuki et al., 2010; Jicha and Kay, 2018; Safonova and Khanchuk, 2021). The early-middle Cambrian magmatic rocks and detrital zircons of Central Kazakhstan, West Junggar and Northern Tianshan yielded positive whole-rock and zircon $\varepsilon Nd_t$ and $\varepsilon Hf_t$ values (Table 4).

In Early Ordovician time, an intra-oceanic arc, Baidaulet-Akbastau (Degtyarev, 2012) or its coeval analogue, was active north of the TFTB as well (Fig. 1) leaving ca. 472 Ma granitoids in the mélange of the TFTB (Degtyarev et al., 2022). Therefore, we place the early Ordovician arc, the analogue or extension of the Baidaulet-Akbastau arc, only to the left side of the model (Fig. 18B). No traces of a coeval early Ordovician arc have been recorded south of the TFTB axis, i.e. in the right side of the model. By the Middle Ordovician, the regime of tectonic erosion changed to the regime of accretion at both sides of the ocean to initiate

**Table 3**
A summary of geochronological, geochemical and isotope data from greywacke sandstones of the TFTB.

| | North Group | | South Group | | North group | South group | UCC |
|---|---|---|---|---|---|---|---|
| | Nura | Bazarbai | Tekturmas | Uspenka | | | |
| **U-Pb ages**[a] | 453 (unimodal) | – | – | 450, 510 (bimodal) | 453 (unimodal) | 450, 510 (bimodal) | – |
| **$SiO_2$** | 50–58 (av. 54) | 60–68 (av. 63) | 58–61 (av. 59) | 60–69 (av. 66) | 50–68 (av. 59) | 58–69 (av. 64) | 66.6 |
| **MgO** | 3.9–6.5 (av. 5.2) | 2.2–3.4 (av. 2.7) | 3.5–3.7 (av. 3.56) | 2.2–3.9 (av. 3) | 2.2–6.5 (av. 3.7) | 2.2–3.9 (av. 3.1) | 2.48 |
| **Rb** | 5–15 (av. 10) | 2–12 (av. 6) | 27–50 (av. 38) | 34–113 (av. 56) | 2–15 (av. 8) | 27–113 (av. 52) | 84 |
| **Cs** | 0.4–0.8 (av. 0.57) | 0.2–0.4 (av. 0.31) | 1.1–2.4 (av. 1.8) | 0.9–5.8 (av. 2.4) | 0.2–0.8 (av. 0.4) | 0.9–5.8 (av. 2.2) | 4.9 |
| **Ba** | 80–161 (av. 121) | 56–102 (av. 76) | 298–379 (av. 339) | 250–643 (av. 401) | 56–161 (av. 94) | 250–643 (av. 388) | 628 |
| **Zr** | 46–53 (av. 50) | 51–86 (av. 68) | 102–118 (av. 110) | 40–192 (av. 119) | 46–86 (av. 61) | 40–192 (av. 117) | 193 |
| **Nb** | 1.4–3.7 (av. 2.5) | 2.4–2.6 (av. 2.5) | 6.8–8.5 (av. 7.7) | 4–11 (av. 9) | 1.4–3.7 (av. 2.5) | 4–11 (av. 9) | 12 |
| **∑REE** | 89–110 (av. 99) | 60–115 (av. 89) | 123–149 (av. 136) | 82–169 (av. 135) | 60–115 (av. 93) | 82–169 (av. 135) | 183 |
| **εNd** | −2.4 | +5.8 | – | +2.3, +2.5 | −2.4, +5.8 | +2.3, +2.5 | – |
| **εHf** | −3…+7 | – | – | +8…+18 | −3…+7 | +8…+18 | – |

Samples: TK-27, TKS-21-60, Nura Zone; TKS-21-51, TKS-21-55, TKS-21-67, Bazarbai Zone; TKS-21-44, TKS-21-45, Tekturmas Zone; TK-17, TK-18, TKS-21-24, TKS-21-25, TKS-21-39, TKS-21-40, TKS-21-43, Uspenka Zone; av. – average value. The values for the upper continental crust are after (Rudnick and Gao, 2003). The concentrations of $SiO_2$ and MgO are in wt%, the others are in ppm (Perfilova et al., 2022a; Safonova and Perfilova, 2023; Perfilova, 2023).

[a] Character of distribution of U-Pb detrital zircon ages.

two new subduction zones (Fig. 18C), which trench axes were located more oceanward relative the previous ones (Fig. 18A), and, respectively, two more intra-oceanic arcs (Figs. 10, 17). The Middle-Late Ordovician arc magmatism (Fig. 18C) was accompanied by accretionary growth and formation of accretionary prisms hosting OPS magmatic (OIB and MORB) and sedimentary (chert, siliceous mudstone, turbidites) rocks (Table 1; Figs. 5, 8D, H, I).

The Late Ordovician Nura-Bazarbai arc (left of the mid-ocean ridge in Fig. 18C) produced magmatic series compositionally ranging from basalt to rhyolite (Figs. 12, 13D, H). Its age is constrained by the ca. 449 Ma rhyolite (Fig. 10B) and by the 453 Ma peak of U-Pb age of detrital zircons from a Nura sandstone (Fig. 16; Perfilova et al., 2022a). The Bazarbai arc magmatic rocks are characterized by the extremely juvenile character of their sources, i.e., highly positive $\varepsilon Nd_t$ and $\varepsilon Hf_t$ (Fig. 14A, D). More evidence for its intra-oceanic nature comes from the unimodal distribution of the ages of zircons from the Nura sandstone and from the positive values of $\varepsilon Nd_t$ of a sandstone of the Bazarbai Zone (Safonova and Perfilova, 2023; Fig. 14A; Supplementary figure S2). The Nura sandstones yielded negative values of $\varepsilon Nd_t$ (−2.4) and negative to positive values of $\varepsilon Hf_t$ (−3 to +7; sample TK-27 in Table 3, Figs. 3, 14, 17). On the contrary, the Bazarbai sandstone is characterized by a higher positive value of $\varepsilon Nd_t$ in (+5.8; Safonova and Perfilova, 2023) and the Bazarbai magmatic rocks yielded strongly positive values of $\varepsilon Nd_t$ (+6.0 to +10.8) and $\varepsilon Hf_t$ (+17 to +19) (Table 3; Supplementary table S3; Fig. 14A, D). This suggests that the Nura and Bazarbai sandstones deposited in different basins: back-arc (Nura) and fore-arc (Bazarbai) (Fig. 18C). The Late Ordovician juvenile magmatism has been also recorded in the Maikain zone of the Baidaulet-Akbastau arc more to the north-east of the TFTB hosting 459 ± 5 Ma island-arc andesite with $\varepsilon Hf_t$ = +4… +15 (Pan et al., 2015).

The Late Ordovician Uspenka-Tekturmas intra-oceanic arc was reconstructed based on the 450 Ma peak in the U-Pb detrital zircon age histogram from the Uspenka sandstone, which also yielded positive values of $\varepsilon Nd_t$ (+2.5) and highly positive values of $\varepsilon Hf_t$ (+8 to +18) (sample TK-17 in Table 3, Figs. 3, 14A, 17). Although there are few magmatic rocks in the area south of the MORB-axis, except for several accreted oceanic rises having OIB geochemical affinities (Figs. 6, 13A, B, E, F), we think that the magmatic protoliths of the Uspenka sandstones were formed at a young intra-oceanic arc. An actualistic analogue of such an arc could be the youngest lavas of the Izu-Bonin-Mariana intra-oceanic arc system, which lavas are also compositionally variable and also derived from very depleted mantle sources (see section 6; Straub et al., 2010). The Uspenka sandstones were likely deposited in a fore-arc basin and accretionary prism. In general, most Ordovician magmatic rocks and greywacke sandstones of Central Kazakhstan, West Junggar, Russian Altai and Northern Tienshan, all in the western CAOB, yielded positive $\varepsilon Nd_t$ and $\varepsilon Hf_t$ values (Table 4; Fig. 14A, D).

The pieces of all arcs were tectonically juxtaposed in the TFTB during the early Paleozoic subduction and accretion of the PAO (Safonova et al., 2020; Degtyarev et al., 2022; Gurova et al., 2022). The MDA ages from detrital zircons (Fig. 17) indicate that the intra-oceanic arc magmatism fully ceased in early Silurian time (Fig. 18D). This model matches the tectonic model of the adjacent Itmurundy Zone implying double-sided subduction as well but under two type of Pacific-type convergent margins, intra-oceanic and continental (Safonova et al., 2024b). All such settings, intra-oceanic arc and continental arc, are currently active around the Circum-Pacific (Safonova and Khanchuk, 2021). The intra-oceanic arcs of the TFTB can be compared with juvenile Cambrian and Ordovician arcs of West Junggar (Liu et al., 2016), Central Kazakhstan (Degtyarev, 2012; Safonova et al., 2020, 2022, 2024b; Gurova et al., 2022; Perfilova et al., 2022a, 2022b), Russian Altai (Buslov et al., 2001; Chen et al., 2016; Safonova et al., 2024a), Tienshan (Gao et al., 2009; Ma et al., 2013; Wang et al., 2015) and the Lake Zone of Mongolia (Janoušek et al., 2018) that resulted from magmatism at convergent margins between the Paleo-Asian Ocean and Gondwana-derived continents and microcontinents all detached during the break-up of the Rodinia supercontinent (Dobretsov et al., 1995; Buslov et al., 2001; Domeier and Torsvik, 2014).

Conclusively, the new data from Tekturmas and the previous age and isotope data from surrounding terranes of the western CAOB show that the early Paleozoic magmatism at active margins of the PAO was dominantly juvenile. The juvenile magmas were highly likely generated at intra-oceanic arcs. That time continental or mature magmatic arcs were present around the PAO, although in minority, as well. However, our recent data from Kazakhstan (Safonova et al., 2020, 2022, 2024b) and Russian Altai (Safonova et al., 2024a) allow us to suggest that a part of the early Paleozoic intra-oceanic arcs, which produced that juvenile magma, were tectonically eroded.

## 10. Conclusions

In this paper we presented new geological, geochronological (U-Pb zircon ages) and geochemical data and first isotope data (Sm-Nd, Pb-Pb, Lu-Hf) from the Tekturmas Fold-and-Trust Belt (TFTB) in Central Kazakhstan and reviewed geological and isotope data from coeval complexes of the western CAOB. The TFTB hosts various magmatic rocks, plutonic and volcanic, forming coherent units or occurring as blocks in serpentinite mélange. In this paper we reviewed available and presented new geochronological and geochemical data plus we pioneered to obtain and discus first bulk-rock Nd and Pb and Hi-in-zircon isotope data. Granite and rhyolite yielded late Ordovician U-Pb zircon ages, 462 and 449 Ma, respectively, that match the microfossil data from

**Table 4**
Data on whole-rock Sm-Nd and Hf-in-zircon isotope systematics from magmatic rocks and greywacke sandstones of adjacent island-arc and accretionary terranes of the western CAOB.

| Region | Complex | Rock type | εNd(t) | εHf(t) | Age, Ma | Reference |
|---|---|---|---|---|---|---|
| **West Junggar, NW China** | | | | | | |
| Tangbale-Mayile arc | Northen Aibi Lake plutons | Diorite | +6.4…+6.7 | n/a | 532 ± 4 | Zheng et al., 2020 |
| | | Qtz-diorite | +6.8…+8.0 | n/a | 505 ± 3 | |
| | Yushitasi plutons | Diorite | +3.4…+6.4 | n/a | 501 ± 3 | Zheng et al., 2020; Xu et al., 2012 |
| | | Granite | +6.8...+8.3 | n/a | 493 ± 5 | |
| | Shandebulake pluton | Diorite | +6.0 | n/a | 488 ± 5 | |
| | Saleinuohai Mts. plutons | Granite | +5.7…+7.2 | n/a | 514 ± 2 | Zheng et al., 2020; Ren et al., 2014 |
| | | Granite | +7.4 | n/a | 509 ± 2 | |
| | | Diorite | +5.1...+6.4 | n/a | 500-493 ± 2 | |
| | | Gabbro | +5.3...+6.1 | n/a | 495 ± 2; 498 ± 2 | |
| Northern West Junggar | Chagantaolegai ophiolite | Diorite | +4.4…+4.6 | +10.2…+14.7 | 503 ± 2 | Yang et al., 2019b |
| | | Granite | +3.7…+4.6 | +10.5…+13.7 | 481 ± 3 | |
| | | Granite | +2.2…+2.4 | +9.5…+15.0 | 435 ± 2 | |
| | | Granodiorite | +2.8…+3.0 | +10.5…+14.0 | 428 ± 2 | |
| Northern West Junggar | Hebukesaier ophiolitic mélange | Rhyolite | n/a | +12.1…+15 | 435 ± 2 | Yang et al., 2018; Yang et al., 2019a |
| Chingiz–Tarbagatai zone | Chagantaolegai ophiolite | Metagabbro | +0.8…+9.5 | n/a | 519 ± 3; 517 ± 3 | Zhao and He, 2014 |
| **Central Kazakhstan** | | | | | | |
| Boshchekul area | Boshchekul group | Dacite | +6.2 | +9.7…+17 | 502 ± 2 | Shen et al., 2015 |
| | | Tonalite | +4.9…+5.7 | +10.6…+17.2 | 489 ± 3 | |
| | | Basalt | +5.6…+6.7 | n/a | n/a | |
| | | Andesite | +5.4…+5.9 | n/a | n/a | |
| Baidaulet-Akbastau arc | Maikain-Kyzyltas zone | Andesite | n/a | +4.3…+14.8 | 459 ± 5 | Pan et al., 2015 |
| Chingiz segment | Central Chingiz zone | Basalt | +5.0…+5.6 | n/a | 470 (m/f) | Degtyarev, 2012 |
| | | Granodiorite | +4.1 | n/a | 470 (m/f) | |
| | Chunai zone, Abaev Fm. | Basalt | +4.2…+6 | n/a | 465 (m/f) | |
| | Stepnyak zone | Dacite | +1.5…+4.4 | n/a | 480 (m/f) | |
| | | Granodiorite | +3.5…+3.4 | n/a | 450 (m/f) | |
| Itmurundy zone | Itmurundy mélange | Diorite | +4 | n/a | 502 ± 4 | Safonova et al., 2020 |
| | Itmurundy ophiolite | SSZ basalt | +7.8 | n/a | 470 (m/f) | |
| | | SSZ gabbro | +4.7…+9.2 | n/a | n/a | |
| | Itmurundy AC | Sandstone, Kazyk Fm. | +0.9 | +9.2…+14.9 | 507-458 | Safonova et al., 2022 |
| | | Sandstone, Itmurundy Fm. | +5.3 | +13.3...+14.5 | 473-452 | |
| | | Sandstone, Tyuretai Fm. | –7.2 | –11.4...+7.7 | 470-437 | |
| Tekturmas belt | Tekturmas ophiolite | SSZ granite, tonalite | +3.0…+5.6 | n/a | 485 (m/f) | Khassen et al., 2020 |
| | Bazarbai ophiolite | SSZ diorite, basalt | +7.4…+7.7 | n/a | 465 (m/f) | |
| | Bazarbai Fm. | Sandstone | +7.7 | n/a | 437 | Perfilova et al., 2022a; Safonova and Perfilova, 2023 |
| | Uspenka zone: Silurian olistostrome | Sandstone | +2.3…+2.5 | +8… +18.4 | 440 | |
| | Nura zone: Yermek Fm. | Sandstone | –2.3 | –3...+6.9 | 440 | |
| **Russian Altai** | | | | | | |
| Gorny Altai terrane | Gorny Altai Series | Metasandstone | n/a | −9.3…+16.1 | 520-463 | Chen et al., 2015 |
| | | Metasandstone | n/a | −5.9…+17.5 | 515-455 | |
| | | Turbidite | +4.4…+5.4 | n/a | 520-500 (m/f) | Kruk et al., 2010 |
| | Zasur'ya Series | Sandstone | +1.3…+9.3 | +3.8…+19.2 | 500-485 | Safonova et al., 2024a |
| Charysh–Terekta–Ulagan–Sayan suture zone | Teletsk complex | Metasandstone | n/a | −18…+12.4 | 517-504 | Chen et al., 2016 |
| | | | n/a | −1.6…+7.4 | 492-472 | |

(*continued on next page*)

**Table 4** (*continued*)

| Region | Complex | Rock type | εNd(t) | εHf(t) | Age, Ma | Reference |
|---|---|---|---|---|---|---|
| | Ulagan complex | Metabasalt | −3.3…+ 9.8 | n/a | 500 (m/f) | Kruk et al., 2010 |
| | | Metasandstone | –5.2...–6.3 | n/a | 420 | Chen et al., 2016 |
| Salair arc | Pechanka Fm. | Clastic rock | +4.7 | n/a | 500 (m/f) | Kruk et al., 2010 |
| **Northern Kyrgyz Tien Shan** | | | | | | |
| Kyrgyz Range | Song-Kul arc | Qtz-diorite | +3.8 | +13.5 | 506 ± 5 | Konopelko et al., 2021 |
| | | Diorite | n/a | +12.3 | 498 ± 6 | De Grave et al., 2011 |

oceanic sediments. There are three main groups of volcanic, subvolcanic and plutonic rocks: (1) high-Ti, (2) mid-Ti, and (3) low-Ti. The high-Ti varieties ($TiO_{2av.} = 2.4$), basalts and andesites, are typically associated with volcaniclastic rocks, i.e. slope facies. They are enriched in LREE ($La/Sm_{n, av.} = 2.1$) and HFSE (Nb, Th, Zr; $Nb/Th_{n, av.} = 1.9$; $Nb/La_{n, av.} = 1.5$) and have differentiated HREE ($Gd/Yb_{n, av.} = 2.3$). The high-Ti lavas were derived at 2–4 % melting of an enriched garnet-bearing peridotite ($\varepsilon Nd_t = +2.1 - +6.8$; $^{206}Pb/^{204}Pb = 19.1–22.8$). The compositional affinity of the high-Ti rocks to OIB and association with volcaniclastic slope facies suggest their eruption on an oceanic island or seamount. The mid-Ti gabbro ($TiO_{2av.} = 1.1$) is compositionally close to N-MORB and is characterized by medium mean values of $La/Sm_n$ (0.6), $Gd/Yb_n$ (1.1), $Nb/Th_{pm}$ (2.1), and $Nb/La_{pm}$ (1.1). It formed from a 15 % melted depleted mantle source ($\varepsilon Nd_t = +8.1$; $^{206}Pb/^{204}Pb = 18.9$). The low-Ti group shows low-enriched LREE ($La/Sm_{n, av.} = 1.4$) and weakly differentiated heavy REE ($Gd/Yb_{n, av.} = 1.3$) and Nb troughs in multi-element diagrams ($Nb/Th_{pm, av.} = 0.3$, $Nb/La_{pm, av.} = 0.4$). All these features are typical of supra-subduction magmatic series. They formed at high degrees of melting (15–30 %) of depleted and ultra-depleted mantle sources ($\varepsilon Nd_t = +6.1 - +10.8$; $\varepsilon Hf_t = +17.6 - +19.3$) suggesting their emplacement in a supra-subduction setting. The highly positive values of $\varepsilon Hf_t$ recorded in zircons from low-Ti rhyolite match those measured in zircons from a greywacke sandstone ($\varepsilon Hf_t = +8 - +18$), that, coupled with the unimodal distributions of U-Pb detrital zircon ages and positive values of $\varepsilon Nd_t$, allowed us to conclude about the intra-oceanic character of magmatic arcs.

The whole set of new and reviewed data, geological, structural, geochronological and isotope-geochemical, allowed us to propose a new tectonic model for the establishment of the TFTB. We concluded that there were totally four intra-oceanic arcs, early-middle Cambrian, Early Ordovician and two Late Ordovician arcs, that were active at two opposite Pacific-type convergent margins, both intra-oceanic, in early Paleozoic time. The early-middle Cambrian and early Ordovician arcs were tectonically eroded and their fragments have been preserved as blocks of mélange and as traces in greywacke sandstones only. The Late Ordovician arc magmatism was active at both convergent margins and has been recorded by coherent magmatic units and unimodal peaks in the U-Pb detrital zircon age histograms. The early Paleozoic magmatism ceased in early Silurian time. The pieces of all arcs were probably tectonically juxtaposed in the TFTB during the suturing of the PAO in middle-late Paleozoic time.

## CRediT authorship contribution statement

**Inna Safonova:** Funding acquisition, Conceptualization, Supervision, Validation, Writing – original draft, Writing – review & editing. **Alexandra Gurova:** Investigation, Data curation, Formal analysis, Methodology, Writing – original draft. **Alina Perfilova:** Data curation, Investigation, Validation, Writing – review & editing. **Wenjiao Xiao:** Validation. **Pavel Kotler:** Validation, Methodology. **Reimar Seltmann:** Validation, Writing – review & editing. **Natalia Soloshenko:** Validation, Methodology. **Alla Dolgopolova:** Validation.

## Declaration of competing interest

The authors declare that they have no known competing financial interests or personal relationships that could have appeared to influence the work reported in this paper.

## Acknowledgements

We appreciate mutual discussions about the Tekturmas Fold-and-Thrust Belt with RAS Academician K. Degtyarev and Dr. A. Yakubchuk. The study was supported by the Ministry of Science and Higher Education of Russia, State Assignment Projects (122041400044-2, FSUS-2025-0008; 123011800012-9), National Natural Science Foundation of China (W2431031), State Administration of Foreign Experts Affairs (Y20240079).

## Appendix A. Supplementary data

Supplementary data to this article can be found online at https://doi.org/10.1016/j.earscirev.2025.105120.

## Data availability

No data was used for the research described in the article.

## References

Abrajevitch, A.V., Van der Voo, R., Bazhenov, M.L., Levashova, N.M., McCausland, P.J. A., 2008. The role of the Kazakhstan orocline in the late Paleozoic amalgamation of Eurasia. Tectonophysics 455, 61–76.
Afonichev, N.A., 1976. On the age of the Urtynzhalskaya series of Central Kazakhstan. Izv. Akad. Nauk KazSSR Ser. Geol. 5 (in Russian).
Albarède, F., 1995. Introduction to Geochemical Modelling. Cambridge University Press, Cambridge, 543 p.
An, A., Hi, C.S., Yu, Y., Lee, D., 2016. Petrogenesis of Late Cenozoic basaltic rocks from southern Vietnam. Lithos 272-273, 192–204.
Antonyuk, R.M., 1974. Oceanic Crust of the Eugeosynclinal Region of the East of Central Kazakhstan. Tectonics of the Ural-Mongolian Fold Belt. M.: Moscow State University Publishing House, pp. 67–74 (in Russian).
Antonyuk, R.M., Evseenko, R.D., Stepanets, V.G., Galley, M.S., Malchenko, E.G., 1995. Geodynamic Map of Kazakhstan. Central Kazakhstan Series. Moscow, 1: 1500000, 251 p. (in Russian).
Antonyuk, R.M., Maslova, I.G., Mukhtarov, Zh.M., 2015. The Tekturmas ophiolite belt: Structure, age, geodynamics. Geology, mineralogy and prospects for the exploration mineral resources of the Republic of Kazakhstan. In: Materials of the International Scientific-Practical Conference. Almaty, 7–28 (in Russian).
Badarch, G., Cunningham, W.D., Windley, B.F., 2002. A new terrane subdivision for Mongolia: implications for the Phanerozoic crustal growth of Central Asia. J. Asian Earth Sci. 21, 87–110.
Baraboshkin, E.Yu., Chitalin, A.F., 1989. Structure and conditions of formation of the Nurcheken strata of the Tekturmas anticlinorium. In: Bulletin of Moscow University. Series 4: Geology 1, pp. 34–45 (in Russian).
Bédard, J.H., 1994. A procedure for calculating the equilibrium distribution of trace elements among the minerals of cumulate rocks, and the concentration of trace elements in the coexisting liquids. Chem. Geol. 118, 143–153.
Bespalov, V.F., 1976. Tectonic nappes in the central Kazakhstan. Dokl. Akad. Nauk SSSR 227 (3), 676–680 (in Russian).
Bezard, R., Fischer-Gödde, M., Hamelin, C., Brennecka, G.A., Kleine, T., 2016. The effects of magmatic processes and crustal recycling on the molybdenum stable isotopic composition of Mid-Ocean Ridge Basalts. Earth Planet. Sci. Lett. 453, 171–181.
Bogdanov, A.A., 1939. New data on the geological structure of the southern and western margins of the Karaganda Basin. In: Proceedings of the USSR Academy of Sciences. Geological Series, p. 4 (in Russian).
Buslov, M.M., 2011. Tectonics and geodynamics of the Central Asian Foldbelt: the role of Late Paleozoic large-amplitude strike-slip faults. Russ. Geol. Geophys. 52 (1), 52–71.
Buslov, M.M., Safonova, I.Yu., Watanabe, T., Obut, O.T., Fujiwara, Y., Iwata, K., Semakov, N.N., Sugai, Y., Smirnova, L.V., Kazansky, A.Yu., Itaya, T., 2001. Evolution of the Paleo-Asian Ocean (Altai-Sayan Region, Central Asia) and collision of possible

Gondwana-derived terranes with the southern marginal part of the Siberian continent. Geosci. J. 5, 203–224.
Cawood, P.A., Kröner, A., Collins, W.J., Kusky, T.M., Mooney, W.D., Windley, B.F., 2009. Accretionary orogens through Earth history. Geol. Soc. Lond. Spec. Publ. 318 (1), 1–36.
Chappell, B.W., White, A.J.R., 1992. I- and S-type granites in the Lachlan Fold Belt. Earth and Environmental Science Transactions of the Royal Society of Edinburgh 83 (1–2), 1–26.
Chauvel, C., Hofmann, A.W., Vidal, P., 1992. HIMU-EM: the French Polynesian connection. Earth Planet. Sci. Lett. 110, 99–119.
Chen, M., Sun, M., Buslov, M., Cai, K., Zhao, G., Zheng, J., Rubanova, E., Voytishek, E., 2015. Neoproterozoic–middle Paleozoic tectono-magmatic evolution of the Gorny Altai terrane, northwest of the Central Asian Orogenic Belt: Constraints from detrital zircon U–Pb and Hf-isotope studies. Lithos 233, 223–236.
Chen, M., Sun, M., Cai, K., Buslov, M., Zhao, G., Jiang, Y., Rubanova, E., Kulikova, A., Voytishek, E., 2016. The early Paleozoic tectonic evolution of the Russian Altai: implications from geochemical and detrital zircon U–Pb and Hf isotopic studies of meta-sedimentary complexes in the Charysh–Terekta–Ulagan–Sayan suture zone. Gondwana Res. 34, 1–15.
Chetverikova, N.P., Sytova, V.A., Ushatinskaya, G.T., et al., 1996. Stratigraphy and Fauna of Silurian and Lower Devonian Deposits of the Nura Synclinorium. Moscow State University Publishing House, M, 256 p. (in Russian).
Clift, P.D., Pecher, I., Kukowski, N., Hampel, A., 2003. Tectonic erosion of the Peruvian forearc, Lima Basin, by subduction and Nazca Ridge collision. Tectonics 22 (3), 1023.
Cohen, R.S., O'Nions, R.K., 1982. The lead, neodymium and strontium isotopic structure of ocean ridge basalts. J. Petrol. 23 (3), 299–324.
Collins, W.J., Belousova, E.A., Kemp, A.I.S., Murphy, J.B., 2011. Two contrasting Phanerozoic orogenic systems revealed by hafnium isotope data. Nat. Geosci. 4, 333–337.
Dagva-Ochir, L., Oyunchimeg, T., Enkhdalai, B., Safonova, I., Li, H., Otgonbaatar, D., Tamehe, L.S., Sharav, D., 2020. Middle Paleozoic intermediate-mafic rocks of the Tsoroidog Uul' accretionary complex, Central Mongolia: Petrogenesis and tectonic implications. Lithos 376-377, 105795.
De Grave, J., Glorie, S., Buslov, M.M., Izmer, A., Fournier-Carrie, A., Batalev, V., Vanhaecke, F., Elburg, M., Van den haute, P., 2011. The thermo-tectonic history of the Song-Kul Plateau, Kyrgyz Tien Shan: constraints by apatite and titanite thermochronometry and zircon U/Pb dating. Gondwana Res. 20 (4), 745–763.
Degtyarev, K.E., 1999. Tectonic Evolution of the Early Paleozoic Active Margin in Kazakhstan. Nauka, Moscow, 123 p. (in Russian).
Degtyarev, K.E., 2011. Tectonic evolution of Early Paleozoic island-arc systems and continental crust formation in the Caledonides of Kazakhstan and the North Tien Shan. Geotectonics 45 (1), 23–50.
Degtyarev, K.E., 2012. Tectonic Evolution of the Early Paleozoic Island Arcs and Continental Crust Formation in the Caledonides of Kazakhstan. GEOS, Moscow, 289 p. (in Russian).
Degtyarev, K.E., Ryazantsev, A.V., 2007. Model of the Cambrian arc–continent collision for the paleozoids of Kazakhstan. Geotectonics 1, 71–96 (in Russian).
Degtyarev, K.E., Tolmacheva, T.Y., Tretyakov, A.A., Kotov, A.B., Yakubchuk, A.S., Salnikova, E.B., Wang, K.-L., 2017. Polychronous formation of the ophiolite association in the Tekturmas zone of Central Kazakhstan inferred from geochronological and biostratigraphic data. Dokl. Earth Sci. 472, 26–30.
Degtyarev, K.E., Tolmacheva, T.Y., Tretyakov, A.A., 2020. Siliceous–volcanic associations of the Northern Balkhash ophiolite zone (Central Kazakhstan): biostratigraphy, sedimentation and tectonic evolution in the Middle-Late Ordovician. Palaeogeogr. Palaeoclimatol. Palaeoecol. 551, 109748.
Degtyarev, K., Yakubchuk, A.S., Luchitskaya, M.V., Tolmacheva, T.Y., Skoblenko, A.V., Tretyakov, A.A., 2022. Ordovician supra-subduction, oceanic and within-plate ocean island complexes in the Tekturmas ophiolite zone (Central Kazakhstan): age, geochemistry and tectonic implications. Int. Geol. Rev. 64 (15), 2108–2150.
Degtyarev, K.E., Luchitskaya, M.V., Tretyakov, A.A., 2023. The first discovery of Cambrian volcanic rocks and plagiogranites in the Tekturmas Ophiolite Zone (Central Kazakhstan): age and composition. Dokl. Earth Sci. 513, 1096–1103.
Didenko, A., Mossakovsky, A., Pechersky, D., Ruzhentsev, S., Samygin, S., Kheraskova, T., 1994. Geodynamics of Paleozoic oceans of Central Asia. Geol. Geofiz. 35 (7–8), 59–75 (in Russian).
Dobretsov, N.L., Berzin, N.A., Buslov, M.M., 1995. Opening and tectonic evolution of the Paleo-Asian Ocean. Int. Geol. Rev. 37, 335–360.
Domeier, M., Torsvik, T.H., 2014. Plate tectonics in the late Paleozoic. Geosci. Front. 5 (3), 303–350.
Filippova, I.B., Bush, V.A., Didenko, A.N., 2001. Middle Paleozoic subduction belts: the leading factor in the formation of the Central Asian fold-and-thrust belt. Russ. J. Earth Sci. 3 (6), 405–426.
Gao, J., Long, L.L., Klemd, R., Qian, Q., Liu, D.N., Xiong, X.M., Su, W., Liu, W., Wang, Y. T., Yang, E.Q., 2009. Tectonic evolution of the south Tianshan orogen and adjacent regions, NW China: geochemical and age constraints of granitoid rocks. Int. J. Earth Sci. 98, 1221–1238.
Gerasimova, N.A., Novikova, M.Z., Kurkovskaya, L.A., Yakubchuk, A.S., 1992. New data on the stratigraphy of the Lower Paleozoic Tekturmas ophiolite belt (Central Kazakhstan). Bull. MSNT Geol. Dep. 67 (3), 60–76 (in Russian).
Glorie, S., De Grave, J., Buslov, M.M., Zhimulev, F.I., Izmer, A., Vandoorne, W., Ryabinin, A., Van den Haute, P., Vanhaecke, F., Elburg, M.A., 2011. Formation and Palaeozoic evolution of the Gorny-Altai–Altai-Mongolia suture zone (South Siberia): zircon U/Pb constraints on the igneous record. Gondwana Res. 20 (2–3), 465–484.
Gridina, N.M., 2003. Conodonts in siliceous deposits of the northeast of Central Kazakhstan. In: Geosciences in Kazakhstan. MGK-32. Reports of Kazakhstan Geologists, pp. 135–140 (in Russian).
Gurova, A.V., Safonova, I.Y., Savinsky, I.A., Antonyuk, R.M., Orynbek, T.Z., 2022. Magmatic rocks of the Tekturmass accretionary complex, Central Kazakhstan: geological position and geodynamic settings of formation. Geodyn. Tectonophys. 13 (5), 0673.
Hanyu, T., Tatsumi, Y., Senda, R., Miyazaki, T., Chang, Q., Hirahara, Y., Takahashi, T., Kawabata, H., Suzuki, K., Kimura, J.-I., Nakai, S., 2011. Geochemical characteristics and origin of the HIMU reservoir: a possible mantle plume source in the lower mantle. Geochem. Geophys. Geosyst. https://doi.org/10.1029/2010GC003252.
Hirschmann, M.M., Stolper, E.M., 1996. A possible role for garnet pyroxenite in the origin of the "garnet signature" in MORB. Contrib. Mineral. Petrol. 124, 185–208.
Hofmann, A.W., 1988. Chemical differentiation of the Earth: the relationship between mantle, continental crust, and oceanic crust. Earth Planet. Sci. Lett. 90 (3), 297–314.
Hofmann, A.W., 1997. Mantle geochemistry: the message from oceanic volcanism. Nature 385, 219–229.
Hori, R., 1992. Radiolarian biostratigraphy at the Triassic/Jurassic period Boundary in bedded cherts from the Inuyama Area, Central Japan. Austrian J. Geosci. 35, 53–65.
Humphris, S.E., Thompson, G., 1978. Hydrothermal alteration of oceanic basalts by seawater. Geochim. Cosmochim. Acta 42, 107–125.
Ichiyama, Y., Ishiwatari, A., Koizumi, K., 2008. Petrogenesis of greenstones from the Mino–Tamba belt, SW Japan: evidence for an accreted Permian oceanic plateau. Lithos 100, 127–146.
Ichiyama, Y., Ishiwatari, A., Kimura, J.-I., Senda, R., Miyamoto, T., 2014. Jurassic plume-origin ophiolites in Japan: accreted fragments of oceanic plateaus. Contrib. Mineral. Petrol. 168, 1019.
Isozaki, Y., Maruyama, S., Fukuoka, F., 1990. Accreted oceanic materials in Japan. Tectonophysics 181, 179–205.
Jahn, B.M., 2004. The Central Asian Orogenic Belt evolution and growth of the continental crust in the Phanerozoic. In: Malpas, J., Fletcher, C.J.N., Ali, J.R., Aichison, J.C. (Eds.), Aspects of the Tectonic Evolution of. Geological Society of London, Special Publication, China, pp. 73–100, 226 p.
Jahn, B., Wu, F., Chen, B., 2000. Granitoids of the Central Asian Orogenic Belt and continental growth in the Phanerozoic. Trans. R. Soc. Edinb. 91, 181–193.
Janoušek, V., Jiang, Y., Buriánek, D., Schulmann, K., Hanžl, P., Soejono, I., Kröner, A., Altanbaatar, B., Erban, V., Lexa, O., Ganchuluun, T., Košler, J., 2018. Cambrian–Ordovician magmatism of the Ikh-Mongol Arc System exemplified by the Khantaishir Magmatic Complex (Lake Zone, south–central Mongolia). Gondwana Res. 54, 122–149.
Jensen, L.S., 1976. A new cation plot for classifying subalkalic volcanic rocks. In: Ontario Division Mines, Miscellaneous Paper, 66, 22 p.
Jian, P., Liu, D.Y., Shi, Y.R., Zhang, F.Q., 2005. SHRIMP dating of SSZ ophiolites from northern Xinjiang Province, China: Implications for generation of oceanic crust in the Central Asian orogenic belt. In: Sklyarov, E.V. (Ed.), Structural and Tectonic Correlation across the Central Asia Orogenic Collage: North-Eastern Segment. Guidebook and Abstract Volume of the Siberian Workshop IGCP-480. Institute of the Earth Crust, Siberian Branch of Russian Academy of Sciences, Irkutsk, 246 p.
Jicha, B.R., Kay, S.M., 2018. Quantifying arc migration and the role of forearc subduction erosion in the central Aleutians. J. Volcanol. Geotherm. Res. 360, 84–99.
Johnson, K.T.M., 1998. Experimental determination of partition coefficients for rare earth and high-field-strength elements between clinopyroxene, garnet, and basaltic melt at high pressures. Contrib. Mineral. Petrol. 133, 60–68.
Katz, H.R., 1973. Contrasts in tectonic evolution of orogenic belts in the south-East Pacific. J. R. Soc. N. Z. 3 (3), 333–361.
Kemp, A.I., Hawkesworth, C.J., Foster, G.L., Paterson, B.A., Woodhead, J.D., Hergt, J.M., Gray, C.M., Whitehouse, M.J., 2007. Magmatic and crustal differentiation history of granitic rocks from Hf-O isotopes in zircon. Science 315 (5814), 980–983.
Khassen, B.P., Safonova, I.Yu., Yermolov, P.V., Antonyuk, R.M., Gurova, A.V., Obut, O. T., Perfilova, A.A., Savinskiy, I.A., Tsujimori, T., 2020. The Tekturmas ophiolite belt of Central Kazakhstan: geology, magmatism, and tectonics. Geol. J. 55, 2363–2382.
Kojima, S., Kemkin, I.V., Kametaka, M., Ando, A., 2000. A correlation of accretionary complexes of southern Sikhote-Alin of Russia and the Inner Zone of Southwest Japan. Geosci. J. 4, 175–185.
Konopelko, D., Seltmann, R., Dolgopolova, A., Safonova, I., Glorie, S., De Grave, J., Sun, M., 2021. Adakite-like granitoids of Songkultau: a relic of juvenile Cambrian arc in Kyrgyz Tien Shan. Geosci. Front. 12 (1), 147–160.
Korobkin, V.V., Buslov, M.M., 2011. Tectonics and geodynamics of the western Central Asian fold belt (Kazakhstan Paleozoides). Russ. Geol. Geophys. 52 (12), 1600–1618.
Kröner, A., Windley, B.F., Badarch, G., Tomurtogoo, O., Hegner, E., Jahn, B.M., Gruschka, S., Khain, E.V., Demoux, A., Wingate, M.T.D., 2007. Accretionary growth and crust formation in the Central Asian Orogenic Belt and comparison with the Arabian-Nubian shield. Geol. Soc. Am. Mem. 200, 181–209.
Kröner, A., Kovach, V., Belousova, E., Hegner, E., Armstrong, R., Dolgopolova, A., Seltmann, R., Alexeiev, D.V., Hofmann, J.E., Wong, J., Sun, M., Cai, K., Wang, T., Tong, Y., Wilde, S.A., Degtyarev, K.E., Rytsk, E., 2014. Reassessment of continental growth during the accretionary history of the Central Asian Orogenic Belt. Gondwana Res. 25, 103–125.
Kröner, A., Kovach, V., Alexeiev, D., Wang, K.-L., Wong, J., Degtyarev, K., Kozakov, I., 2017. No excessive crustal growth in the Central Asian Orogenic Belt: further evidence from field relationships and isotopic data. Gondwana Res. 50, 135–166.
Kruk, N.N., Vladimirov, A.G., Babin, G.A., Shokalsky, S.P., Sennikov, N.V., Rudnev, S.N., Volkova, N.I., Kovach, V.P., Serov, P.A., 2010. Continental crust in Gorny Altai: nature and composition of protoliths. Russ. Geol. Geophys. 51, 431–446.
Kurkovskaya, L.A., 1985. Conodonts from Ordovician Siliceous and Volcanogenic Formaitons of Central Kazakhstan. Geology of Early Geosynclinal Complexes of

Central Kazakhstan. Moscow State University Publishing House, Moscow, pp. 164–177 (in Russian).
Kusky, T., Windley, B., Safonova, I., Wakita, K., Wakabayashi, J., Polat, A., Santosh, M., 2013. Recognition of Ocean Plate Stratigraphy in accretionary orogens through Earth history: a record of 3.8 billion years of sea floor spreading, subduction, and accretion. Gondwana Res. 24, 501–547.
Kwon, S.-T., Tilton, G.R., Coleman, R.G., Feng, Y., 1989. Isotopic studies bearing on the tectonics of the West Junggar region, Xinjiang, China. Tectonics 8 (4), 719–727.
Le Maitre, R.W., Streckeisen, A., Zanettin, B., Le Bas, M.J., Bonin, B., Bateman, P., Bellieni, G., Dudek, A., Efremova, S., Keller, J., Lamere, J., Sabine, P.A., Schmid, R., Sorensen, H., Woolley, A.R., 2002. Igneous rocks: A classification and glossary of terms. In: Recommendations of the International Union of Geological Sciences, Subcommission of the Systematics of Igneous Rocks. Cambridge University Press, 236 p.
Levashova, N.M., Degtyarev, K.E., Bazhenov, M.L., Collins, A.Q., Van der Voo, R., 2003. Permian palaeomagnetism of East Kazakhstan and the amalgamation of Eurasia. Geophys. J. Int. 152, 677–687.
Levashova, N.M., Degtyarev, K.E., Bazhenov, M.L., 2012. Oroclinal bending of the Middle and Late Paleozoic volcanic belts in Kazakhstan: paleomagnetic evidence and geological implications. Geotectonics 46 (4), 285–302.
Li, P., Sun, M., Rosenbaum, G., Yuan, C., Safonova, I., Cai, K., Jiang, Y., Zhang, Y., 2018. Geometry, kinematics and tectonic models of the Kazakhstan orocline, Central Asian orogenic belt. J. Asian Earth Sci. 153, 42–56.
Linnen, R.L., Keppler, H., 2002. Melt composition control of Zr/Hf fractionation in magmatic processes. Geochim. Cosmochim. Acta 66, 3293–3301.
Liu, B., Han, B.F., Xu, Z., Ren, R., Zhang, J.R., Zhou, J., Su, Li, Li, Q.L., 2016. The Cambrian initiation of intra-oceanic subduction in the southern Paleo-Asian Ocean: further evidence from the Barleik subduction related metamorphic complex in the West Junggar region, NW China. J. Asian Earth Sci. 123, 1–21.
Liu, B., Han, B.F., Chen, J.F., Ren, R., Zheng, B., Wang, Z.Z., Feng, L.X., 2017. Closure time of the Junggar-Balkhash Ocean: Constraints from Late Paleozoic volcano-sedimentary sequences in the Barleik Mountains, West Junggar, NW China. Tectonics 36 (12), 2823–2845.
Ma, X.X., Shu, L.S., Santosh, M., Li, J.Y., 2013. Petrogenesis and tectonic significance of an early Palaeozoic mafic-intermediate suite of rocks from the Central Tianshan, Northwest China. Int. Geol. Rev. 55, 548–573.
Magmatic complexes of Central Kazakhstan, 1988. Guidebook of the Excursion of the IV Kazakhstan Petrographic Conference, Karaganda, 62 p.
Maniar, P.D., Piccoli, P.M., 1989. Tectonic Discrimination of Granitoids. Geol. Soc. Am. Bull. 101, 635–643.
Maruyama, S., Isozaki, Y., Kimura, G., Terabayashi, M., 1997. Paleogeographic maps of the Japanese Islands: Plate tectonic synthesis from 750 Ma to the present. Island Arc 6, 121–142.
Maruyama, S., Omori, S., Sensu, H., Kawai, K., Windley, B.F., 2011. Pacific-type orogens: new concepts and variations in space and time from present to past. J. Geogr. 120, 115–223 (in Japanese with English abstract and captions).
Matsuda, T., Uyeda, S., 1971. On the Pacific-type orogeny and its model: Extension of the paired metamorphic belt concept and possible origin of marginal basins. Tectonophysics 11, 5–27.
Mullen, E.D., 1983. MnO-$TiO_2$-$P_2O_5$. A minor element discrimination for basaltic rocks of oceanic environments and its implications for petrogenesis. Earth Planet. Sci. Lett. 62, 53–62.
Nazarov, B.B., 1975. Lower and Middle Paleozoic Radiolarians of Kazakhstan. Nauka, M, 203 p. (in Russian).
Nikitin, I.F., 1991. Decisions of the III Kazakhstan Stratigraphic Conference on the Precambrian and Phanerozoic. Part 1: Precambrian and Paleozoic. Satpaev Institute of Geological Sciences Publishing House, Alma-Ata, 148 p. (in Russian).
Nikitin, I.F., 2002. Ordovician siliceous and siliceous-basaltic complexes of Kazakhstan. Russ. Geol. Geophys. 43 (6), 512–527 (in Russian).
Niu, Y.L., O'Hara, M.J., 2008. Global correlations of ocean ridge basalt chemistry with axial depth: a new perspective. J. Petrol. 49, 633–664.
Novikova, M.Z., Kuznetsov, I.E., Ryakhovsky, V.M., Sigachev, S.P., 1988. Lower Paleozoic Early Geosynclinal Volcanism of Central Kazakhstan. Geology and Minerals of Central Kazakhstan. Nauka, M, pp. 44–71 (in Russian).
Novikova, M.Z., German, L.L., Kuznetsov, I.E., Yakubchuk, A.S., 1991. Ophiolites of the Tekturmas Zone. Magmatism and Ore Potential of Kazakhstan. Gylym, Alma-Ata, pp. 92–102 (in Russian).
Orlov, I.V., Bespalov, V.F., 1981. Geological Map of the Kazakhstan SSR. Scale 1: 500000. Aerogeology, Central Kazakhstan Series, Moscow, 21 p. (in Russian).
Pan, H., Shen, P., Zhang, L., Seitmuratova, E., Jakupova, S., 2015. Geochemistry, U-Pb dating, Lu-Hf isotopic analysis and geological significance of volcanic rocks in Maikain deposit, Kazakhstan. Acta Petrol. Sin. 31 (2), 401–414.
Parkinson, I.J., Pearce, J.A., 1998. Peridotites from Izu-Bonin-Mariana forearc (ODP Leg 125): evidence for mantle melting and melt-mantle interaction in a supra-subduction zone setting. J. Petrol. 39 (9), 1577–1618.
Pearce, J.A., 1983. Role of the sub-continental lithosphere in magma genesis at active continental margins. In: Hawkesworth, C.J., Norry, M.J. (Eds.), Continental Basalts and Mantle Xenoliths. Shiva Cheshire, UK, pp. 230–249.
Pearce, J.A., 2008. Geochemical fingerprinting of oceanic basalts with applications to ophiolite classification and the search for Archean oceanic crust. Lithos 100, 14–48.
Pearce, J.A., Peate, D.W., 1995. Tectonic implications of the composition of volcanic arc magmas. Annu. Rev. Earth Planet. Sci. 23, 251–285.
Pearce, J.A., Harris, N.B., Tindle, A.G., 1984. Trace element discrimination diagrams for the tectonic interpretation of granitic rocks. J. Petrol. 25 (4), 956–983.
Perfilova, A.A., 2023. Age, Composition and Sources of Paleozoic Greywacke Sandstones of Central and Eastern Kazakhstan. PhD Dissertation,. IGM SB RAS, Novosibirsk, 242 p.
Perfilova, A.A., Safonova, I.Y., Degtyarev, K.E., Savinskiy, I.A., Kotler, P.D., Khassen, B. P., 2022a. Composition and sources of Silurian terrigenous rocks at the periphery of the Tekturmas ophiolite zone (Central Kazakhstan). Dokl. Earth Sci. 505 (1), 11–17.
Perfilova, A.A., Safonova, I.Y., Gurova, A.V., Kotler, P.D., Savinskiy, I.A., 2022b. Tectonic settings of formation of volcanic and sedimentary rocks of the Itmurundy zone, Central Kazakhstan. Geodyn. Tectonophys. 13 (1), 0572.
Pfänder, J.A., Jochum, K.P., Kozakov, I., Kröner, A., Todt, W., 2002. Coupled evolution of back-arc and island arc-like mafic crust in the late-Neoproterozoic Adardagh Tes-Chem ophiolite, Central Asia: evidence from trace element and Sr-Nd-Pb isotope data. Contrib. Mineral. Petrol. 143, 154–174.
Polat, A., Kerrich, R., Wyman, D.A., 1999. Geochemical diversity in oceanic komatiites and basalts from the late Archean Wawa greenstone belts, Superior Province, Canada: trace element and Nd isotope evidence for a heterogeneous mantle. Precambrian Res. 94, 139–173.
Regelous, M., Hofmann, A.W., Abouchami, W., Galer, S.J.G., 2003. Geochemistry of lavas from the Emperor Seamounts, and the geochemical evolution of Hawaiian magmatism from 85 to 42 Ma. J. Petrol. 44, 113–140.
Ren, R., Han, B.-F., Xu, Zh., Zhou, Y.-Zh., Liu, B., Zhang, L., Chen, J.-F., Su, L., Li, J., Li, X.-H., Li, Q.-L., 2014. When did the subduction first initiate in the southern Paleo-Asian Ocean: New constraints from a Cambrian intra-oceanic arc system in West Junggar, NW China. Earth Planet. Sci. Lett. 388, 222–236.
Rudnick, R.L., Gao, S., 2003. Vol. 3: The Crust, 3.01—The Composition of the Continental Crust. In: Holland, H.D., Turekian, K.K. (Eds.), Treatise on Geochemistry. Elsevier-Pergamon, Oxford, pp. 1–64.
Safonova, I.Yu., 2008. Geochemical evolution of intraplate magmatism in the Paleo-Asian Ocean from the Late Neoproterozoic to the Early Cambrian. Petrology 16 (5), 492–511.
Safonova, I.Y., 2017. Juvenile versus recycled crust in the Central Asian Orogenic Belt: implications from ocean plate stratigraphy, blueschist belts and intra-oceanic arcs. Gondwana Res. 47, 6–27.
Safonova, I.Y., Khanchuk, A.I., 2021. Subduction erosion at Pacific-type convergent margins. Russ. J. Pac. Geol. 15 (6), 495–509.
Safonova, I., Perfilova, A., 2023. Survived and disappeared intra-oceanic arcs of the paleo-Asian Ocean: evidence from Kazakhstan. Natl. Sci. Rev. 10 (2), nwac215.
Safonova, I., Santosh, M., 2014. Accretionary complexes in the Asia-Pacific region: tracing archives of ocean plate stratigraphy and tracking mantle plumes. Gondwana Res. 25, 126–158.
Safonova, I., Seltmann, R., Kröner, A., Gladkochub, D., Schulmann, K., Xiao, W., Kim, T., Komiya, T., Sun, M., 2011a. A new concept of continental construction in the Central Asian Orogenic Belt (compared to actualistic examples from the Western Pacific). Episodes 34, 186–194.
Safonova, I.Yu., Buslov, M.M., Simonov, V.A., Izokh, A.E., Komiya, T., Kurganskaya, E. V., Ohno, T., 2011b. Geochemistry, petrogenesis and geodynamic origin of basalts from the Katun' accretionary complex of Gorny Altai (southwestern Siberia). Russ. Geol. Geophys. 52 (4), 421–442.
Safonova, I.Y., Sennikov, N.V., Komiya, T., Bychkova, Y.V., Kurganskaya, E.V., 2011c. Geochemical diversity in oceanic basalts hosted by the Zasur'ya accretionary complex, NW Russian Altai, Central Asia: implications from trace elements and Nd isotopes. J. Asian Earth Sci. 42 (3), 191–207.
Safonova, I.Y., Simonov, V.A., Kurganskaya, E.V., Obut, O.T., Romer, R.L., Seltmann, R., 2012. Late Paleozoic oceanic basalts hosted by the Char suture-shear zone, East Kazakhstan: geological position, geochemistry, petrogenesis and tectonic setting Original Research Article. J. Asian Earth Sci. 49, 20–39.
Safonova, I., Kojima, S., Nakae, S., Romer, R., Seltmann, R., Sano, H., Onoue, T., 2015. Oceanic island basalts in accretionary complexes of SW Japan: tectonic and petrogenetic implications. J. Asian Earth Sci. 113, 508–523.
Safonova, I., Biske, G., Romer, R.L., Seltmann, R., Simonov, V., Maruyama, S., 2016. Middle Paleozoic mafic magmatism and ocean plate stratigraphy of the South Tianshan, Kyrgyzstan. Gondwana Res. 30, 236–256.
Safonova, I., Kotlyarov, A., Krivonogov, S., Xiao, W., 2017. Intra-oceanic arcs of the Paleo-Asian Ocean. Gondwana Res. 50, 167–194.
Safonova, I., Savinskiy, I., Perfilova, A., Gurova, A., Maruyama, S., Tsujimori, T., 2020. The Itmurundy Pacific-type orogenic belt in northern Balkhash, Central Kazakhstan: revisited plus first U-Pb age, geochemical and Nd isotope data from igneous rocks. Gondwana Res. 79, 49–69.
Safonova, I., Perfilova, A., Savinskiy, I., Kotler, P., Sun, M., Wang, B., 2022. Sandstones of the Itmurundy accretionary complex, Central Kazakhstan, as archives of arc magmatism and subduction erosion: evidence from U-Pb zircon ages, geochemistry and Hf-Nd isotopes. Gondwana Res. 111, 35–52.
Safonova, I., Krutikova, A., Perfilova, A., Obut, O., Kovach, V., Kulikova, A., 2024a. Early Paleozoic juvenile crustal growth in the Paleo-Asian Ocean: a contribution from the Zasur'ya accretionary complex of NW Altai. Earth Sci. Rev. 249, 104648.
Safonova, I., Savinskiy, I., Perfilova, A., Obut, O., Gurova, A., Krivonogov, S., 2024b. A new tectonic model for the Itmurundy Zone, Central Kazakhstan: linking ocean plate stratigraphy, timing of accretion and subduction polarity. Geosci. Front. 15, 101814.
Seitmuratova, E.Y., Goryaeva, V.S., Saidasheva, F.F., Arshamov, Y.K., Baratov, R.T., Dautbekov, D.O., Shadiyev, N.S., Mashrapova, M.A., Dauletuly, A., Karimbekov, T. K., 2023. The current state of research on secondary quartzites of the northern segment of the Jungar-Balkhash folded system and their Au mineralization (Central Kazakhstan). Minerals 13 (6), 813.

Seltmann, R., Soloviev, S., Shatov, V., Pirajno, F., Naumov, E., Cherkasov, S., 2010. Metallogeny of Siberia: tectonic, geologic and metallogenic settings of selected significant deposits. Aust. J. Earth Sci. 57 (6), 655–706.
Sengör, A.M.C., Natal'in, B.A., Burtman, V.S., 1993. Evolution of the Altaid tectonic collage and Paleozoic crustal growth in Eurasia. Nature 364, 299–307.
Shen, P., Pan, H., Seitmuratova, E., Yuan, F., Jakupova, S., 2015. A Cambrian intra-oceanic subduction system in the Bozshakol area, Kazakhstan. Lithos 224-225, 61–77.
Stepanets, W.G., 2016. Ophiolites of Kazakhstan. Geology and Geodynamics. Acad. Pub. House Lambert, 251 p. (in Russian).
Stern, C.R., 2011. Subduction erosion: rates, mechanisms, and its role in arc magmatism and the evolution of the continental crust and mantle. Gondwana Res. 20, 284–308.
Stern, R.J., Scholl, D.W., 2010. Yin and Yang of continental crust creation and destruction by plate tectonic processes. Int. Geol. Rev. 52, 1–31.
Straub, S.M., Goldstein, C.L., Class, C., Schmidt, A., Gomez-Tuena, A., 2010. Slab and Mantle Controls on the Sr-Nd-Pb-Hf Isotope Evolution of the Post 42Ma Izu-Bonin Volcanic Arc. J. Petrol. 51 (5), 993–1026.
Sun, S., McDonough, W.F., 1989. Chemical and isotopic systematics of oceanic basalts: implications for mantle composition and processes. Magmatism in the Ocean Basins. Geol. Soc. Spec. Publ. 42, 313–345.
Sun, M., Yuan, C., Xiao, W., Long, X., Xia, X., Zhao, G., Lin, S., Wu, F., Kroner, A., 2008. Zircon U–Pb and Hf isotopic study of gneissic rocks from the Chinese Altai: progressive accretionary history in the early to middle Palaeozoic. Chem. Geol. 247, 352–383.
Suzuki, K., Maruyama, S., Yamamoto, S., Omori, S., 2010. Have the Japanese Islands grown?: five "Japans" were born, and four "Japans" subducted into the mantle. J. Geogr. (Chigaku Zasshi) 119, 1173–1196 (in Japanese).
Thompson, G., 1991. Metamorphic and hydrothermal processes: Basalt-seawater interactions. In: Floyd, P.A. (Ed.), Oceanic Basalts. Blachie and Sons Ltd., Glasgow, pp. 148–173.
Turmanidze, T.L., Grishin, D.M., Pechersky, D.M., Stepanets, V.G., 1991. Paleomagnetic data from Ordovician ophiolites of the allochthonous Karaulcheku, Tolpak, and Bazarbay massifs (Central Kazakhstan). Geotectonics 4, 54–69 (in Russian).
Utsunomiya, A., Jahn, B.-M., Ota, T., Safonova, I.Yu., 2009. A geochemical and Sr-Nd isotopic study of the Vendian greenstones from Gorny Altai, southern Siberia: implications for the tectonic setting of the formation of greenstones and the role of oceanic plateaus in accretionary orogeny. Lithos 113, 437–453.
Volkova, N.I., Budanov, V.I., 1999. Geochemical discrimination of metabasalt rocks of the Fan–Karategin transitional blueschist/greenschist belt, South Tianshan, Tajikistan: seamount volcanism and accretionary tectonics. Lithos 47 (3–4), 201–216.
Volkova, N.I., Sklyarov, E.V., 2007. High-pressure complexes of Central Asian Fold Belt: geologic setting, geochemistry, and geodynamic implications. Russ. Geol. Geophys. 48, 83–90.
Wakita, K., 2012. Mappable features of mélanges derived from Ocean Plate Stratigraphy in the Jurassic accretionary complexes of Mino and Chichibu terranes in Southwest Japan. Tectonophysics 568-569, 74–85.
Wang, Z.H., Sun, S., Li, J.L., Hou, Q.L., Qin, K.Z., Xiao, W.J., Hao, J., 2003. Paleozoic tectonic evolution of the northern Xinjiang, China: geochemical and geochronological constrains from the ophiolites. Tectonics 22, 1014.
Wang, B., Shu, L.S., Liu, H.S., Gong, H.J., Ma, Y.Z., Mu, L.X., Zhong, L.L., 2014. First evidence for ca. 780 Ma intra-plate magmatism and its implications for Neoproterozoic rifting of the North Yili Block and tectonic origin of the continental blocks in SW of Central Asia. Precambrian Res. 254, 258–272.
Wang, M., Zhang, J.J., Zhang, B., Qi, G.W., 2015. An Early Paleozoic collisional event along the northern margin of the Central Tianshan Block: constraints from geochemistry and geochronology of granitic rocks. J. Asian Earth Sci. 113, 325–338.
Wang, T., Xiao, W., Collins, W.J., Tong, Y., Hou, Z., Huang, H., Wang, X., Lin, S., Seltmann, R., Wang, Ch., Han, B., 2023. Quantitative characterization of orogens through isotopic mapping. Nat. Commun. Earth Environ. 4 (1), 110.
Weit, A., Trumbull, R.B., Keiding, J.K., Geissler, W.H., Gibson, S.A., Veksler, I.V., 2017. The magmatic system beneath the Tristan da Cunha Island: insights from thermobarometry, melting models and geophysics. Tectonophysics 716, 64–76.
Wen, Z.G., Zhao, W.P., Liu, T.F., Liu, S.B., 2016. Formation age and geotectonic significance of Baerluke ophiolite in west Junggar, Xinjiang. Geol. Bull. China 35, 1401–1410 (in Chinese with English abstract).
Weng, K., Xu, X.Y., Ma, Z.P., Chen, J.L., Sun, J.M., Zhang, X., 2016. The geochemistry and chronology characteristics and the geological significance of ultramafic rock in Mayile ophiolite, West Junggar, Xinjiang. Acta Petrol. Sin. 32 (5), 1420–1436 (in Chinese with English abstract).
White, W.M., Hofmann, A.W., Puchelt, H., 1987. Isotope geochemistry of Pacific mid-ocean ridge basalts. J. Geophys. Res. 92, 4881–4893.
Winchester, J.A., Floyd, P.A., 1977. Geochemical discrimination of different magma series and their differentiation products using immobile elements. Chem. Geol. 20, 325–343.
Windley, B.F., Alexeiev, D., Xiao, W., Kröner, A., Badarch, G., 2007. Tectonic models for accretion of the Central Asian Orogenic Belt. J. Geol. Soc. Lond. 164, 31–47.
Wood, D.A., Joron, J.-L., Treuil, M., 1979. A re-appraisal of the use of trace elements to classify and discriminate between magma series erupted in different tectonic settings Earth Planet. Sci. Lett. 45, 326–336.
Xiao, W., Santosh, M., 2014. The western Central Asian Orogenic Belt: a window to accretionary orogenesis and continental growth. Gondwana Res. 25, 1429–1444.
Xiao, W.J., Huang, B., Han, C., Sun, S., Li, J., 2010. A review of the western part of the Altaids: a key to understanding the architecture of accretionary orogens. Gondwana Res. 18, 253–273.
Xiao, W., Windley, B.F., Sun, S., Li, J., Huang, B., Han, C., Yuan, C., Sun, M., Chen, H., 2015. A tale of amalgamation of three Permo-Triassic Collage Systems in Central Asia: oroclines, sutures, and terminal accretion. Annu. Rev. Earth Planet. Sci. 43, 477–507.
Xu, Z., Han, B.-F., Ren, R., Zhou, Y.-Z., Zhang, L., Chen, J.-F., Su, L., Li, X.-H., Liu, D.-Y., 2012. Ultramafic–mafic mélange, island arc and post-collisional intrusions in the Mayile Mountain, West Junggar, China: implications for Paleozoic intra-oceanic subduction–accretion process. Lithos 132-133, 141–161.
Yakubchuk, A.S., 1991. Tectonic Position and Structure of Ophiolites of Central Kazakhstan Using the Tekturmas and Southwestern Maykain-Kyzyltas Zones as Examples. Autoreferate Diss. Cand. Geol. and Min. Sci. Moscow State University Publishing House, Moscow, 16 p. (in Russian).
Yakubchuk, A.A., Stepanets, V.G., German, L.L., 1988. Swarms of subparallel sheeted dikes in ophiolite complexes as evidence of spreading. Doklady USSR Acad. Sci. 298 (5), 1193–1197 (in Russian).
Yakubchuk, A.S., Chitalin, A.F., Baraboshkin, E.Yu., 1989. Variscan tectonics of the Tekturmas ophiolite zone (Central Kazakhstan). Geotectonics 5, 61–70 (in Russian).
Yang, Y.Q., Zhao, L., Xu, Q.Q., Zheng, R.G., Niu, B.G., 2018. Defining components of the Hebukesaier ophiolitic mélange in the northern West Junggar and its tectonic implication. Acta Geol. Sin. 92 (2), 298–312 (in Chinese with English abstract).
Yang, Y., Zhao, L., Zheng, R., Xu, Q., 2019a. Evolution of the early Paleozoic Hongguleleng–Balkybey Ocean: evidence from the Hebukesaier ophiolitic mélange in the northern West Junggar, NW China. Lithos 324-325, 519–536.
Yang, Y., Zhao, L., Xu, Q., Zheng, R., Liu, J., Zhang, J., 2019b. Early Paleozoic tectonic evolution of the northern West Junggar (NW China): Constraints from Early Cambrian – Middle Silurian felsic plutons of the Chagantaolegai ophiolitic mélange. Lithos 350-351, 105225.
Yin, R., Wang, R.C., Zhang, A.C., Hu, H., Zhu, J.C., Rao, C., Zhang, H., 2013. Extreme fractionation from zircon to hafnon in the Koktokay No. 1 granitic pegmatite, Altai, northwestern China. Am. Mineral. 98, 1714–1724.
Zaitsev, Yu.A., 1977. Some aspects of the geological history of the Paleozoic fold belt of Kazakhstan. In: Geology and Mineral Resources of Central Kazakhstan. Nauka, Moscow, 19-46 pp. (in Russian).
Zartman, R.E., Doe, B.R., 1981. Plumbotectonics – the model. Tectonophysics 75, 135–162.
Zhang, L.F., 1997. $^{40}Ar/^{39}Ar$ age and its geological significance of the blueschists from the western Junggar, Xinjiang. Chin. Sci. Bull. 42, 2178–2181 (in Chinese).
Zhang, J.E., Xiao, W.J., Luo, J., Chen, Y.C., Windley, B.F., Song, D.F., Han, C., Safonova, I., 2018. Collision of the Tacheng block with the Mayile- Barleik-Tangbale accretionary complex in Western Junggar NW China: implication for Early-Middle Paleozoic architecture of the western Altaids. J. Asian Earth Sci. 159, 259–278.
Zhang, J., Chen, Y., Xiao, W., Wakabayashi, J., Song, S., Luo, J., Zhao, Y., 2023. Architecture of ophiolitic mélanges in the Junggar region, NW China. Geosyst. Geoenviron. 2, 100175.
Zhao, L., He, G., 2014. Geochronology and geochemistry of the Cambrian (~518 Ma) Chagantaolegai ophiolite in northern West Junggar (NW China): constraints on spatiotemporal characteristics of the Chingiz–Tarbagatai megazone. Int. Geol. Rev. 56 (10), 1181–1196.
Zheng, B., Han, B.F., Wang, Z.Z., Liu, B.L., Feng, X., 2020. An example of Phanerozoic continental crustal growth: the West Junggar Orogenic Belt, Northwest China. Lithos 376-377, 105745.
Zholtaev, G.Zh., Nikitina, O.I., Zhaimina, V. Ya, Seitmuratova, E. Yu, Pirogova, T.E., Ivanova, N.I., Fazylov, E.M., Musina, E.S., Nigmatova, S.A., Bayshashov, B.U., 2021. Decisions of the meeting on the unification of Phanerozoic Stratigraphic Schemes of Kazakhstan, Almaty, November 25–29, 2021. In: Explanatory note to the stratigraphic schemes developed and approved by the Meeting within the framework of the project "Modernization of stratigraphic schemes of the Phanerozoic of Kazakhstan based on the International chronostratigraphic chart - 2016-2021". Almaty, LLP «378», 236 p. (in Russian).
Zindler, A., Hart, S.R., 1986. Chemical geodynamics. Annu. Rev. Earth Planet. Sci. 14, 493–571.
Zonenshain, L.P., Kuzmin, M.I., Natapov, L.M., 1990. Geology of the USSR: A plate tectonic synthesis. In: Geodynamic Monograph Series. Am. Geoph. Union, 328 p.